Fall 2014

# Effects of grain properties and compaction on single-tool normal indentation of granular materials

Dennis Chieze Duru



Department:

# EFFECTS OF GRAIN PROPERTIES AND COMPACTION ON SINGLE-TOOL NORMAL INDENTATION OF GRANULAR MATERIALS

**by**

**DENNIS CHIEZE DURU**

**A THESIS**

**Presented to the Graduate Faculty of the**

**MISSOURI UNIVERSITY OF SCIENCE AND TECHNOLOGY**

**In Partial Fulfillment of the Requirements for the Degree**

**MASTER OF SCIENCE**

**in**

**GEOLOGICAL ENGINEERING**

**2014**

**Approved by**

**Leslie Gertsch, Advisor**
**Norbert Maerz**
**David Rogers**

## ABSTRACT

The behavior of three granular materials; filter sand, crushed garnet, and shale cutting, were investigated in an effort to evaluate the effect of grain size and shape, and material compaction under single tool load-indentation test. Force-penetration data was collected continuously through the end of each test and specific energy and specific penetration was calculated from the data.

Grain size and compaction affected the force penetration behavior. The higher the grain size, the more the fluctuation in the force of penetration. In addition, compaction reduces the force fluctuation in the fine aggregate grains, but increases the magnitude of the force fluctuations in the coarse aggregate grains.

Specific energy SE (energy required to indent a unit volume of the material) and Specific penetration SP (maximum force required to indent the material a given depth) were computed from the force-penetration curve. SE correlated with grain size and Aspect ratio for uncompacted materials and correlated with grain size and bulk density for the compacted materials. SP correlated with grain size and aspect ratio of the uncompacted sample and correlated with grain size, bulk density and solid density when the compacted data was introduced. This indicates that for uncompacted materials, grain size and aspect ratio are the dominant variable affecting SP and SE. However, when compaction is introduced, grain size and bulk density become dominant.

## ACKNOWLEDGEMENTS

I want to thank God for his gifts of strength, good health, wisdom and understanding during the period of this project.

My absolute gratitude goes to my adviser, Dr. Leslie Gertsch, for her financial support, encouragement and the opportunity given to me to carry out this project. I also want to thank the committee members, Dr. Norbert Maerz and Dr. David Rogers for accepting to be part of this project. I appreciate your individual contributions and corrections.

I wish to thank Paula Cochran, the Secretary of the Department of Geological Sciences and Engineering for all her help, the other staff and faculty of Geological Engineering for their role in my completion of my Master's program and to my colleague Azupuri Kaba for his support in making this project a reality. I also want to thank Dr. Galecki, Mr. Michael Bassett, Mr. John Tyler, Levi and Alex of the Rock Mechanic and Explosive Research Center for their technical support in making sure all the apparatus in the lab worked properly. I also thank the chemistry department for giving a helping hand with some of their chemistry apparatus.

Finally, I wish to thank my family, friends and relatives for their prayers and support during this period. I am most grateful to you all.

# TABLE OF CONTENTS

Page

# LIST OF ILLUSTRATIONS

# LIST OF TABLES

# 1. INTRODUCTION

## 1.1. BACKGROUND

The Earth, along with other rocky planets and most asteroids in the inner solar system, is covered with a layer of crushed, broken, and chemically altered rock. These depending on location and perspective are referred to as regolith or soil. The behavior of these unconsolidated granular materials in response to loads and impacts is an important control on much of engineering activity.

There are much of the surface focused engineering activities where solution to soil and regolith constraints are required. In foundation of buildings, road construction, dam construction, and bridge construction, as well as in surface mining, the behaviors of granular materials vary depending on their properties. Clayey materials tend to lead to expansion and contraction on alternate wetting and drying. This poses some level of difficulty in road construction and foundation for building making excavation unavoidable. More angular materials tend to lock tightly together therefore giving the best in terms of compaction. The military use these unconsolidated materials for defense because of their ability to absorb shock with little or no damage to the immediate environment.

The regolith on Earth's moon is different from the soil on the Earth's surface because the lunar regolith has not been subjected to weathering action of oxygen and water, and has not been biological altered by microbes as witnessed on earth. The moon being free of these weathering agents is effectively dry and free of atmosphere. Mars is also mostly dry though it has seen the effect of water in the past and in certain areas in the present. Near-earth asteroids are too small to hold

atmosphere, and are consequently completely dry. As a result, excavation, construction, and mining on the Moon, Mars, and near-Earth asteroids will be conducted mainly in dry granular materials during the early stages of exploration. This implies that planning can be done based on the behavior of dry granular material that lacks the unique organic qualities of true soil.

Neither regolith nor soil behaves as a consolidated rock does under the action of a single indenter, such as a sample scoop or a drill bit. From an engineering point of view, rock is the hard and durable earth materials that do not slake when soaked into water. From an excavation viewpoint, rocks are earth materials that cannot be excavated without blasting. These definition contrast with soil in that rocks have cohesion while regolith and soils are effectively cohesionless. These makes the measured properties of soils quite different from that of rock.

This study investigated the load-indentation (as in cause-effect) behavior of several granular materials in an effort to quantify the effect of grain size and shape, and material compaction, on the excavatability of regolith in a style that has not been conducted previously on this type of material.

## 1.2. OBJECTIVE AND SCOPE

The main purpose of this research is to evaluate the response of natural unconsolidated granular materials to indentation under different conditions of particle size, shape and compaction. In so doing, adds to the compendium of research ongoing in the area of granular physics and lunar exploration.

To achieve the set objective, Five (5) different kinds of dry granular materials were selected and sieved to obtain different grain size fractions for each material; filter sand (8 size fractions), crushed garnet (3 size fractions), shale cuttings (4 size fractions) and steel shots (two size fraction). The experiment was carried out on dry samples only. Loading behavior was evaluated through the force-penetration curves obtained during load indentation experiment. Peak load was measured for each material and maximum depth reached during indentation was recorded too.

The solid density and bulk density of the materials were determined prior to compaction and the bulk density was determined after compaction. The experiment was carried out on each material before compaction and after compaction.

# 2. LITERATURE REVIEW

## 2.1. GENERAL OVERVIEW

During the past decades, there has been much focus on understanding the behavior of granular materials. This is because of the fundamental nature and wide applicability of such knowledge. A large research effort, in both the statistical physics and the mechanics and civil engineering communities, is currently being devoted to granular materials, aiming in particular at a better understanding of the relationships between grain-level micromechanics (inter-granular contact laws) and macroscopic behaviors (global equilibrium conditions, constitutive relations).

There are many geotechnical engineering situations where high stresses may occur in granular materials such as pile end bearing, high earth or rock fill dams, or foundations of offshore gravity structures. These high stresses can lead to particle breakage and thus, for the consideration of wider range of geotechnical situations, it is of utmost importance to quantify and analyze accurately the mechanical properties such as hardness and elastic modulus at the particle level.

An understanding of the mechanical properties; load bearing capacity and compaction effect of fill materials for engineering fills is of great importance for geotechnical engineers.

Some researchers used indentation tests to design drills bits and mechanical excavators and predict machine performance by assessing drillability and boreability of rock samples. The Robbins Company, (a well-known manufacturer of tunnel-boring machine and raise drill) developed indentation testing as one of their principal tools for evaluating the boreability of rock samples

with respect to rock excavator design and performance prediction. The main approach was to predict forces, which would act on an actual cutter, by curve fitting of the force-penetration data obtained from indentation tests. Based on the predicted forces and performance, the machine was designed. The Earth Mechanics Institute of the Colorado School of Mines has also used indentation tests to define rock boreability and cuttability for many years (Copur et al. 2003).

Yagiz (2008)stated that ductile rocks yielded relatively flatter (smoother) force-penetration graphs after macro-scale indentation tests, Similar behavior was observed in the force-penetration graphs from linear cutting tests (Deketh et al. 1998). However, these definitions of brittleness were based on visual observations on force-penetration responses; and therefore, they could be considered as qualitative. The authors cited above considered that if the rock being loaded is comparatively more brittle, it yields relatively more fluctuated force-penetration due to chipping, which means less fluctuation for more ductile rocks. Shapes of force-penetration response depend also on the micro (texture, grain geometry, matrix material) and macro (strength, elasticity) properties of the material, geometry of indenter (sharpness, shape, dimension), and some environmental parameters (type of loading, temperature, confinement amount and material, data sampling rate). This research, considered some of these later- parameters (texture, grain geometry, and compaction) in determining the behavior of load indentation on very granular materials.

Compaction of powders and granular materials is an important process used to manufacture products including pharmaceuticals, ceramics, metals and

explosives. Most of the industrial products are processed, transported and stocked in a granular state. It is important to understand how compaction affects this material when pressure is applied to them and in what condition (coarse verses fine, rounded verses angular) will be suitable for best compaction and storage.

Similarly, due to granular nature of lunar regolith, research has been focusing on understanding the behavior and properties of both terrestrial and lunar regolith. This knowledge will help in lunar exploration and mining. As humanity's activities expand to the Moon, Mars, and other extra-terrestrial bodies, it will be necessary to use local resources rather than bringing everything from the Earth (IAI 2010). Understanding the mechanical behavior of granular materials will aid in both sample collection for early phase of exploration, design of robots for a more detailed sampling and exploration and for subsequent activities that will be carried out in the moon.

## 2.2. UNCONSOLIDATED GRANULAR MATERIALS

A granular material is any material composed of many individual solid particles, irrespective of the particle sizes. Handling of granular material is important in many industries. On weight basis, roughly one-half of commercial products and three-quarters of raw materials are granular solids (Nedderman 1992). When one adds the vast tonnages of wheat, sugar, iron ore, cement etc. that have to be stored and transported together with sand and gravel that are excavated and used as construction materials; the importance of granular materials becomes apparent.

Granular media are neither completely solid-like nor completely liquid-like in their behavior – they pack like solids but flow like liquids, they can like liquids take the shape of their containing vessels, but unlike liquids, they can also adopt a variety of shapes when they are free standing (A Mehta, 2007). Dense granular materials behave like rigid solids at rest, and yet are easily set into liquid-like, quasi-steady motion by gravity or moving boundaries. Dense granular materials exhibit many interesting collective phenomena, such as force chains, slow structural relaxation, and jamming. The properties of granular materials are also known to depend on the degree of order in the arrangement, size segregation effects, particle shape, horizontal compressive forces, and inter-particle friction (Ehlers et al., 2012).

In general, the behavior of a cohesionless granular material like sand is characterized in between fluid and solid, where the solid behavior results from the angle of internal friction and the confining pressure. Although the friction angle is an intrinsic material property, the confining pressure varies with the boundary conditions, thus defining different solid properties like plastic hardening, softening, and failure (Ehlers et al., 2012). Ehlers and Avci (2012) investigated the yield behavior of dense sand using drained monotonic and non-monotonic triaxial experiments. They found out specifically through triaxial-stress-path-dependent compression tests that the standard approach in the description of granular material such as sand is not correct in case of proceeding from a fixed failure surface. They found on various stress paths that the size of the failure surface was not constant. Instead, it changes depending on the current state of hydrostatic

pressure. This finding is in contrast to the standard opinion consisting of the fact that the failure surface remains constant, once it has been reached during an experiment or in situ.

Marston et al., (2012), found that for zero impact velocity, minimum penetration depth is smaller for wet materials than it is for dry materials. On the contrary, for high impact velocities the minimum penetration depth is higher for wet materials than it is for dry materials. They conducted their research with a unique spherical impactor with known constant geometry and density, under a broad range of liquid saturation of the granular material.

Vanel et al. (1999) showed that construction history affects the pressure distribution at the bottom of conical and wedge-shaped piles of sand formed on a rigid base. They observed a pressure dip at the center of a pile when they used a localized source (funnel with small outlet) but the dip disappeared when they used a more uniformly vertical filling via a raining procedure. From their work, it seems likely that the progressive formation of a sand pile by successive avalanche leads to the occurrence of a pressure dip.

The flow of granular systems defies rheological description, in part because shear tends to localize and conventional instruments cannot measure stress and strain. Therefore, an alternative approach is to measure the force on a moving intruder. For slow horizontal motion at a fixed depth, the force is rate independent and proportional to both the projected area of the intruder and its depth; this is due to friction acting at gravity-loaded contact (Albert et al., 2001). For an intruder

vertically penetrating a granular system by free fall, intruder roughness is not crucial to achieve greater depth (Brzinski et al 2014).

## 2.3. PHYSICS OF GRANULAR MATERIAL BEHAVIOR

**2.3.1. Shape and Size.** The shape and size distribution of the grains of a granular material affect the mechanics of the granular system. Much work in this field has been done in the past two decades, usually with idealized particles that are more regular and/or more uniform than natural regolith or soil grains. The mechanics of rough particles are much more difficult to model and predict than those of smooth particles of consistent size. Behringer et al. (2002), for example, is part of a large body of work on the effects of vertical shaking of granular materials.

Huang et al. (2013) investigated the compressibility and the energy-absorption densities of quartz sand. In testing uniformly graded materials, they found that fine sand exhibits a higher yield stress, and a smaller breakage extent than coarse material at the same stress level. Also uniformly graded sand exhibits lower yield stress and a bigger breakage extent than the well-graded material when the biggest grains are approximately the equal. In addition, they found that the compressibility and the energy-absorption capacity of well-graded sand are both smaller than those of uniformly graded material.

Similarly, Lu et al. (2013), discovered that dense smaller-size sand absorbs more energy than dense larger sand. In addition, the sand compressibility as a

function of sand grain particle sizes was gradually inversed with increasing sand particle sizes.

**2.3.2. Density and Compaction.** Another important property of granular materials is the density (mass per unit volume). There are two densities of interest when dealing with granular materials. First is the solid density ($\rho_s$), which is the density of the particles themselves. The bulk density ($\rho_b$) is the density of the mixture of solid plus interstitial gas. Provided the particles are not porous, the solid density can be measured by the technique of liquid displacement and the bulk density can be obtained from the ratio of the mass and volume of a sample.

Whilst the particles themselves may be compressible, the change in the solid density over the range of stresses normally encountered on planetary surfaces is usually small, so the solid density $\rho_s$, is effectively constant for a given material. On the other hand, the bulk density varies significantly with applied stress, mainly because of rearrangement of the particles. Unfortunately, on reduction of the stress, the material does not necessarily re-expand and as a result, the bulk density depends not only on the current stress in the material, but also on its stress history. Therefore, for a given material, solid density $\rho_s$ may be treated as a constant, but the value of the bulk density $\rho_b$ depends on the present and past treatment of the material.

Sand is fragile in the sense that it can barely support the weight of an object (a ball) without the object digging into it on slight tap. Sand also is strong in the sense that if you drop the object from a height, the sand can stop it quickly forming a shallow crater in the process. Uehara et al. (2003), in an experiment to describe

the stopping force of a ball when released from a height into a sand pack of sand, Uehara Ambrose Ojha and Durian showed that the friction between the ball and contact surface has no effect on the stopping force. This means that ball roughness has no effect on the stopping force. They found that the grain size did affect the stopping force. Explaining that as the ball crashes into the medium, it jams together the grains underneath. The normal force between these grains thus becomes much greater than the hydrostatic pressure. As the ball moves, the grain contacts slide so that each dissipates a total amount of energy given by the normal force times grain size. New contacts are formed as the old ones break. This loading and breaking of force chains gives rise to the dissipation force that ultimately stops the ball. Another possibility for the explanation of the stopping force is that dissipation is due to sliding friction between force chains and the surrounding unloaded grains. These suggestive conclusions are backbone for this present research. Rather than measuring stopping force, we are measuring forces necessary to overcome the resistance forces that tend to stop an object (indenter) from continuously penetrating these granular materials. The paper cited above considered only the ball roughness, drop height, grain density and grain size, only grain size had an effect. However, in this work, other factors will be considered alongside grain size. These factors include grain shape, compaction, and depth of penetration.

Bragov et al. (2007), in their work; found that the compressibility of sand decreases slightly with reduction of particle size for all modes of loading but overall, the response is non-linear. The loading deformation diagrams (Figure 2.1) have two main regions, connected to two mechanisms of deformation. In the first

mechanism the particle velocity within the sample is small (approximately 500 m/s) and the sand is very porous. In the first stage, the basic mechanism is the movement of sand particles to fill the pores. With the removal of pores, the second mechanism becomes more dominant. The sample is then at higher density so it transmits more stress. The particles also begin to interact intensively with each other. This is accompanied by an increase of friction at the contact points, elastic deformation and their partial destruction. Recovered material shows this fracture of particles during loading.

## 2.4. LOAD INDENTATION TEST (PUNCH TEST)

The punch test was developed in the late 1960s to provide a direct laboratory measurement of the normal cutter loads that could be expected during mechanical excavation with either button or disc cutters. Since its inception, numerous manufacturers of underground excavation equipment, including the Dresser Company, Hughes Tools, Jarva, Wirth, Calweld, Smith International, Ingersoll-Rand and the Robbins Company, have used the test. Most of the early developments of the test for estimating penetration rates were done at the Raise Drill Division of Ingersoll Rand (Seattle, Wash., U.S.A.) and the Robbins Company (Kent, Wash., U.S.A.). Because each manufacturer interpreted the test results differently, no attempt has been made to standardize the test and no standard method of interpreting the test results has been developed. The punch test is a nonstandard laboratory test that was originally designed to provide a direct method for estimating the normal loads on button and disc cutters (Figure 2.2.) during

mechanical excavation of rock. Dollinger et al. (1998) evaluated the status of the punch test as it relates to raised boring machine (RBM) and Tunnel boring machine (TBM) performance. The earliest method of analysis of punch test results involved the drawing of a best fit straight-line on the force-penetration graph through the origin (Figure 2.2) and then directly estimating from this line the expected cutter loads and penetrations during excavation using the slope of the line measured in lb./in (called the “Penetration Index”).

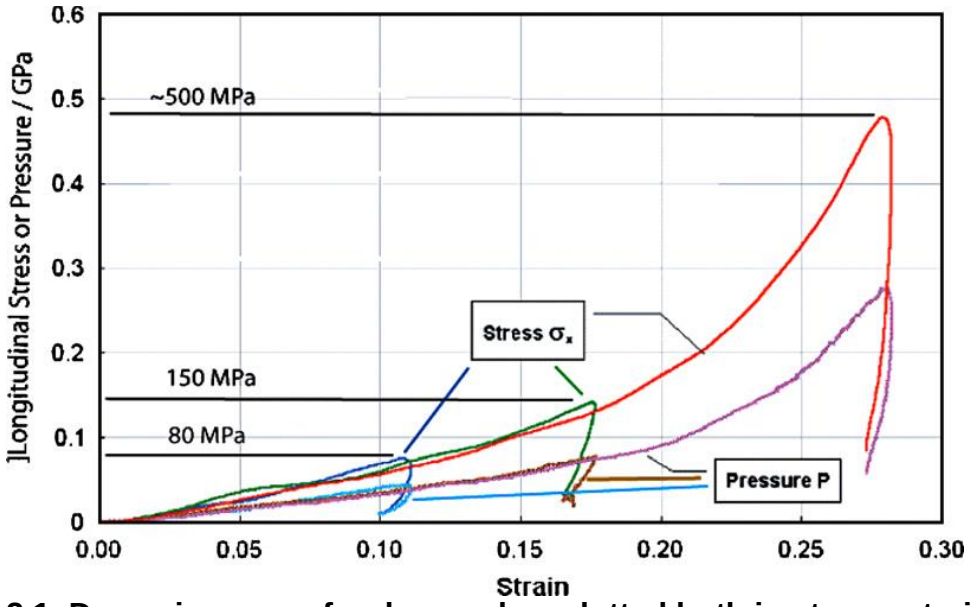


**2.1. Dynamic curves for dry sand as plotted both in stress–strain and pressure–strain axes. The characteristic for experiments with loading stresses ($\sigma_x$) of 80, 150, and 500MPa are shown. P is the applied pressure. The curves lie on the same loading path. After reaching a maximum compressive strain, the curves drop in stress and strain during unloading. (Bragov et al. (2007)).**

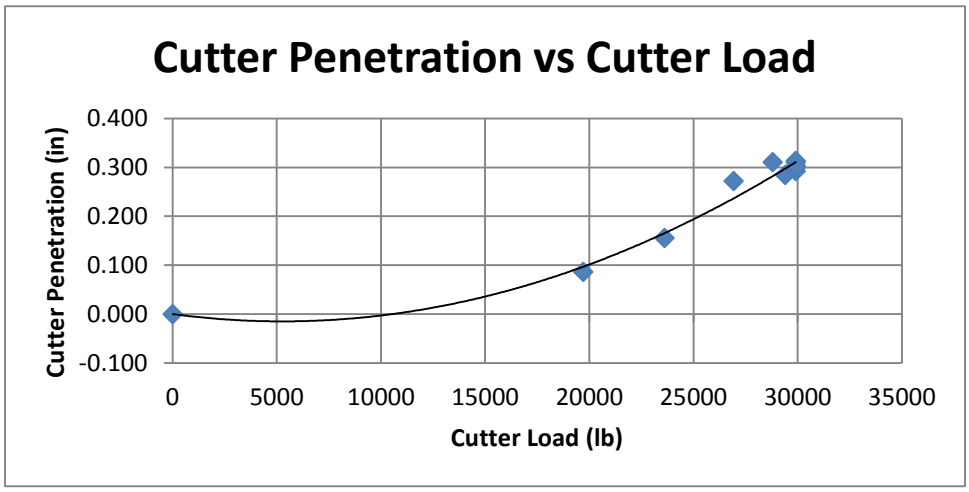


**Figure 2.2. Cutter normal load vs. cutter penetration for Chicago dolomite. Dollinger et al. (1998).**

This method assumed that the relationship between the cutter normal load and cutter penetration is linear and that the penetration index determined by the punch test is equivalent to the penetration index (cutter load divided by cutter penetration) that is measured in the field during boring.

Early application of this method to predicting RBM and TBM performance, in fact, resulted in reasonably good estimates of penetration rates for both low-strength rock conditions and low cutter path loads. In higher strength rock conditions, however, where high cutter path loads are required, the penetration index method tended to underestimate the actual penetration rates.

One of the main reasons why the penetration index method was less successful in high-strength rock conditions is that the true relationship between the cutter load and cutter penetration in such rocks is non-linear, with a critical cutter

load that must be exceeded before increasing cutter load produces significant changes in cutter penetration. This critical load correlates with the appearance of large chips in the muck produced during boring and is the cutter load at which use of the punch test for estimating TBM performance efficient boring begins. Because of this nonlinear relationship, the penetration index method tends to overestimate TBM performance at low cutter loads and to underestimate it at high cutter loads in hard rocks.

## 2.5. MATERIAL CHARACTERIZATION USING THE PUNCH TEST

The punch test has also been used to evaluate certain physical characteristics of rocks (consolidated and unconsolidated) which have been found to affect mechanical excavation rates, and to check penetration rate estimates made from other physical properties of the rock. Included among the physical characteristics of rock that can be evaluated using the punch test are its brittleness (i.e. the ease at which it forms chips during indentation), the strength or weakness of bedding and cleavage planes, and the effect of porosity. This is done by comparing and examining the shape of the force-penetration curves, the maximum forces that occur during a test, the area under the test curves (i.e. work done during a test) and by visually observing how the sample fails during a test (for consolidated rocks) and how the intender penetrates the sample in the case of unconsolidated rocks. Highly brittle materials, for example, show large force drops due to the formation of large chips, while rocks that are more ductile show only minor force drops and, in some cases, no force drops. Due to the force drops, less

work is done during a test (i.e. the area under the test curve) on a brittle rock than on a non-brittle rock if the maximum cutter loads are the same. This agrees with the observation that brittle rocks tend to require less energy to bore than non-brittle rocks of comparable strength. The punch test in an expanded form has also been demonstrated to be a useful tool for studying various machine parameters, such as the effect of cutter tip width and cutter spacing on the forces required to excavate rock (Dollinger et al., 1998).

Saffet Yagiz (2008), introduce direct method to measure rock brittleness as an index via punch penetration test, and also investigated the relationship between intact rock properties (uniaxial compressive strength, Brazilian tensile strength, and density of rock) and the brittleness measured from the test. The force–penetration graph was obtained from the punch penetration test as qualitative indicator of the brittleness. It should be noted that failure of the rock under the indenter is related to initiation of chipping and subsequently brittleness feature of rock. It is known that rock must absorb enough energy before chipping and broken; and then, it suddenly loss its strength with little or no plastic deformation under the indenter. This behavior of rock, also known as brittleness, could be monitored from the beginning of the test to the end by observing the force–penetration data chart. On obtained chart, high brittle rock demonstrates fluctuated force–penetration relationship due to the both large force drops and large chips; on the other hand, moderate brittle rock shows minor force drop with small chips. As the rock has ductile or low brittle features, then there is no force drop and chipping on rock sample. This could be seen from the graph with less or no fluctuation with lower

force as demonstrated in Figure 2.3. Afterward, the brittleness ($B_4$) of rock was quantified by using the slope of force–penetration graph. The slope was obtained by drawing line from origin of the graph to the maximum applied force that rock absorbs until end of the test. So, the ratio of maximum applied force (KN) on specimen to the corresponding penetration (mm) was named as rock brittleness index (BIm) in kN/mm. The brittleness index (BIm), were introduced from the punch penetration test.

As a result, that of conducted laboratory tests, the rock brittleness index was developed and consequently, the classification of rock brittleness was suggested bases on density, strength and type of rocks together with rock brittleness and visual inspection of force–penetration graph obtained from the punch penetration test.

In instrumented indentation testing, especially in the nano and micro scales, low scale artifacts such as sensor sensitivity, surface roughness, imperfect indenter tip geometry and material heterogeneity can create significant deviations of the measured indentation load-depth curve from the ideal curve corresponding to the bulk material.

Brammer et al. (2012), assessed the influence of an offset of the measured penetration depth on the identified bulk mechanical parameter values when using a reverse analysis model based on spherical indentation. It is shown through numerical examples that significant errors arise if the identification procedure is based on the load values recorded at penetration depth values.

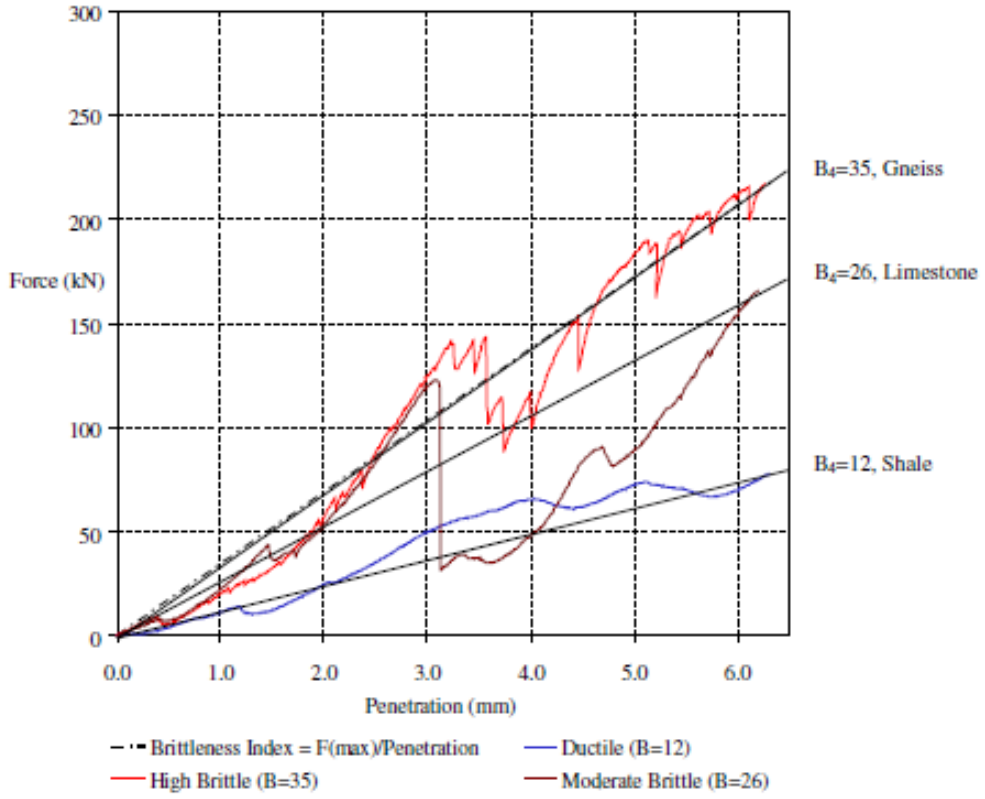


**Figure 2.3. Visual and quantitative brittleness concept based on measured rock brittleness (Yagiz, 2008).**

Therefore, in other to overcome this effect, an alternative exploitation of the reverse analysis model is proposed, which is based on the use of the slope of the indentation curve at indentation load values. In addition, it is proposed to neglect the data at low load values in order to avoid the effect of low scale artifacts on the shape of the indentation curve at low load values. The proposed approach is applied to the numerical examples, and then an experimental case of a blunted indenter tip is presented. In all cases, the proposed approach provides accurate identification results, which are not affected by low scale artifacts. The proposed

approach can be significantly useful when analyzing indentation curves obtained in the nano and micro scales, as well as indentation curves obtained in industrial conditions.

# 3. RESEARCH METHODOLOGY

## 3.1. INTRODUCTION

The experimental program consisted of two major parts: Physical property tests to understand fully the properties of the material being tested, and indentation tests to determine force-penetration behavior of the material.

**3.1.1. Material Types**. To understand largely how compaction, size and shape affects dry unconsolidated granular materials, several granular materials were selected: Filter sand, crushed garnet, shale cuttings. These materials were chosen from readily available granular materials often used for research at the Space Resources Laboratory of the Rock Mechanics and Explosives research Centre, so as to represent a wide range of granular material behavior from very angular to fairly rounded and from very fine to coarse materials.

**3.1.2. Property Tests**. The physical properties measured in these tests include solid density, porosity, specific gravity, bulk density, aspect ratio, roundness and circularity.

**3.1.3. Indentation Tests (Punch Tests).**The punch test was developed in the late 1960s to provide a direct laboratory measurement of the normal cutter loads that could be expected during mechanical excavation with either button or disc cutters. Since its inception, numerous manufacturers of underground excavation equipment, including the Dresser Company, Hughes Tools, Jarva, Wirth, Calweld, Smith International, Ingersoll-Rand and the Robbins Company, have used the test. Most of the early development of the test for estimating penetration rates was done at the Raise Drill Division of Ingersoll Rand (Seattle,

Wash., U.S.A.) and the Robbins Company (Kent, Wash., U.S.A.). Because each manufacturer interprets the test results differently, no standard method of performing or interpreting the test results has been developed (Dollinger et al., 1998).

The primary purpose of conducting load-indentation tests is to obtain a measure of the energy required fragment the rock. This is reflected partly by the specific penetration which is the load required to push the indenter a unit distance into the rock, and more directly by the specific energy , which is the energy required to fragment a unit volume of the rock.

## 3.2. MATERIAL TYPES

The major emphasis of this study is to understand the relationship that exists between the properties of granular materials to their specific energy and specific penetration during single tool indentation. Therefore, materials of varying shapes, sizes and densities were chosen for this research.

**3.2.1. Filter Sand (FS**). Figure 3.1 shows the filter sand before size separation. It is sub-rounded sand. The sand is sieved into eight different size fractions with each fraction having their solid density and bulk density, as well as their shape and area determined. The filter sand is composed mainly of the potassium feldspar with little quartz blend.


**Figure 3.1. Filter sand before sieving.**

**3.2.2. Crushed Garnet (CG).** Figure 3.2 shows the crushed garnet before sieving. This is a material obtained from crushing garnet into fine particles. The crushed particles are angular and locked tightly together when packed. They are sieved into three different size fractions with each fraction having their bulk and solid density as well as their shape and area determined.

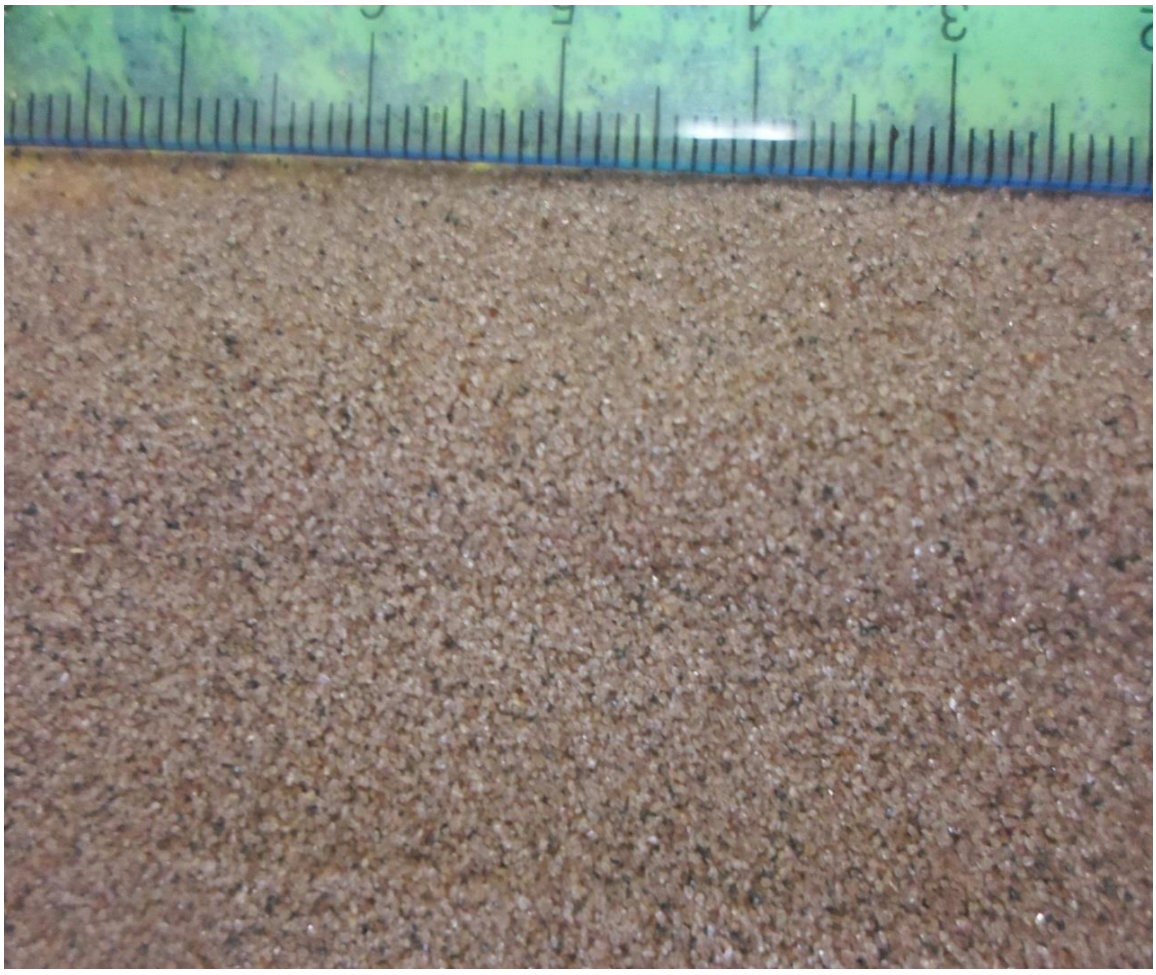

**Figure 3.2. Crushed garnet before sieving.**

**3.2.3. Shale Cuttings (SC).** Figure 3.3 shows the shale cuttings before it is being sieved. This material is from cuttings from shale during drilling. The materials are sub-angular. The material is sieved into four different size fractions, with each fraction having their bulk and solid density as well as their shape and area determined.

**Figure 3.3. Shale cuttings before sieving.**

**3.2.4. Steel spheres (SS).** These are almost well rounded spheres made of steel (Figure 3.4). The material is sieved into two different size fractions, with each fraction having their bulk and solid density as well as their shape and area determined.

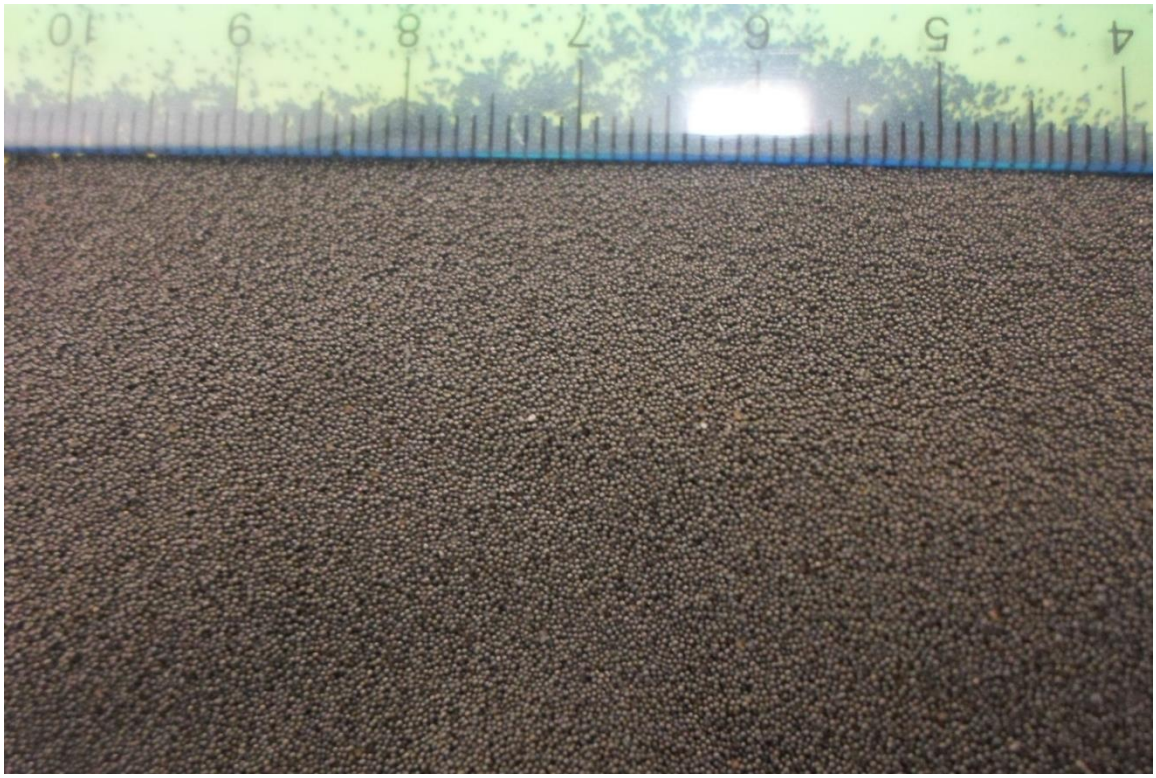

**Figure 3.4. Steel spheres before sieving.**

## 3.3. MATERIAL PROPERTY MEASUREMENT

**3.3.1. Solid Density.** This is the mass of oven-dry samples per unit volume of the sample particles, including the volume of permeable and impermeable pores within particles, but not including the voids between the particles. This test was carried out according to the ASTM C128-12 (Standard Test Method for Density, Relative Density (Specific Gravity), and Absorption of Fine Aggregate). The average density), the relative density and the absorption of the samples were

determined following this standard. The measurements determined are expressed as oven dried.

Procedure: 500g±10g of sample was immersed in water for 24 hours to fill the pores. It is then removed from the water, the water is dried from the surface of the particles, and the mass determined. Afterward, a portion of the sample (Saturated surface-dry) is placed in a graduated cylinder and the volume is determined by the gravimetric method. Finally, the sample is oven-dried at $110^0$C to constant mass and the mass determined. Using the mass values obtained, the Density, Relative Density, and Absorption were calculated thus:

$$\text{Relative Density (Specific Gravity) SG} = \frac{A}{B+S-C} \quad 3.1$$

$$\text{Density } \rho \text{ g/cm}^3 = \frac{0.9975A}{B+S-C} \quad 3.2$$

$$\%\text{Absorption} = 100\left(\frac{S-A}{A}\right) \quad 3.3$$

(Absorption is increase in mass of the sample particles due to water penetrating into the pores of the particle, during a prescribed period of time but not including water adhering to the outside surface of the particles, expressed as a percentage dry mass)

Where A = Mass of oven dried sample, g.

B = Mass of cylinder filled with water to calibration mark, g.

C= Mass of cylinder filled with sample and water to calibration mark, g.

S= Mass of saturated surface-dry sample, g.

0.9975 = Density of water

**3.3.2. Bulk Density Calculation.** This is the mass per unit volume of the material obtained by measuring the mass and the volume of the material. This is done before and after compaction just prior to indentation.

$$\text{Bulk density } \rho b = \frac{mass}{volume} \quad 3.4$$

**3.3.3. Material Shape Analysis**. The material was first sieved into different size fraction using the Shake and Sieve (SS) (Figure 3.5). Then each size fraction was analyzed using the software IMAGEJ. The image of the material was taken using a 4.5-22.5mm zoom camera and microscopic camera was used for very small sized grains (Figure 3.6). The images were then analyzed with the IMAGEJ software (Figure 3.7) to obtain;

- **Grain Roundness**. This is defined mathematically in equation 3.8. It is the inverse of the aspect ratio.

  $$Roundness = \frac{4*area}{\pi*(major\_axis)^2} \quad 3.5$$

- **Aspect Ratio**. This is the ratio of the major axis to the minor axis. It is mathematically described in equation 3.9.

  $$Aspect\ ratio = \frac{major\_axis}{minor\_axis} \quad 3.6$$

- **Circularity**: This is defined mathematically in equation 3.10. A value of 1.0 indicates a perfect circle. As values approach 0.0, it indicates an increasingly elongated shape.

  $$Circularity = \frac{4\pi*area}{(perimeter)^2} \quad 3.7$$


**Figure 3.5. Sieve-shake (SS), used for sieving the materials into their different size fraction (EIE instrument PVT. LTD).**

- **Grain Roundness**. This is defined mathematically in equation 3.8. It is the inverse of the aspect ratio.

$$Roundness = \frac{4*area}{\pi*(major\_axis)^2} \quad 3.5$$

- **Aspect Ratio**. This is the ratio of the major axis to the minor axis. It is mathematically described in equation 3.9.

$$Aspect\ ratio = \frac{major\_axis}{minor\_axis} \quad 3.6$$

- **Circularity**: This is defined mathematically in equation 3.10. A value of 1.0 indicates a perfect circle. As values approach 0.0, it indicates an increasingly elongated shape.

$$Circularity = \frac{4\pi * area}{(perimeter)^2} \quad 3.7$$

## 3.4. INDENTATION (PUNCH PENETRATION) TESTS

**3.4.1. Load Indentation Set-Up.** The indentation apparatus consist of the actuator, an LVDT, a load cell, a data acquisition box, the power pack, and a computer that reads out the output. The actuator provides the thrust at 200mm/sec. The LVDT (linear variable displacement transducer) measures the depth of penetration and the load cell measures the force of indentation (Figure 3.8). The computer outputs the result of the experiment (load cell and LVDT reading). The computer runs on a LABVIEW software programmed to take the measured load and displacement every 0.0002 second (data rate of 5 KHz). All measurements were recorded in volts and were converted respective using the calibration data provided by the FUTEK (load cell designer) for the load cell and the calibration package of LABVIEW software for the LVDT.

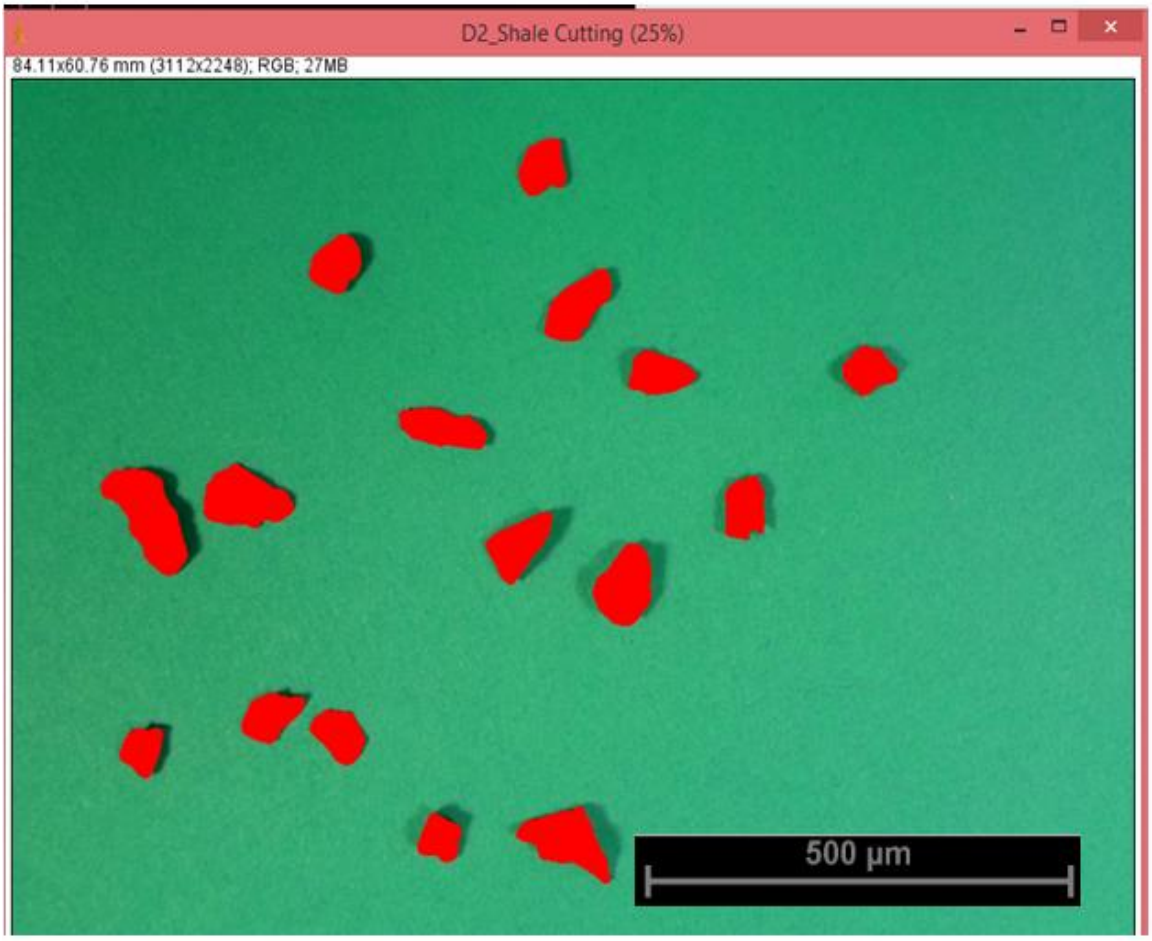


**Figure 3.6. Grain shape after adjusting the threshold on IMAJEJ software.**

**3.4.2. Indenter.** As shown in Figure 3.9, the indenter used was 0.75in (1.905cm) in diameter and hemispherical in shape (round-top insert). It is 1.24inches (3.15cm) long and is made entirely of steel.


**Figure 3.7. Grain image output after analysis.**

**3.4.3. Sample Preparation.** The samples were sieved into different sizes and poured into separate cylindrical sample containers 6in (15.24cm) in diameter and 2.35in to 3.35in (7cm to8.5cm) deep. The containers are made of PVC pipe of wall thickness approximately 0.3in (0.75cm).

The sample container holds (Figure 3.10) the sample before and after indentation. The sample is poured into the container via a funnel and is manually distributed as evenly as possible to avoid non-homogeneity. For the compacted

samples, the container with the material was placed on a vibrator and vibrated at level two for 3-4 minutes.

**3.4.4. Running a Test.** Figure 3.11 shows a picture of the Load indentation. To start a test, the first thing to do was to turn on the power system. All instruments connected to the power (actuator, computer and control box) are checked to ensure they are working properly and at appropriate voltages. The computer was turned on, and a preliminary test was run to ensure the load cell and LVDT (Linear Variable displacement Transducer) are working properly. The prepared sample was placed underneath the frame as shown in Figure 3.12. The material was indented by pressing the “on” button on the actuator control switch and releasing it when the actuator hit the mechanical stop. The LABVIEW program run on Dell computer records the load cell and LVDT reading in Volts.

**3.4.5. Data Collection and Management.** All test data were handled and analyzed using Microsoft Excel spreadsheet (LABVIEW supports direct export of data to excel). The load cell data were reduced by calculating an 83 point running average. The LVDT data were averaged over 10 points. The averaging was to reduce the effect of noise on the data trend. The averaged load cell and LVDT readings in volts were converted to newtons and centimeters, respectively. When the test data was plotted, and compared to the air data, there was an obvious contrast on where the air reading stopped and sample indentation reading started as seen in Figure 3.12.

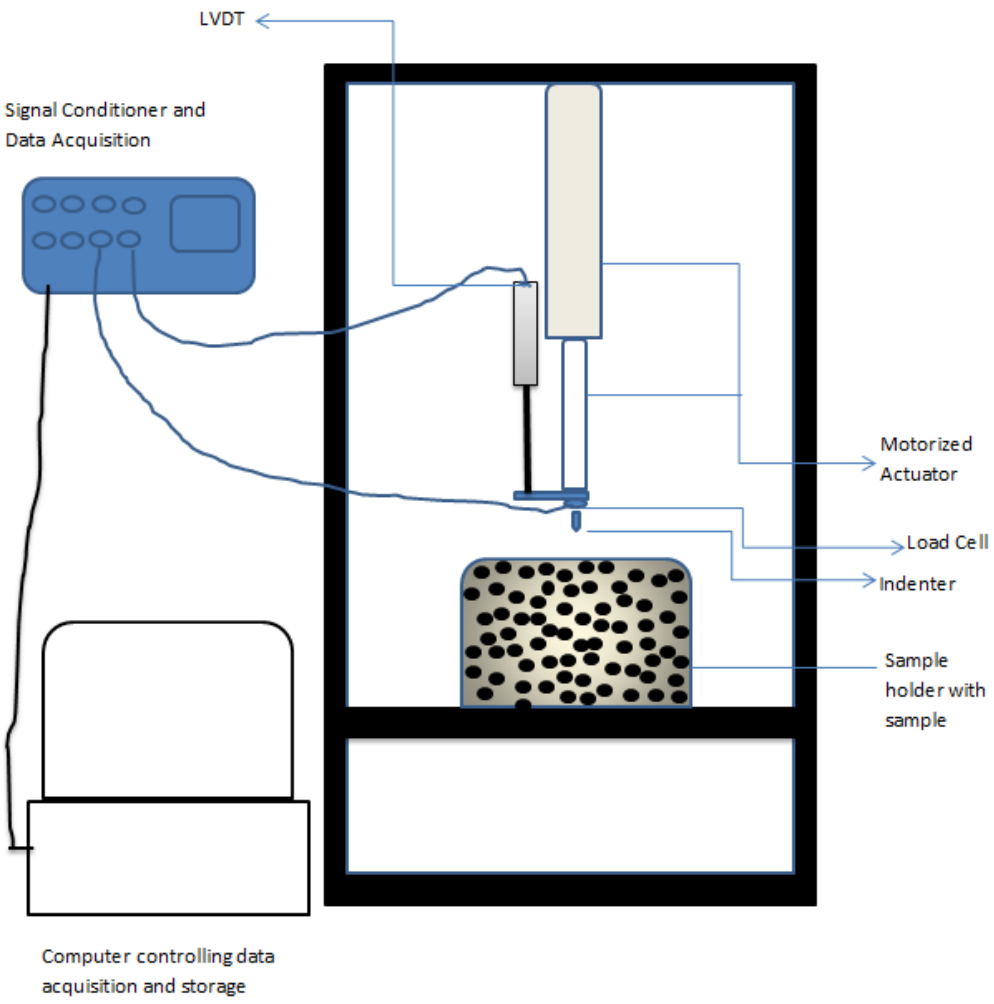


**Figure 3.8. Schematic diagram of the load indentation set-up.**

When the test data was plotted, and compared to the air data, there was an obvious contrast on where the air reading stopped and sample indentation reading started as seen in Figure 3.12.


**Figure 3.9. The 0.75in diameter indenter used in the indentation exercise.**

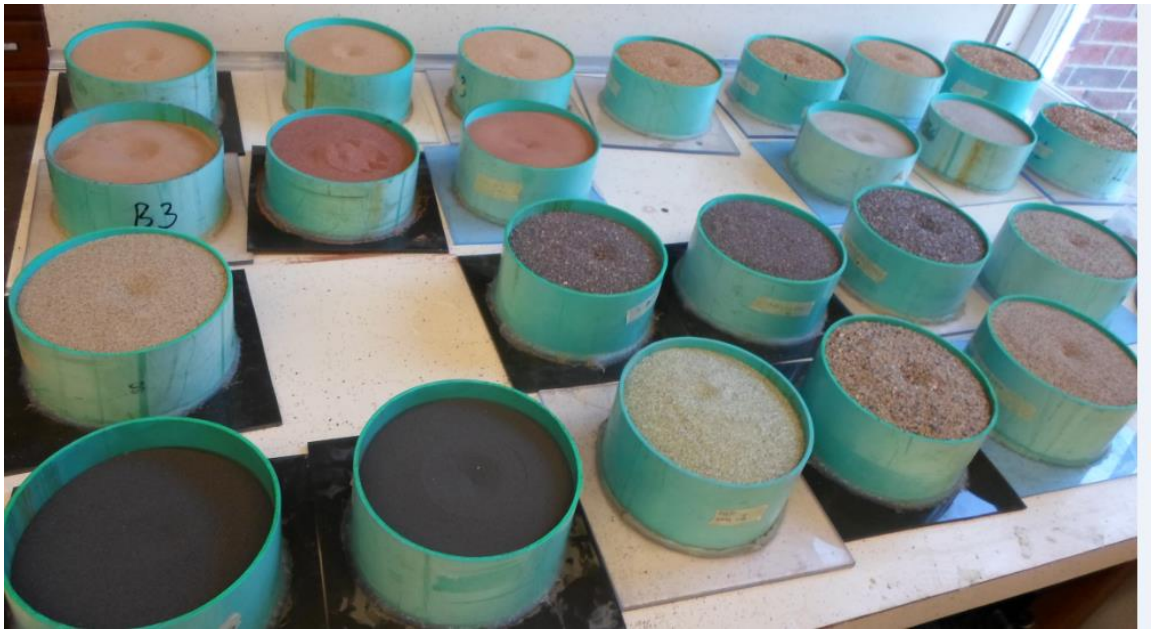


**Figure 3.10. Material in their sample containers.**

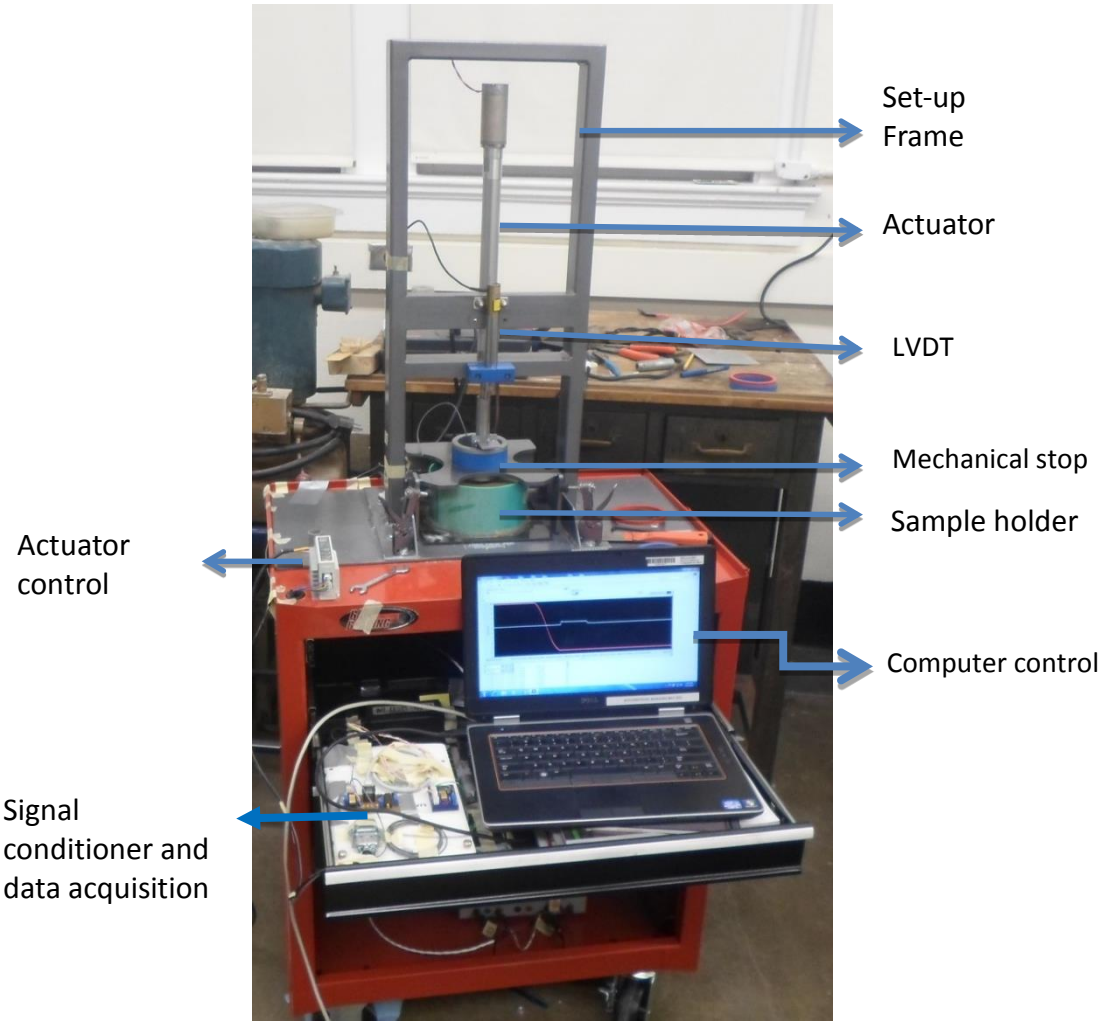


**Figure 3.11. Load indentation apparatus after running a test.**

After determining the contact point, the displacement and load readings were zeroed at this point. The maximum load was then picked at this point and maximum displacement was picked. The maximum load does not always correspond to the maximum displacement.

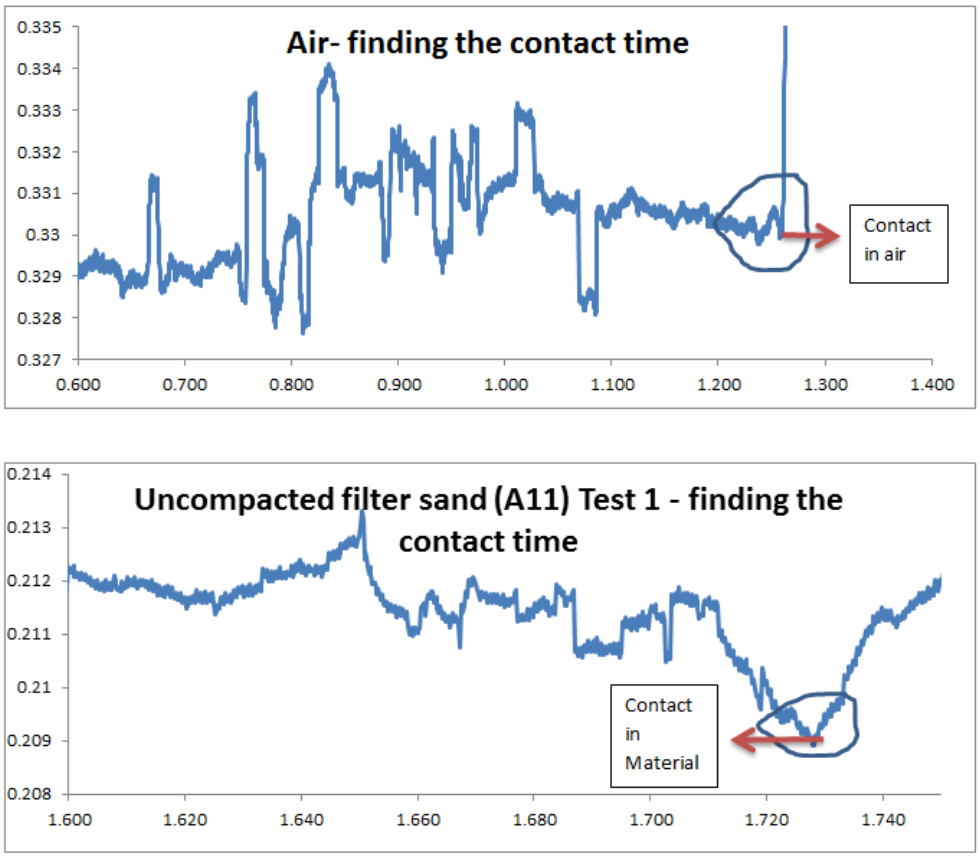


**Figure 3.12. Load-time graph showing how to pick the contact point.**

# 4. EXPERIMENTAL RESULT AND DISCUSSION

This section presents the results of the experiment and discusses the implication of the results to the set objectives.

## 4.1. DERIVED PARAMETERS

**4.1.1. Specific Penetration (SP).** The specific penetration is the force required to indent the material a given depth. For this research, the maximum force and maximum penetration depth were used to compute the specific penetration. Although the slope of the force-penetration curve can be used to estimate the specific penetration, for simplicity, the maximum force and depth at which it occurred were used.

Specific Penetration (SP):

$$SP = \frac{Force(\max)}{Depth(\max)}\left(\frac{N}{cm}\right) \quad 4.1$$

**4.1.2. Specific Energy (SE).** This is the energy required to displace a unit volume of the material. It is the work done per unit volume. The work done is measured by the area under the force-penetration curve and was calculated by discrete integration within the Excel data file after zeroing and truncation of pre- and post-indentation data:

$$work = \int_0^h f(x)dx \quad 4.2$$

$h = depth\ caused\ by\ any\ force\ f$

$$SE = \frac{Work}{volume}\left(\frac{N}{cm2}\right) \quad 4.3$$

## 4.2. BASIC FORCE-PENETRATION BEHAVIOR

The discussion on the forces with illustrations as well as the effect of the different variables will be discussed in later sections. The summary for the load indentation tests is presented in Table 4.1.

**Table 4.1. Load indentation data summary.**

| | Uncompacted | | | | Compacted | | |
|---|---|---|---|---|---|---|---|
| Sample ID | Max Load | Max Indent | Work Done | | Max Load | Max Indent | Work Done |
| | N | cm | N-cm | | N | cm | N-cm |
| FS-1 | 5.69 | 2.50 | 8.13 | | 113.12 | 1.51 | 69.05 |
| | 3.47 | 2.54 | 4.20 | | 431.82 | 4.15 | 19.80 |
| | 5.00 | 2.54 | 3.69 | | 154.84 | 4.30 | 174.80 |
| | 2.99 | 2.10 | 2.22 | | 108.68 | 4.13 | 126.28 |
| | | | | | 300.04 | 3.02 | 494.34 |
| FS-2 | 23.54 | 2.88 | 28.91 | | 77.85 | 2.52 | 70.65 |
| | 24.40 | 2.81 | 17.54 | | 13.27 | 2.54 | 28.55 |
| | 23.07 | 2.85 | 24.14 | | 199.14 | 3.59 | 280.64 |
| | 19.44 | 2.88 | 21.52 | | 322.33 | 2.63 | 392.17 |
| | 21.05 | 2.90 | 18.11 | | 214.53 | 3.18 | 290.54 |
| FS-3 | 16.66 | 2.89 | 7.86 | | 199.40 | 3.87 | 313.65 |
| | 15.00 | 2.87 | 10.82 | | 131.16 | 3.00 | 143.45 |
| | 18.29 | 2.51 | 10.04 | | 77.95 | 3.01 | 82.86 |
| | | | | | 153.76 | 3.06 | 200.98 |
| | | | | | | | |

**Table 4.1. Load indentation data summary (contd.)**

| | Uncompacted | | | | Compacted | | |
|---|---|---|---|---|---|---|---|
| Sample ID | Max Load | Max Indent | Work Done | | Max Load | Max Indent | Work Done |
| | N | cm | N-cm | | N | cm | N-cm |
| FS-4 | 11.86 | 2.21 | 8.29 | | 116.16 | 3.39 | 107.40 |
| | 19.72 | 2.28 | 15.01 | | 264.44 | 3.20 | 275.95 |
| | 5.09 | 2.01 | 3.02 | | 28.19 | 3.43 | 34.93 |
| | 13.75 | 2.26 | 6.05 | | 185.40 | 3.04 | 154.60 |
| | 3.38 | 2.30 | 4.00 | | 259.69 | 3.38 | 243.03 |
| FS-5 | 9.03 | 2.73 | 8.48 | | 252.67 | 2.86 | 344.70 |
| | 4.97 | 2.49 | 5.10 | | 251.30 | 2.85 | 343.25 |
| | 6.43 | 2.70 | 9.89 | | 15.01 | 2.77 | 17.63 |
| | 7.37 | 2.76 | 6.57 | | 252.40 | 2.88 | 345.38 |
| | 13.28 | 2.23 | 9.76 | | 218.60 | 2.38 | 242.36 |
| FS-6 | 19.77 | 2.59 | 13.69 | | 138.33 | 2.45 | 126.62 |
| | 15.49 | 2.51 | 11.51 | | 178.17 | 2.93 | 153.10 |
| | 9.45 | 2.50 | 5.43 | | 249.33 | 2.74 | 303.57 |
| | 12.39 | 2.59 | 9.03 | | 109.66 | 2.80 | 113.18 |
| | 16.69 | 2.49 | 9.17 | | 130.20 | 2.79 | 135.62 |
| FS-7 | 32.58 | 2.95 | 28.93 | | 218.02 | 2.98 | 229.13 |
| | 44.18 | 3.27 | 53.35 | | 459.00 | 2.86 | 571.08 |
| | 34.52 | 3.02 | 28.04 | | 68.71 | 3.00 | 67.34 |
| | 25.95 | 2.96 | 26.04 | | 184.79 | 2.90 | 120.41 |
| | 20.63 | 2.66 | 15.63 | | 439.44 | 3.23 | 846.80 |
| FS-8 | 31.53 | 3.06 | 56.74 | | 248.90 | 2.80 | 246.45 |
| | 41.35 | 3.51 | 80.54 | | 189.66 | 2.81 | 171.10 |
| | 34.48 | 1.97 | 26.59 | | 354.60 | 2.93 | 229.59 |
| | 47.64 | 2.64 | 67.74 | | 115.67 | 2.57 | 120.59 |
| | 38.35 | 3.06 | 38.95 | | 154.99 | 2.39 | 167.45 |
| CG-1 | 8.61 | 2.85 | 10.02 | | 95.84 | 3.95 | 164.25 |
| | 14.58 | 3.77 | 9.84 | | 124.03 | 4.13 | 126.53 |
| | 15.30 | 3.92 | 3.07 | | 108.42 | 4.05 | 227.60 |
| | 14.41 | 3.14 | 6.32 | | 61.82 | 3.22 | 97.64 |
| | 11.23 | 2.13 | 38.54 | | 33.63 | 2.82 | 40.82 |
| CG-2 | 81.33 | 3.66 | 116.54 | | 109.10 | 3.93 | 139.69 |
| | 29.21 | 3.40 | 46.40 | | 166.12 | 3.73 | 190.80 |
| | 48.49 | 2.83 | 50.37 | | 219.65 | 3.83 | 493.01 |
| | 53.47 | 2.48 | 62.53 | | 152.16 | 3.88 | 129.64 |
| | 75.81 | 2.99 | 103.77 | | 417.58 | 3.61 | 442.81 |

**Table 4.1. Load indentation data summary (contd.)**

| | Uncompacted | | | | Compacted | | |
|---|---|---|---|---|---|---|---|
| Sample ID | Max Load | Max Indent | Work Done | | Max Load | Max Indent | Work Done |
| | N | cm | N-cm | | N | cm | N-cm |
| CG-3 | 26.37 | 3.09 | 17.81 | | 97.58 | 2.54 | 64.35 |
| | 9.33 | 2.57 | 12.11 | | 21.57 | 2.47 | 16.28 |
| | 14.46 | 1.88 | 14.83 | | 25.68 | 2.42 | 18.34 |
| | 8.84 | 1.79 | 11.31 | | 122.22 | 2.60 | 156.37 |
| | 14.69 | 1.85 | 12.29 | | 25.32 | 2.30 | 13.98 |
| SC-1 | 12.54 | 3.14 | 8.40 | | 342.85 | 2.68 | 519.16 |
| | 10.15 | 3.98 | 5.63 | | 85.12 | 2.36 | 80.74 |
| | 14.73 | 2.98 | 10.98 | | 284.69 | 1.89 | 206.20 |
| | 10.50 | 2.96 | 6.52 | | 172.95 | 2.68 | 157.50 |
| | 10.39 | 2.13 | 3.64 | | | | |
| SC-2 | 30.46 | 2.98 | 20.90 | | 244.26 | 2.69 | 322.52 |
| | 40.55 | 3.28 | 7.62 | | 15.57 | 3.70 | 28.31 |
| | 37.75 | 8.70 | 24.31 | | 17.57 | 3.62 | 18.44 |
| | 18.29 | 9.28 | 13.52 | | 12.58 | 3.17 | 18.82 |
| | 26.25 | 9.14 | 21.93 | | | | |
| SC-3 | 26.92 | 2.77 | 36.29 | | 679.75 | 3.36 | 1243.17 |
| | 44.01 | 3.21 | 69.85 | | 248.00 | 3.31 | 264.62 |
| | 26.44 | 3.14 | 33.27 | | 154.12 | 3.33 | 191.60 |
| | 36.36 | 3.20 | 43.77 | | 251.54 | 2.89 | 287.60 |
| | 31.84 | 2.72 | 38.80 | | 486.93 | 2.83 | 596.21 |
| SC-4 | 90.74 | 3.67 | 120.30 | | 220.81 | 3.19 | 235.94 |
| | 74.19 | 3.89 | 152.76 | | 124.30 | 2.38 | 113.53 |
| | 82.57 | 3.66 | 130.16 | | 294.07 | 2.98 | 271.52 |
| | 71.84 | 2.60 | 86.25 | | 159.20 | 3.12 | 220.30 |
| | 108.28 | 2.93 | 157.39 | | 219.59 | 2.78 | 254.64 |
| | | | | | | | |
| FS = Filter Sand | | | CG = Crushed Garnet | | | SC = Shale Cutting | |

The force measured from the indentation test is the normal force with which the indenter penetrates the sample. In discussing the forces, first, the general force-displacement curve is discussed, followed by the effect of the characteristics of the grains on the forces.

For the uncompacted grains, there is a significantly pattern in their force-penetration curves (Figures 4.1, 4.2, 4.3). First, the force builds up sharply (stick) and drops (slip) marking the first failure (Figure 4.1). After dropping, it picks up again increasing more than the first peak, and then it drops and this trend continues. This behavior is also observed in brittle rocks (Yagiz 2009). In brittle rocks, it is attributed to chip formation. However, for uncemented granular materials, where chip formation is not observed, the force drops can be linked to the materials building up resistance through gravity-loaded frictional grain-grain contacts, which gives rise to changes in normal force (Brzinkski et al. 2013), and how the indenter overcomes this resistance. This frictional resistance is due to the gravity and physical properties of the grain where gravity leads to compaction and the grain properties account for the level of compaction reached prior to the end of indentation.

This can be hypothesized as follows. Primarily, the indenter penetrates the sample by displacing the grains (no crushing). If the grains are too compact and cannot be displaced, then crushing occurs as observed in rocks. This means there are spaces, which constitute weak zones within the material. Therefore, when the indenter hits the first set of grains to be displaced in an uncompacted material, there is a compaction (jamming) at the lower part of the grains being displaced

due to the action of the indenter pressure on the material (Uehara et al. 2003), and gravity.

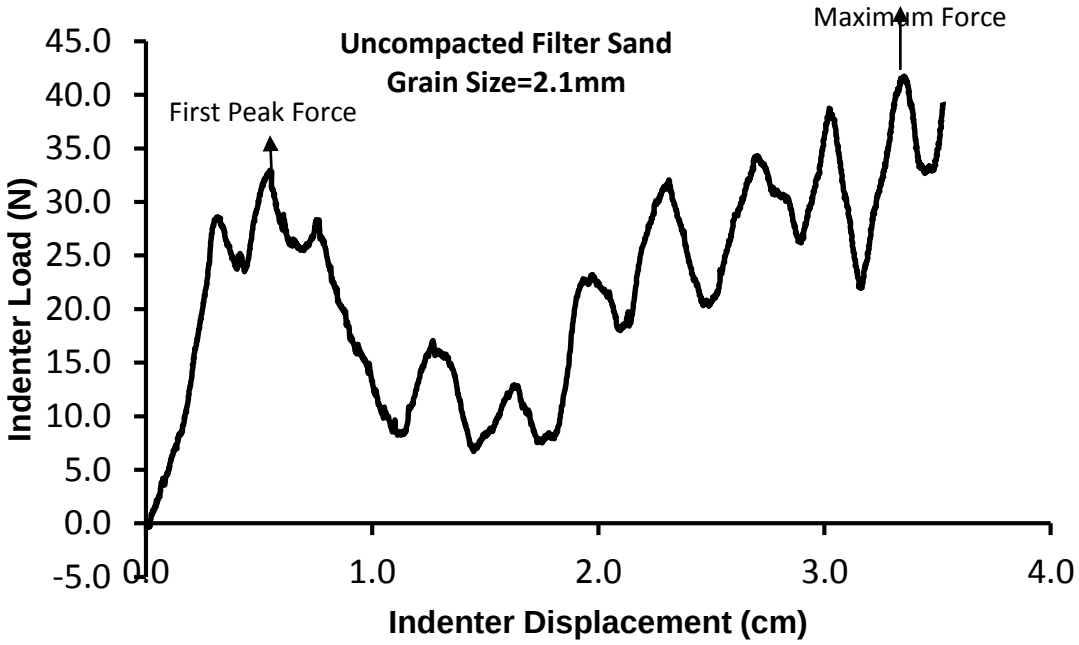


**Figure 4.1. Example of a typical force-penetration curve for filter sand. This indicates the first peak force and the maximum force which correspond to the last peak force of the test. (Refer to appendix B for other charts of same test).**

When the first set of grains are displaced, the force drops because of the roominess in the material and distance to the next set of grains determines to what extent the force will drop. In other words, if the material is too loose, there will be more number of force drop and vice versa.

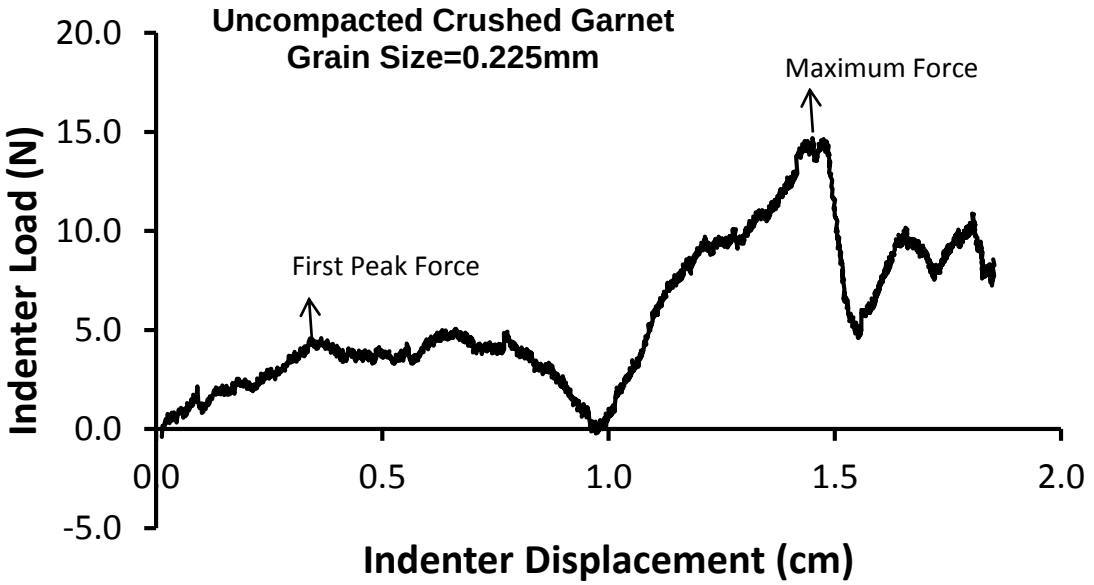


**Figure 4.2. Example of a typical force-penetration curve for crushed garnet. The maximum force was reached prior to the last peak force. (Refer to appendix B for other charts of same test).**

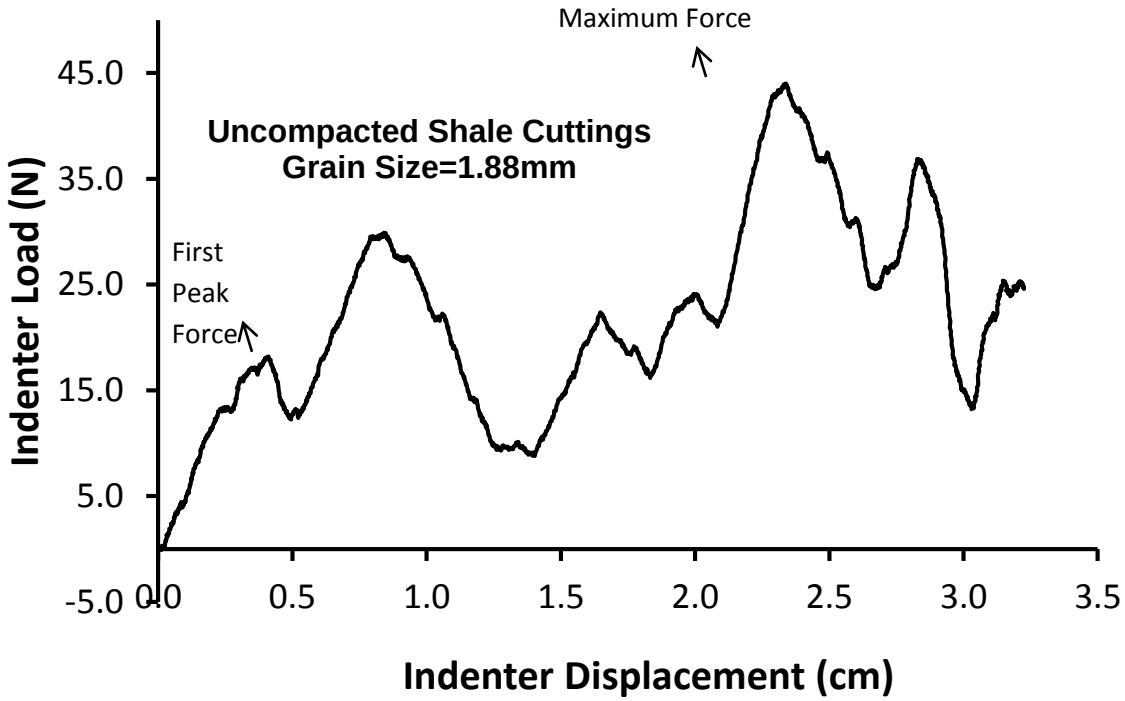


**Figure 4.3. An example of a typical force-penetration curve for shale cuttings. The maximum force was reached prior to the last peak force. (Refer to appendix B for other chart of same test)**

When the indenter hits the next set of grains, it will require greater force to displace it because of its initial compacting action while displacing the grains. At this point, the set of grains being displaced will have more frictional resistance than the previous ones therefore more force will be required and the force drop will be minimal in number due to little room for the indenter to hit the next set of grains and high in magnitude (Figure 4.4.). This continues and the force builds progressively with depth with successive rise and fall in forces, with each successive rise greater than the former and each successive drop less that the former. It was also observed that in some samples, the maximum peak force does not correspond to the last peak force at the end of the indentation. This means that the last rise is not always the peak. This observation can be explained from the fact that during indentation the buildup resistance due to the action of the indenter reaches its peak at the depth corresponding to the maximum force. The indenter feels the compaction effect of the indenter most during indentation at this force. Therefore, it does not necessarily mean that the peak build up resistance must correspond to the maximum depth.

This general pattern observed in the force-penetration curve for uncompacted materials is also observed in the compacted materials (Figure 4.4). In the compacted materials, there is little room for grain movement. Therefore, more force is required to achieve the first displacement. Also depending on the level of compaction, the force drop is considerable minimal in number but higher in magnitude as compared to the uncompacted materials. In summary, the major effect the compaction may have on the behavior of the force-penetration curve is

that it reduces the room for grain movement thereby increasing the force required to displace the grains. The compaction effect also varies with grain size as discussed in the next section.

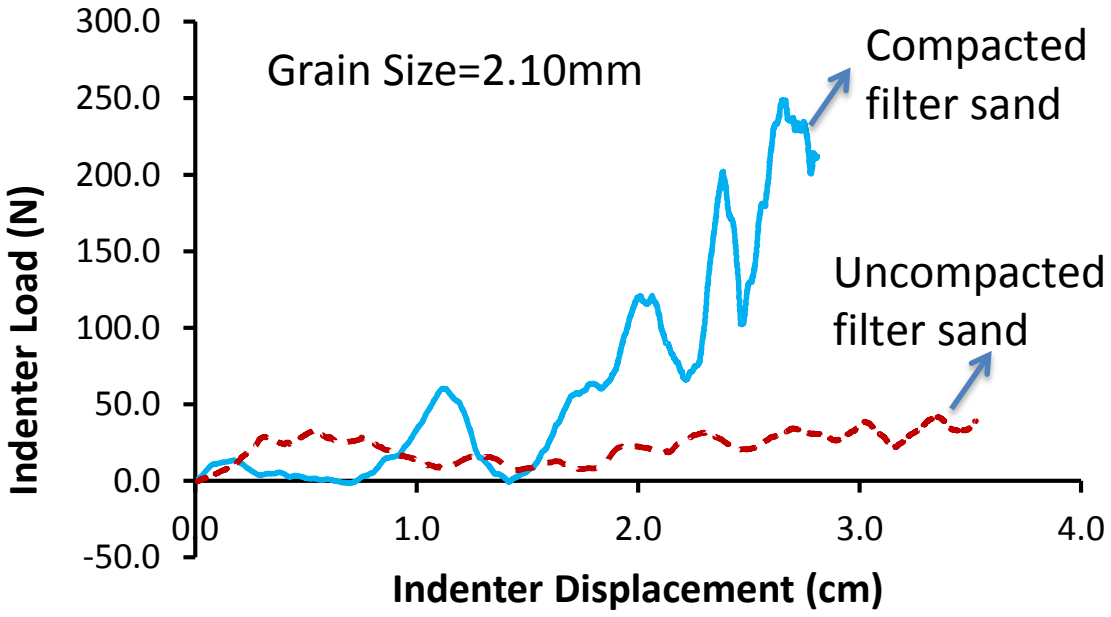


**Figure 4.4. Examples of typical curves comparing the behavior of compacted and uncompacted samples of filter sand.**

## 4.3. VARIABLES AFFECTING THE FORCE-PENETRATION CURVE

Previously, the force-penetration curve was discussed with respect to compaction. It is important to know that compaction accounts for the general trend, but specific behavior of different materials is due to some variables specific

to that material. The frictional resistance is contributed partly by gravity, and partly by the characteristics of the indenter (size) as well as the grain properties (Birzinski2013, Uehara 2003). In this research, gravity, indenter speed and indenter size were kept constant. The properties of the grains as measured had some dissimilarities. No individual variable has a monopoly of effect over the behavior of the force-penetration curve or the force required to penetrate the sample to a given depth. For an individual independent variable to be studied exclusively, all other independent variables must be kept constant. This was not feasible in the present study. It is difficult to produce grains of exactly the same aspect ratio, circularity, solid density as well as to achieve the same bulk density (compaction level). Because of these difficulties, multiple linear regression analysis was applied to better understand the interactions between these variables within and between each material. All analyses were done at 90% confidence. Equation, 4.1 is the model used.

$$Y = b0 + b1X1 + \cdots + bnXn \qquad 4.4$$

Where b0 is the intercept, b1…n are the slopes, X1…Xn are the independent variables and Y is the dependent variable of interest.

The purpose of this research is to understand the effect of the variations in physical properties of these dry granular materials. In this section, the effect of these variables will be discussed based on the behavior of the force-penetration curve as well as the result of the multiple linear regression carried out on the entire data. Tables 4.2 and 4.3 summarizes the regression analysis result for the various variables.

**Table 4.2. Regression summary table for the entire uncompacted sample**.

| Uncompacted Material | | | | | | | | |
|---|---|---|---|---|---|---|---|---|
| Specific Energy | | | | | Specific Penetration | | | |
| | *t Stat* | *P-value* | R^2 | | | *t Stat* | *P-value* | R^2 |
| Grain size | 3.25 | 0.01 | 0.49 | | Grain size | 3.11 | 0.01 | 0.56 |
| Aspect Ratio | 3.75 | 0.00 | 0.41 | | Aspect Ratio | 2.18 | 0.06 | 0.24 |
| Bulk Density | 0.49 | 0.64 | 0.00 | | Bulk Density | 0.75 | 0.47 | 0.03 |
| Circularity | -0.68 | 0.51 | 0.21 | | Circularity | -1.07 | 0.31 | 0.11 |
| Solid Density | -0.10 | 0.93 | 0.37 | | Solid Density | -1.12 | 0.29 | 0.17 |
| | | | | | | | | |
| | | | t-table | 1.83 | | | | |

**Table 4.3. Regression summary table for the entire uncompacted sample.**

| Compacted Material | | | | | | | | |
|---|---|---|---|---|---|---|---|---|
| Specific Energy | | | | | Specific Penetration | | | |
| | *t Stat* | *P-value* | R^2 | | | *t Stat* | *P-value* | R^2 |
| Grain size | -1.32 | 0.22 | 0.15 | | Grain size | 1.47 | 0.18 | 0.61 |
| Aspect Ratio | 0.43 | 0.68 | 0.03 | | Aspect Ratio | 0.47 | 0.65 | 0.02 |
| Bulk Density | -2.38 | 0.04 | 0.26 | | Bulk Density | -0.94 | 0.37 | 0.45 |
| Circularity | 1.07 | 0.31 | 0.05 | | Circularity | 0.37 | 0.72 | 0.07 |
| Solid Density | 2.00 | 0.08 | 0.00 | | Solid Density | 0.06 | 0.95 | 0.00 |
| | | | | | | | | |
| | | | t-table | 1.83 | | | | |

**4.3.1. Compaction.** When the sample is uncompacted, the indentation force fluctuates about the same relative amount in both fine and coarse grains (Figure 4.5). However, on compaction, the fine grain aggregates shows approximately zero force fluctuations (Figure 4.6), whereas coarse grained samples experience increased force fluctuation.

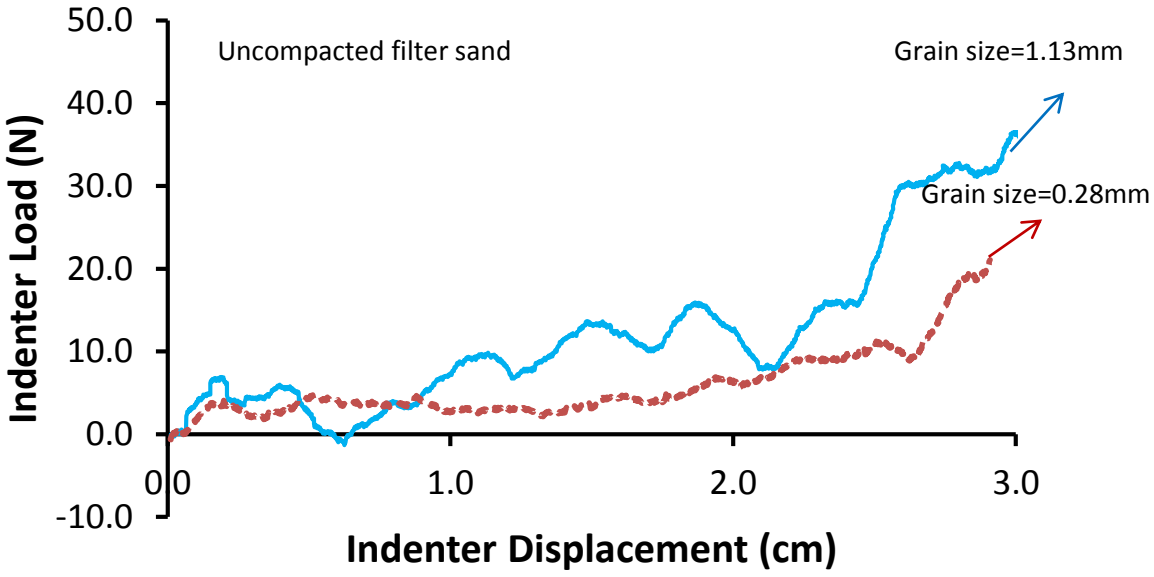


**Figure 4.5. Uncompacted filter sand showing force fluctuation in both fine and coarse grains. The force fluctuation is higher for coarse than for fine. The highest magnitude force-drop is approximately 10N for coarse grains (blue) and about 2N for fine grains (red).**

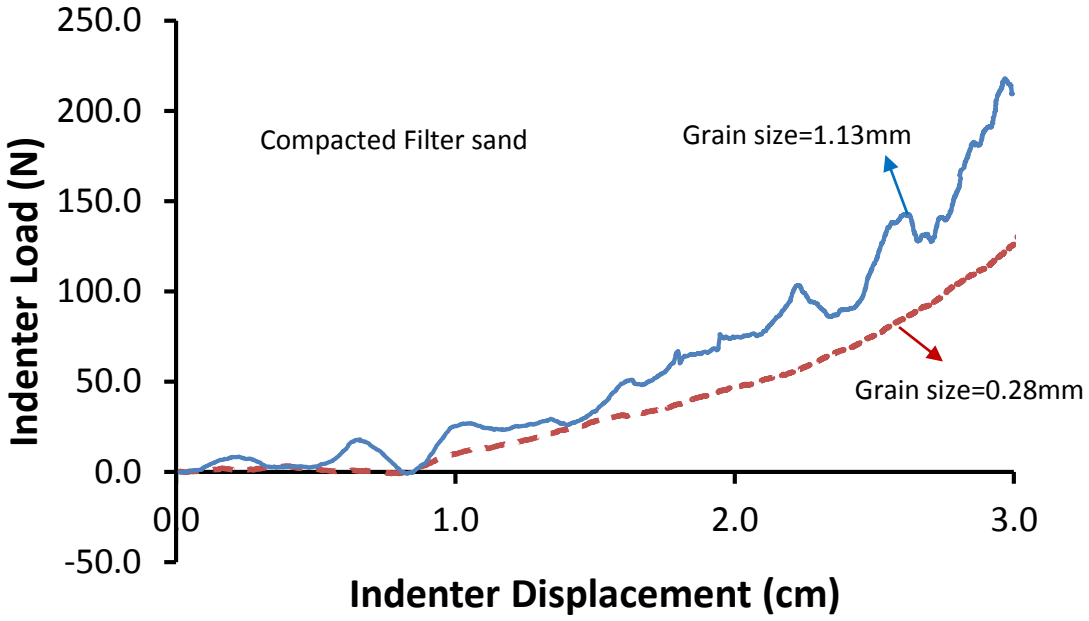


**Figure 4.6. Compacted filter sand showing maximum force drop magnitude of about 20N for coarse grains (blue) and approximately zero force-drop for the fine grains (red).**

**4.3.2. Grain Size Effects.** Table 4.1 summarizes the data from the tests conducted. Filter sand (FS_1-FS_8) and shale cuttings (SC_1-SC_4) had the most grain-size components of all the materials tested. This permitted examination of the effect of grain size on the results.

The grain size is the average of the minimum and maximum grains within each sieved size fraction. The grain size is a major variable that greatly affects the force-penetration behavior. For the larger diameter grains, the force drops after each peak force is apparent (Figure 4.7). This behavior can be explained

because, the indenter-grain ratio is low (the grain size is closer to the indenter size when compared to the small diameter grain). This ratio hypothetically affects the ease of the indenter displacing the grains during penetration. This can be modeled simply by inserting a finger in a pile of dry sand, and then into a pile of gravel. The first is easier. In the same way, the indenter requires more force to penetrate coarse-grained samples (given that other variables remain constant). In addition, returning to the finger model, the finger penetrates the sand pile smoothly with less stick-slip frictional resistance than while penetrating the gravel. This stick-slip is expressed in the force-penetration curves as saw-tooth waveforms; this is what makes the force drop in coarse grained samples (Figure 4.7) more distinctive than in fine grained samples.

In addition, specific energy and specific penetration, correlated with grain size with a $R^2$ value of 0.49 and 0.56, respectively, for the uncompacted materials (Figure 4.8), and 0.15 and 0.61, respectively, for the compacted materials (Figure 4.9). The multiple linear regression result indicated that for the uncompacted material, the correlation of grain size with both the SE and SP is significant whereas, for compacted materials, the correlation is significant for SP but not for SE.

**4.3.3. Density Effects.** The effect of bulk and solid densities will be evaluated in this section.

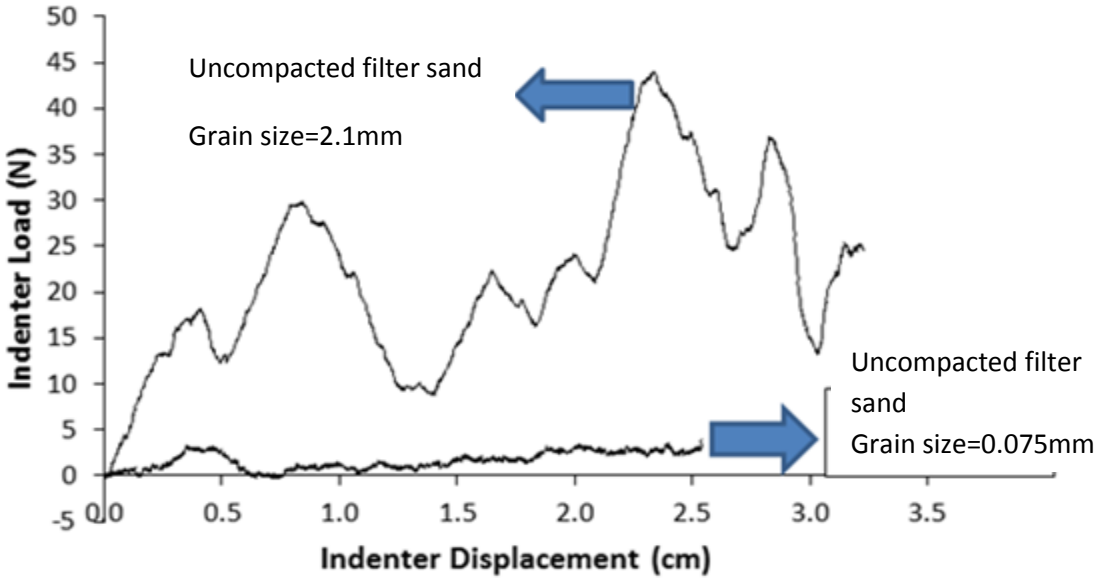


**Figure 4.7. Typical curves comparing the behavior of fine-grained filter sand to coarse-grained filter sand.**

**4.3.3.1. Bulk density**. There is no significant correlation for the uncompacted material with bulk density (Figure 4.10). However, bulk density for the compacted material correlated significantly with SE and SP at $R^2$ value of 0.26 and 0.45, respectively, (Figure 4.11). In addition, regression analysis indicates an inverse relationship of bulk density with specific energy. This inverse relationship supports the work of Saffet Yagiz (2009) where he found that the more ductile a rock is, the less the force fluctuation and the more the work done during indentation. This means that the higher the magnitude of the force fluctuation, the less the work done during the indentation hence the lower the specific energy of indentation.

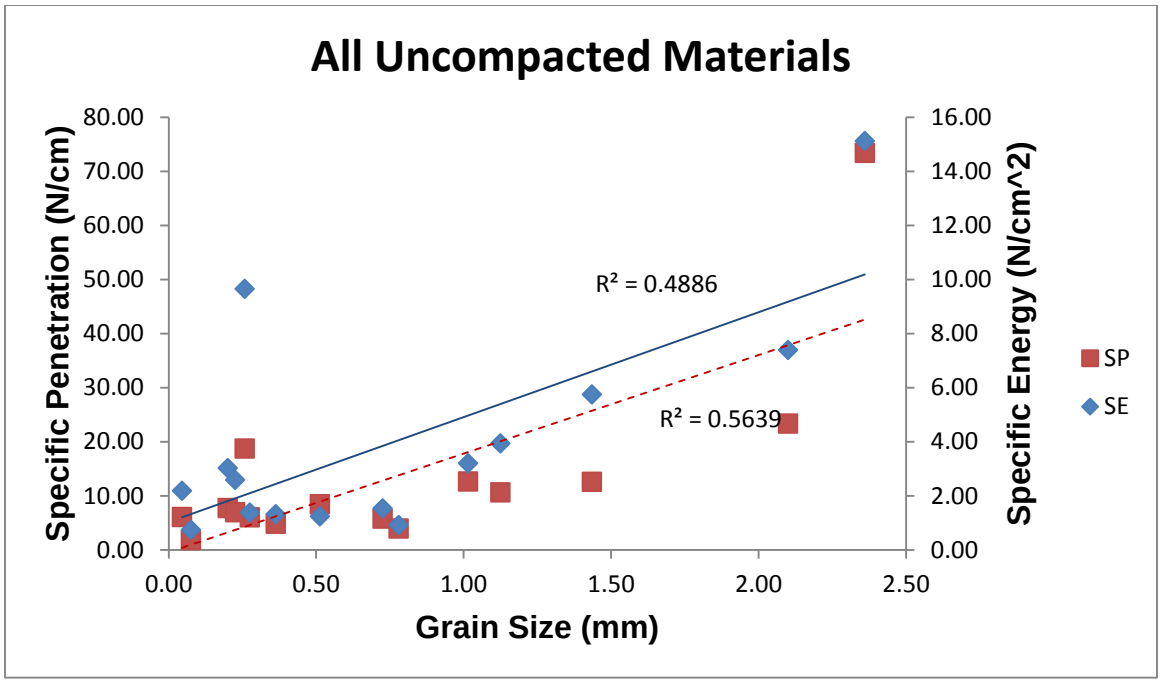


**Figure 4.8. Chart showing the linear relationship of grain size with SE and SP for all uncompacted materials.**

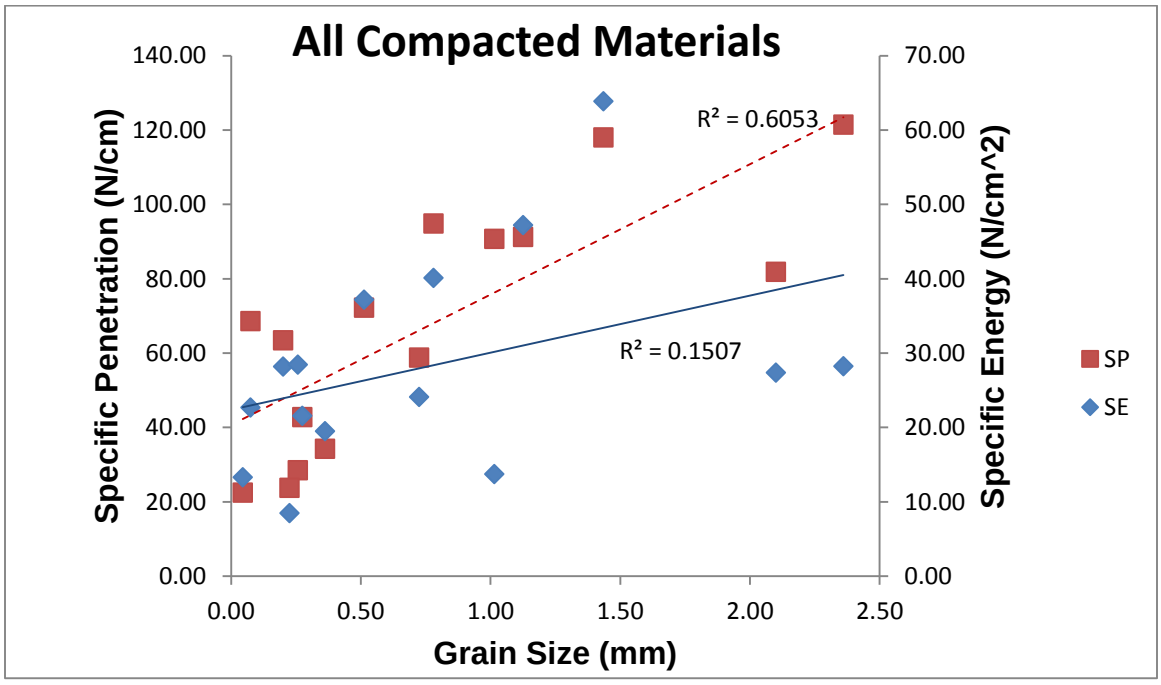


**Figure 4.9. Charts showing the relationship of grain size with SP and SE for compacted materials.**

As explained in Section 4.2 and observed in Figure 4.6 the compacted material shows high magnitude of force fluctuation, therefore less energy is required to indent it as compared to an uncompacted material with the same average indentation force magnitude.

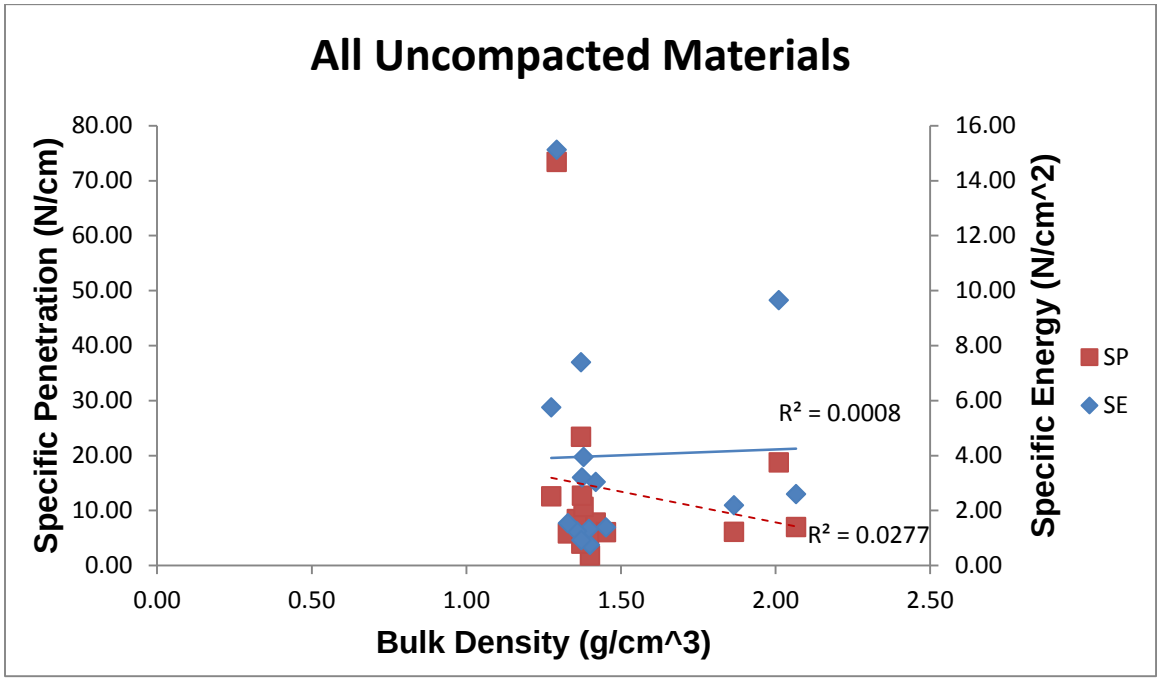


**Figure 4.10. Chart showing the relationship of bulk density with SE and SP for uncompacted materials.**

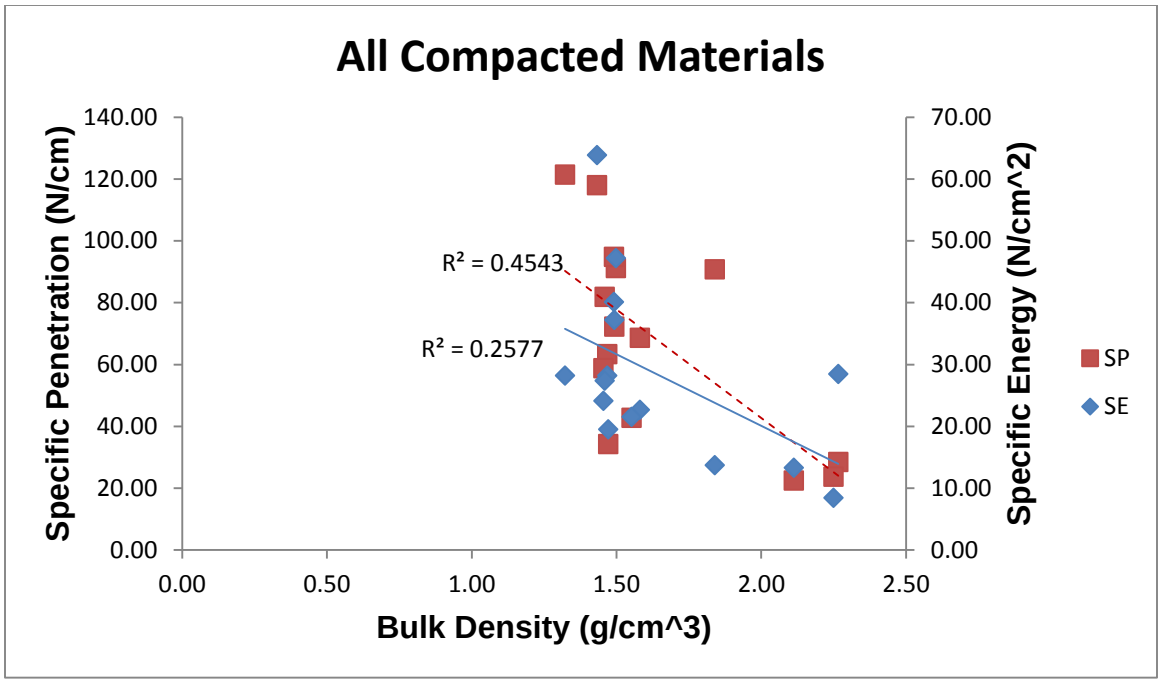


**Figure 4.11. Charts showing the relationship bulk density with SE and SP for compacted materials.**

**4.3.3.2. Solid density.** The solid density is the density of the solids only (without the interstitial spaces). Although there was significant correlation of specific energy with solid density for compacted materials, the correlation coefficient is very low ($R^2$ = 0.0001). When all the results are analyzed together (combination of compacted and uncompacted materials), there was a significant correlation of solid density with specific penetration, like the result of the compaction, the $R^2$ value was also low (0.0036) and the relationship was inverse in this case. The reason for the inverse relationship is still unknown within the scope of this work and because of the low correlation coefficients, it could be concluded that based on this research, solid density was not a major variable.

**4.3.4. Grain Shape Effects.** The effect of Aspect ratio, grain roundness and circularity will be evaluated in this section.

**4.3.4.1. Aspect ratio.** The aspect ratio is the ratio of the major axis to the minor axis (axis of the circumscribed circle). As the ratio approaches one, the grain becomes more rounded. As the aspect ratio increases, the grain becomes more angular. Aspect ratio was found to correlate with both SE and SP for the uncompacted materials at $R^2$ of 0.41 and 0.24, respectively, (Figure 4.12). However, when the materials get compacted, the effect of aspect ratio becomes insignificant (Figure 4.13). It is rationally easier to displace a rounded material than to displace an angular material of the same density. Therefore, the indenter displaces easily rounded grains than angular grains when the grains are packed together. In addition, the rounded grains provides more room for grain movement since the loosely lock together as compared to the angular ones that tightly binds to the sharp edges of each other. In order words, more force is required to penetrate the angular grains than the rounded grains.

**4.3.4.2. Grain roundness.** Just like aspect ratio, the circularity of the grains affects the force-penetration behavior. The circularity is simply how elongated the materials are. If the circularity approaches one, it indicates closeness to perfect circle. On the other hand, if the circularity approaches zero, it indicates an increasingly elongated shape.

This research found no correlation of circularity with either SE or SP (Figures 4.14, 4.15). This could be because a perfect circle just like a perfectly rounded grain will require less force to be moved or rolled around. However, as

the circularity reduces in other words increasing elongation, the displacement of grains requires more force. However, with extreme elongation (circularity tending to zero), the grain breaks and significant force drop will be observed. When the circularity of the grains is too long, hypothetically, the indenter will no longer penetrate the sample via displacement method, rather by breakage depending on the grain size of the materials in general. Therefore, the effect of circularity should not be treated as linear. The effect of circularity on the individual type of material is discussed along with the effect of other variables in the Section 4.4.

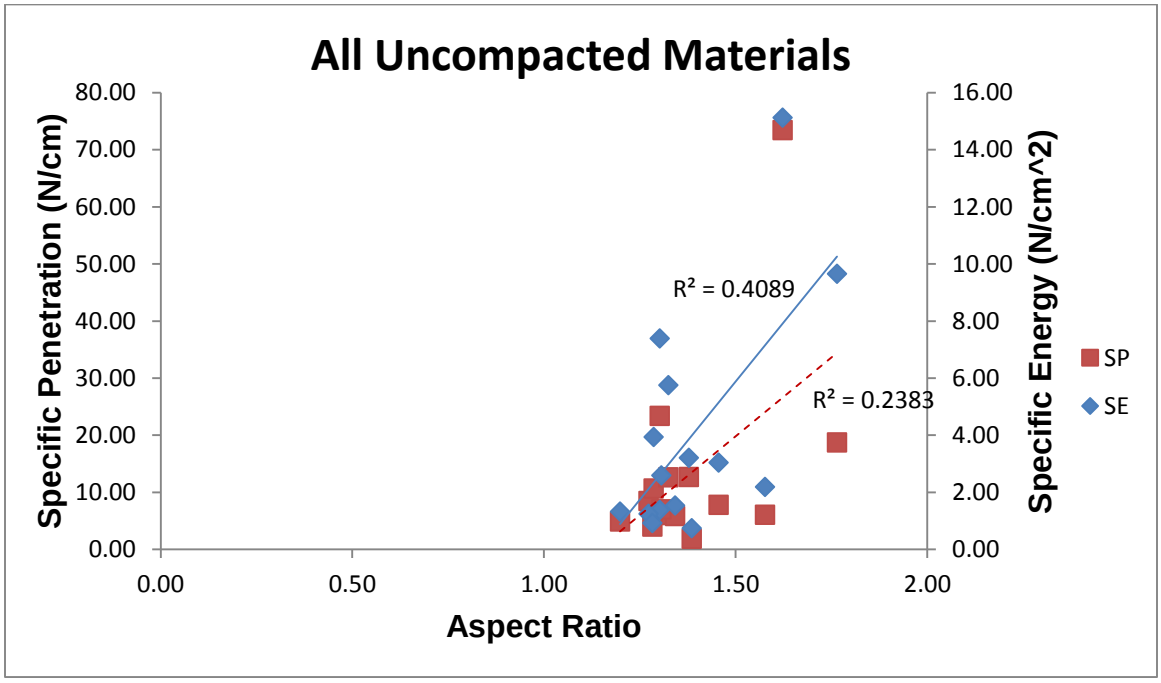


**Figure 4.12. Charts showing the relationship of aspect ratio with SE and SP for uncompacted materials.**

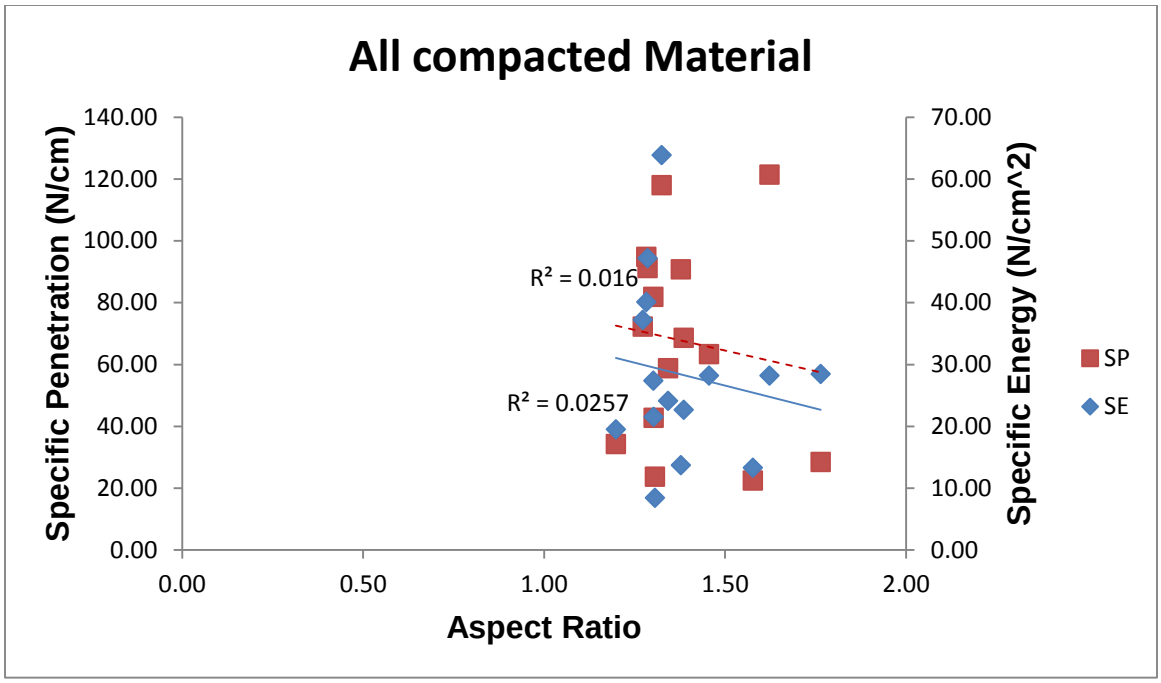


**Figure 4.13. Charts showing the relationship of aspect ratio with SE and SP for compacted materials.**

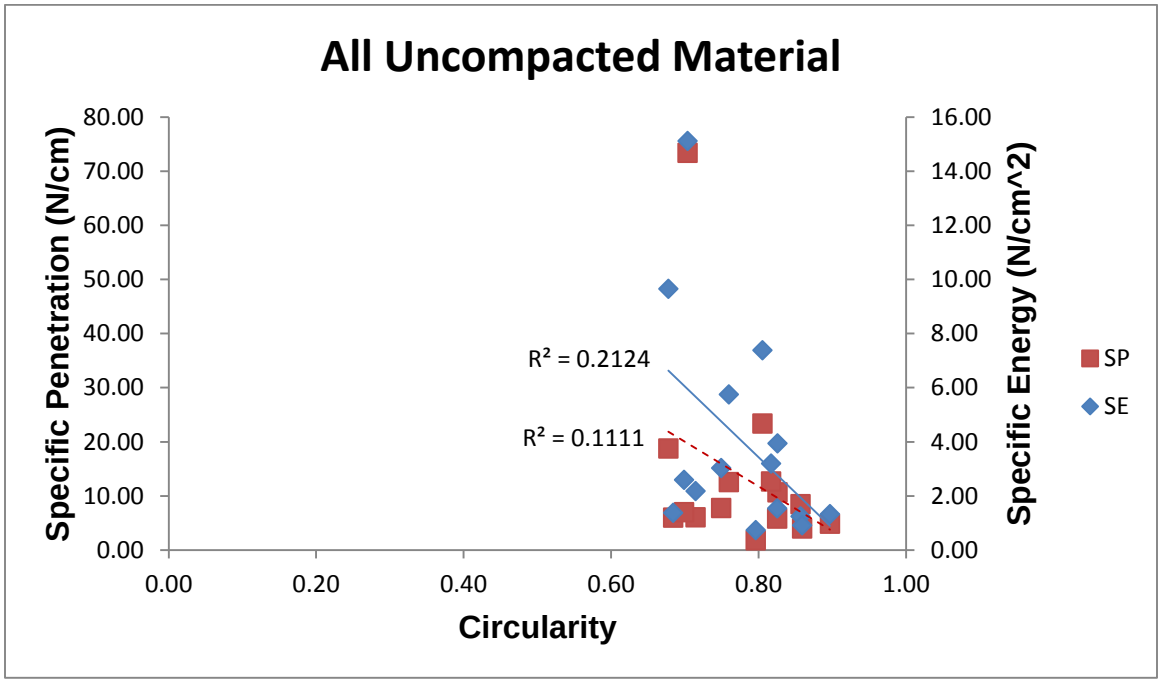


**Figure 4.14. Charts showing the relationship of circularity with SE and SP for uncompacted materials.**

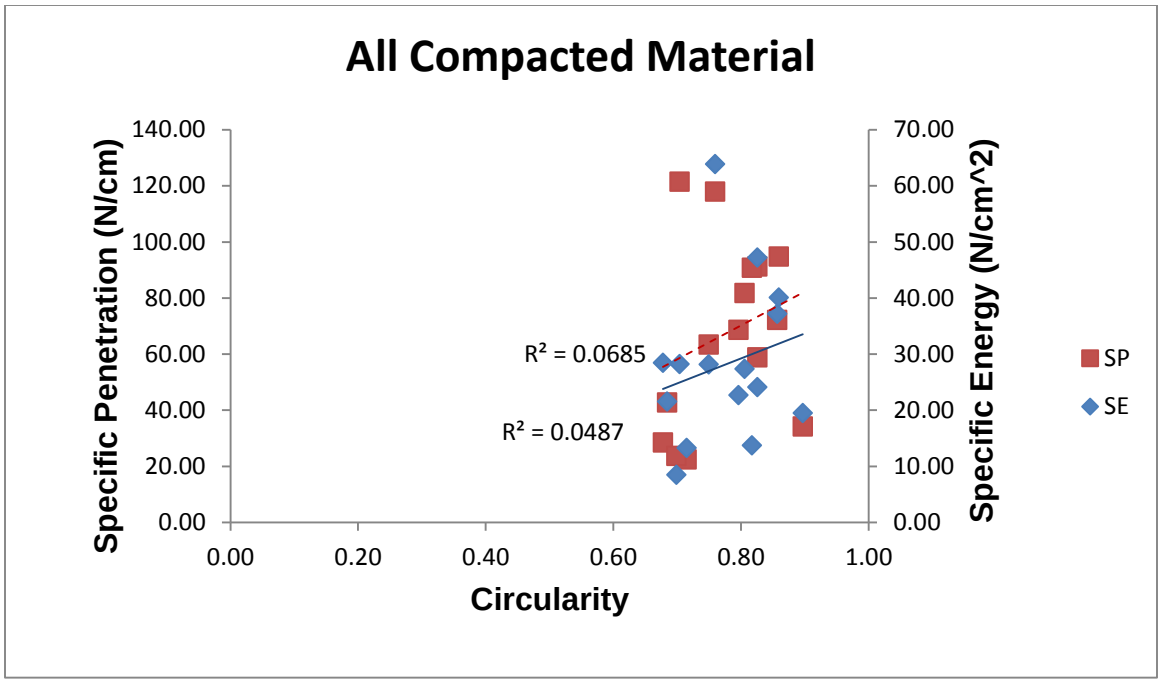


**Figure 4.15. Charts showing the relationship of circularity with SE and SP for compacted materials.**

## 4.4. COMBINED EFFECT ON ONE MATERIAL TYPE

In the preceding section, effects of the various variables were discussed based on the combination of all the materials tested. In this section, the effect of the variables will be discussed based on the material with the greatest number of size fractions tested (filter sand). First, a multiple linear regressions were carried out on the uncompacted and compacted material separately. Then, multiple linear regressions were carried out with compacted and uncompacted results combined. All analyses were done at 90% confidence. Equation, 4.4 is the model used.

For uncompacted filter sand regression result (Table 4.4), specific energy (SE) significantly correlated linearly with grain size, aspect ratio, bulk density, and

circularity at $R^2$ values of 0.82 (Figure 4.16), 0.0003 (Figure 4.17), 0.023 and 0.0016, respectively. The correlation was weak for the shape descriptors and was strong for the grain size. For the uncompacted sample, Specific penetration correlated with only the grain size at $R^2$ value of 0.88.

In the compacted material, the linear regression (Table 4.5) model did not show any correlation of either SP or SE with any of the independent variables. Combining the compacted and uncompacted (Table 4.6), SE linearly correlated with grain size and bulk density with $R^2$ values of 0.03 (Figure 4.18) and 0.49 (Figure 4.19), respectively, while specific penetration (SP) correlated linearly with grain size, aspect ratio, bulk density, and circularity with $R^2$ values of 0.07 (Figure 4.18), 0.0004(Figure 4.19), 0.51 (Figure 4.20), and 0.0007 (Figure 4.21), respectively.

In the entire regressions, correlation was weak for the shape parameters. The grain size dominated in the uncompacted samples and the bulk density dominated whenever there is compaction.

**Table 4.4. Regression result of uncompacted filter sand.**

| Uncompacted Filter Sand | | | | | | | | |
|---|---|---|---|---|---|---|---|---|
| Specific Energy | | | | | Specific Penetration | | | |
| | *t Stat* | *P-value* | R^2 | | | *t Stat* | *P-value* | R^2 |
| Grain size | 3.25 | 0.01 | 0.83 | | Grain size | 3.50 | 0.07 | 0.88 |
| Aspect Ratio | 3.75 | 0.00 | 0.03 | | Aspect Ratio | 1.58 | 0.25 | 0.02 |
| Bulk Density | 0.49 | 0.64 | 0.02 | | Bulk Density | 2.04 | 0.18 | 0.05 |
| Circularity | -0.68 | 0.51 | 0.0016 | | Circularity | 1.06 | 0.40 | 0.00004 |
| Solid Density | -0.10 | 0.93 | 0.86 | | Solid Density | -1.61 | 0.25 | 0.76 |
| | | | t-table | 2.92 | | | | |

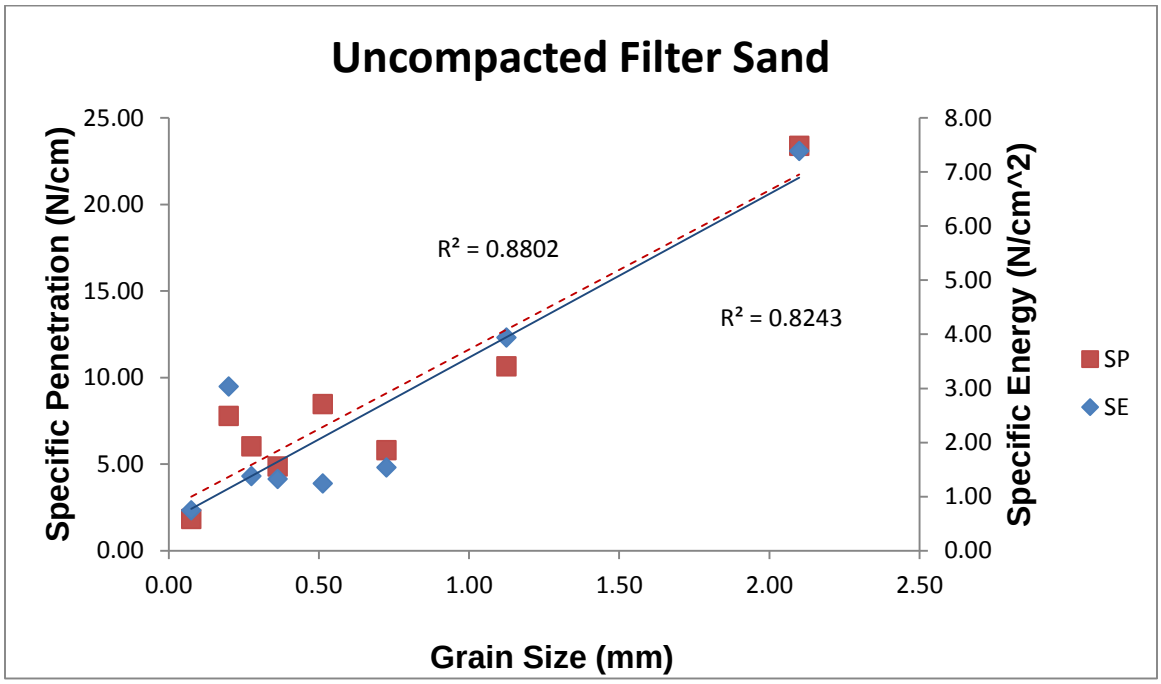


**Figure 4.16. Chart showing the relationship of grain size with SE and SP in the uncompacted filter sand.**

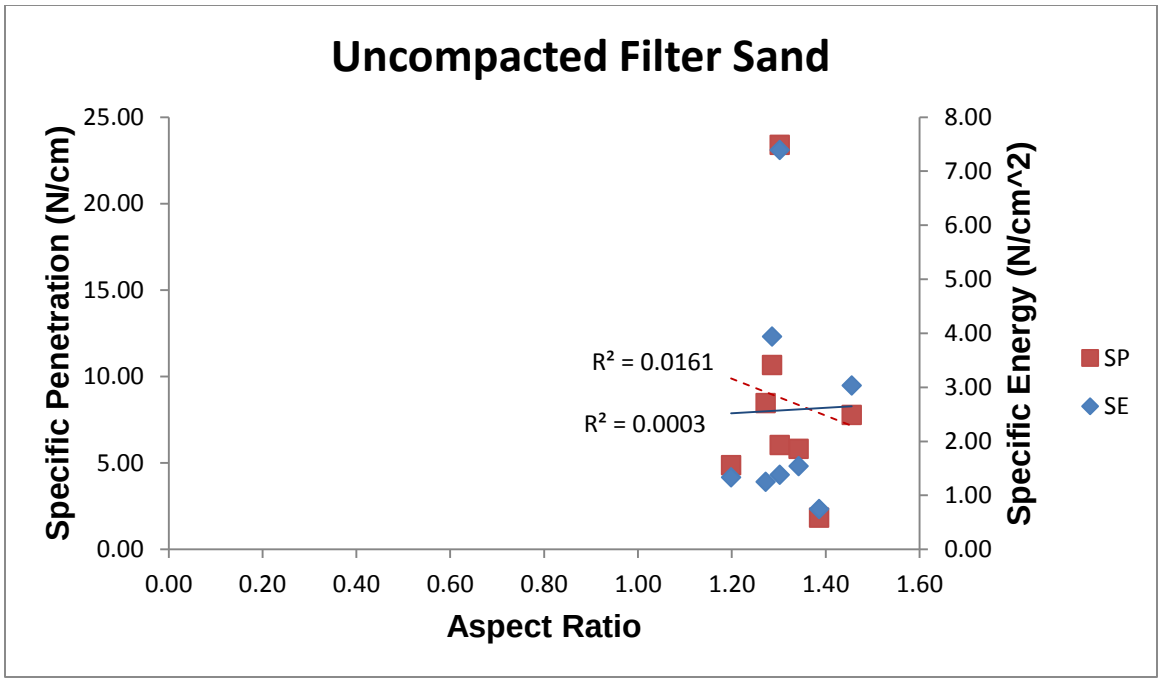


**Figure 4.17. Charts showing the relationship of aspect ratio with SE and SP for uncompacted filter sand.**

**Table 4.5. Regression result for compacted filter sand.**

| Compacted Filter Sand | | | | | | | | |
|---|---|---|---|---|---|---|---|---|
| Specific Energy | | | | | Specific Penetration | | | |
| | *t Stat* | *P-value* | R^2 | | | *t Stat* | *P-value* | *R^2* |
| Grain size | -0.16 | 0.89 | 0.11 | | Grain size | 0.43 | 0.71 | 0.34 |
| Aspect Ratio | 0.10 | 0.93 | 0.0045 | | Aspect Ratio | 1.30 | 0.32 | 0.06 |
| Bulk Density | -0.07 | 0.95 | 0.02 | | Bulk Density | 0.66 | 0.58 | 0.00 |
| Circularity | 0.33 | 0.77 | 0.04 | | Circularity | 1.00 | 0.42 | 0.00 |
| Solid Density | 0.33 | 0.77 | 0.14 | | Solid Density | 0.17 | 0.88 | 0.44 |
| | | | | | | | | |
| | | | t-table | 2.92 | | | | |

**4.6. Regression result for compacted and uncompacted filter sand.**

| Compacted and Uncompacted | | | | | | | | |
|---|---|---|---|---|---|---|---|---|
| Specific Energy | | | | | Specific Penetration | | | |
| | *t Stat* | *P-value* | R^2 | | | *t Stat* | *P-value* | *R^2* |
| Grain size | 1.82 | 0.10 | 0.03 | | Grain size | 3.09 | 0.01 | 0.07 |
| Aspect Ratio | 1.24 | 0.24 | 0.00 | | Aspect Ratio | 2.63 | 0.03 | 0.00 |
| Bulk Density | 5.24 | 0.00 | 0.49 | | Bulk Density | 7.84 | 0.00 | 0.51 |
| Circularity | 1.67 | 0.13 | 0.00 | | Circularity | 2.54 | 0.03 | 0.00 |
| Solid Density | -1.04 | 0.32 | 0.03 | | Solid Density | -1.60 | 0.14 | 0.08 |
| | | | t-table | 1.81 | | | | |

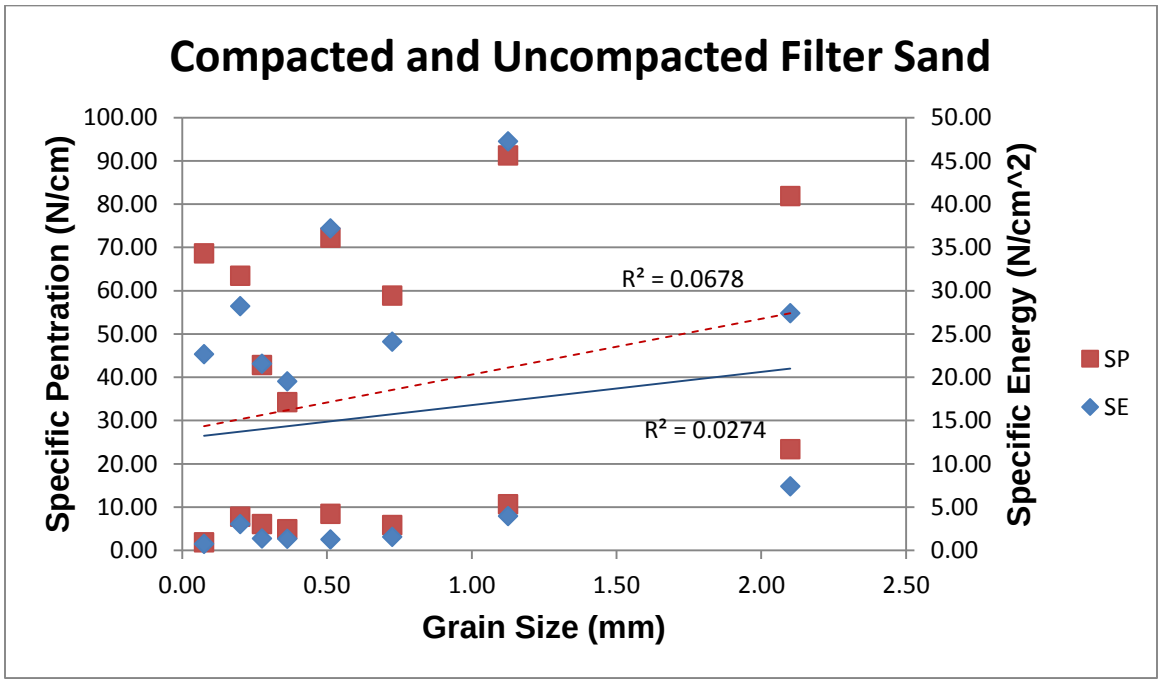


**Figure 4.18. Charts showing the relationship of grain size with SE and SP in both the compacted and uncompacted filter sand materials.**

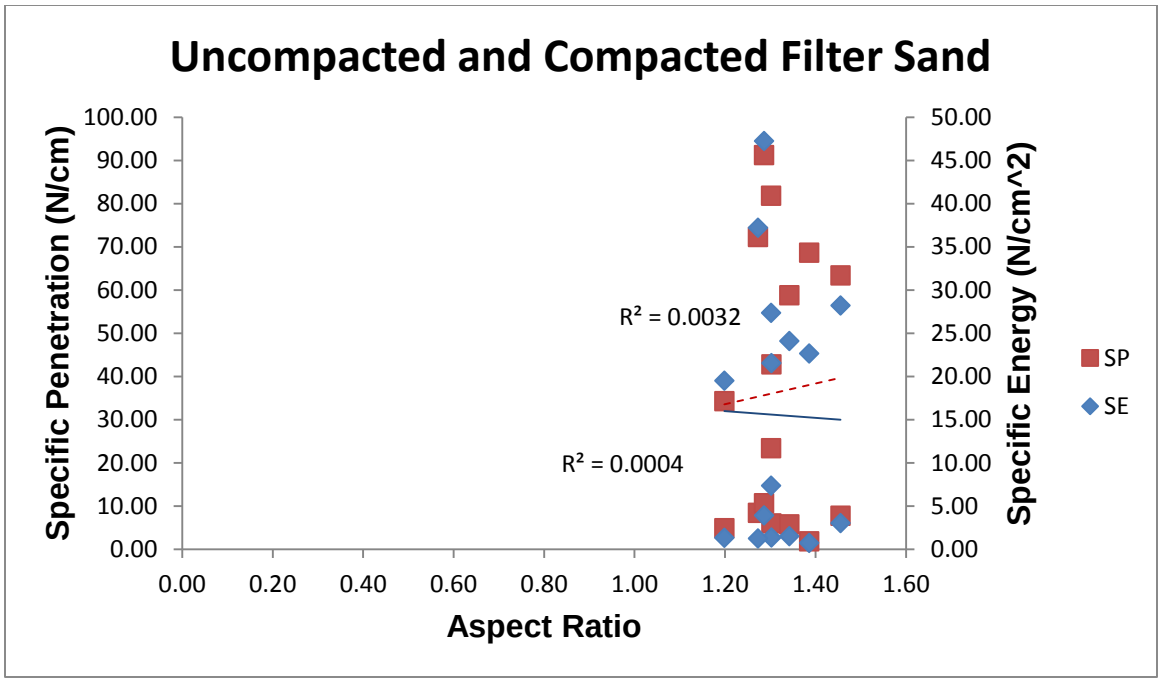


**Figure 4.19. Charts showing the relationship of aspect ratio with SE and SP for compacted and uncompacted filter sand materials combined.**

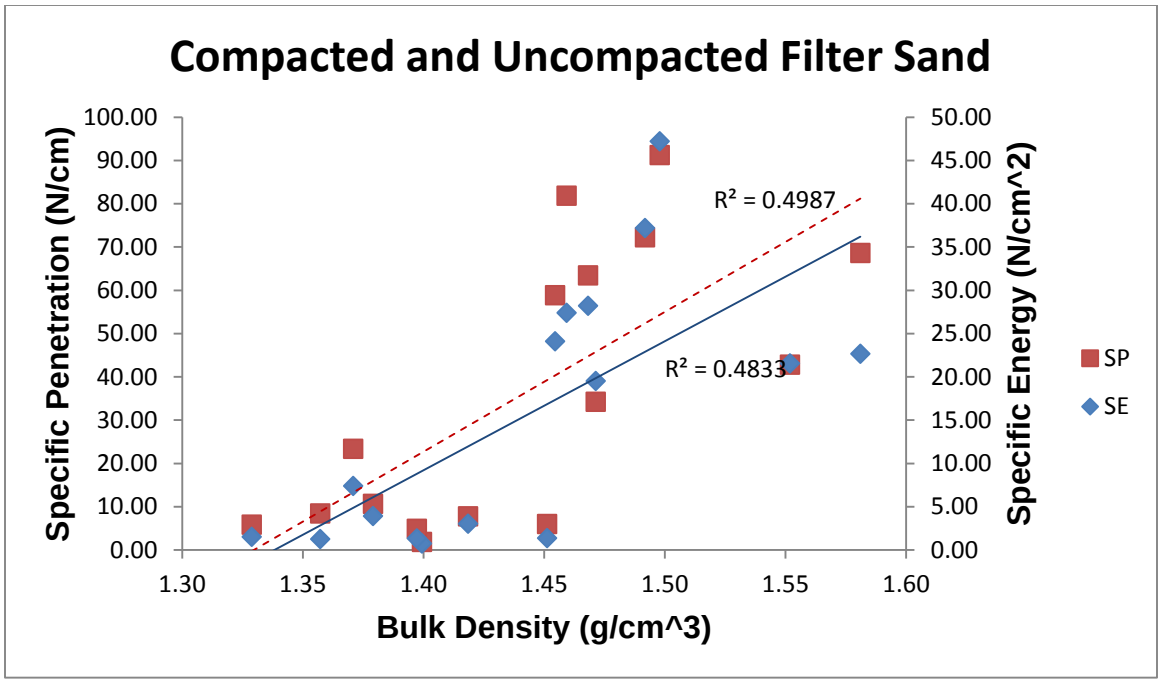


**Figure 4.20. Charts showing the relationship of bulk density with SE and SP in the compacted and uncompacted filter sand materials.**

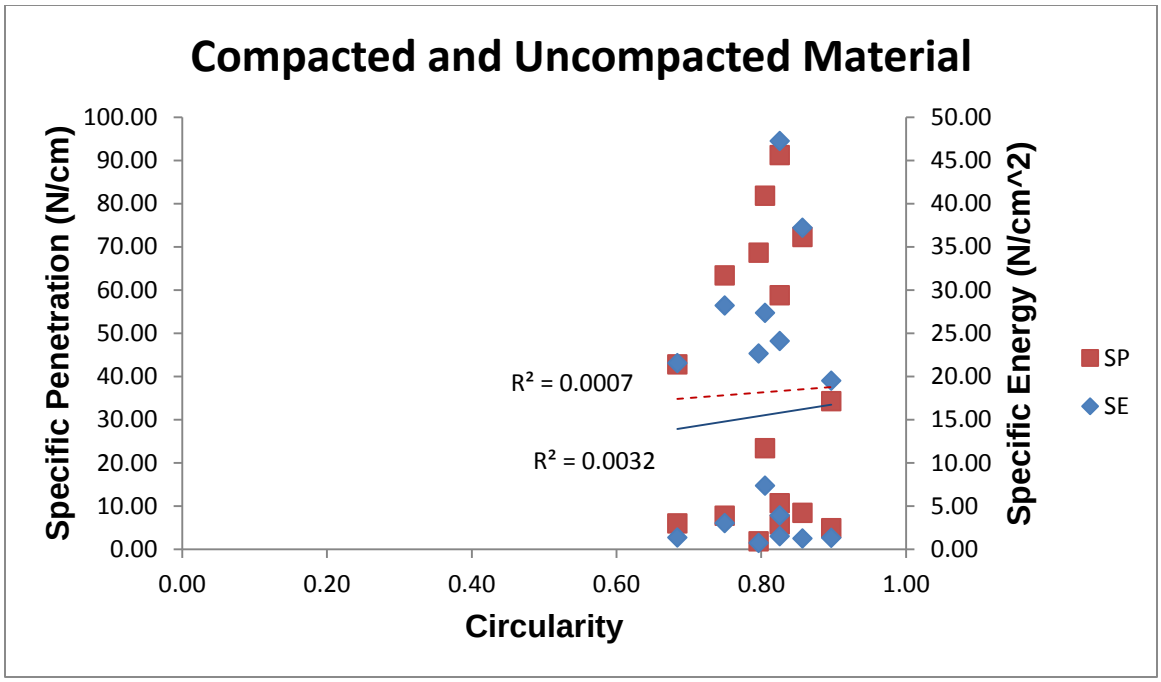


**Figure 4.21. Charts showing the relationship of circularity with SE and SP for compacted and uncompacted filter sand combination.**

# 5. CONCLUSIONS AND RECOMMENDATIONS

## 5.1. CONCLUSIONS

The objective of this research was to evaluate qualitatively and quantitatively the effect of compaction, grain size and grain shape on the behavior of various granular materials under normal indentation by a single tool.

Overall, since the initial speed of indentation and the indenter geometry are constant throughout the experiment, it can be deduced that the changes in specific penetration and specific energy were due to the properties of the sample aggregates of grains. In addition, grain indentation occurs through grain displacement rather than fragmentation.

Particle size, with compaction level was responsible for the drop in forces observed in the force-penetration curve during a single tool indentation of a granular material. Increase in particle size leads to increase in the force required to indent a material. Furthermore, increase in grain size leads to increased force drop (stick-slip frictional resistance). A coarse grain material increases the roominess of the sample unlike the fine grains that leaves little room within the grains. In coarse materials, the indenter takes much time moving from one grain to the other and vice versa in fine materials. This accounts for the increased force drop observed in the force-penetration curve of coarse grain materials. Compaction effect varies depending on the grain size of the material. For fine grain material, compaction reduces significantly the force fluctuation effect. For coarse grained materials, compaction increases the magnitude of the force fluctuation but reduces the number of fluctuations in a given depth of penetration.

Grain size and aspect ratio was the dominating variables affecting SE and SP in uncompacted sample. When compaction is introduced, grain size and bulk density becomes the dominant variables affecting SE and SP for all materials tested.

For the material with the highest size fraction; filter sand (seven-size fraction), grain size, aspect ratio, bulk density, and circularity affected the specific energy significantly and specific penetration was affected only by the grain size for uncompacted sample. This could be due to the fact that SE is a volume measurement whereas SP is length measurement. However, on adding the data for compacted samples, SE correlated with only grain size and bulk density significantly, whereas SP correlated significantly with grain size, aspect ratio, bulk density and circularity.

## 5.2. RECOMMENDATIONS

Based on the design, conduct, and results of this research, the following recommendations were made in other to improve future work and ensure research continuity on this field

- Continuing to develop more predictive models. The linear model used in this research may not be the best model, therefore other models can be tested to better understand the interaction of the variable.
- Repeating the experiment with varying initial indenter speed, water/ice content and introducing gravel size and larger particles to understand fully how these later parameters affect the force of indentation.

- Using an improved method of measuring the bulk density and producing a 3-D image analysis of the grains. Then repeat the experiment with these improved methods.
- Modeling with a numerical method such as DEM, FEM, or hybrid approaches will be helpful to study the behavior of the highly heterogeneous dry granular materials.

# APPENDIX A

# PHYSICAL PROPERTY TEST DATA

| Filter Sand | | | | |
|---|---|---|---|---|
| Sample ID | Grain Size (mm) | Solid Density (g/cm^3) | Specifc Gravity | Porosity (%) |
| A1 | 0.075 | 1.57 | 1.58 | 28.34 |
| A2 | 0.2 | 1.54 | 1.55 | 28.98 |
| A3 | 0.275 | 1.56 | 1.56 | 28.43 |
| A4 | 0.3625 | 1.53 | 1.53 | 29.32 |
| A5 | 0.5125 | 1.51 | 1.51 | 29.58 |
| A6 | 0.725 | 1.53 | 1.54 | 29.95 |
| A7 | 1.125 | 1.81 | 1.82 | 22.92 |
| A8 | 2.1 | 1.97 | 1.98 | 19.47 |

| Filter Sand | | | | |
|---|---|---|---|---|
| Sample ID | Roundness | Aspect Ratio | Circularity | Grain Size |
| | | | | |
| A1 | 0.75 | 1.39 | 0.80 | 0.075 |
| A2 | 0.70 | 1.46 | 0.75 | 0.2 |
| A3 | 0.78 | 1.30 | 0.68 | 0.275 |
| A4 | 0.85 | 1.20 | 0.90 | 0.3625 |
| A5 | 0.80 | 1.27 | 0.86 | 0.5125 |
| A6 | 0.76 | 1.34 | 0.83 | 0.725 |
| A7 | 0.79 | 1.29 | 0.83 | 1.125 |
| A8 | 0.81 | 1.30 | 0.81 | 2.1 |

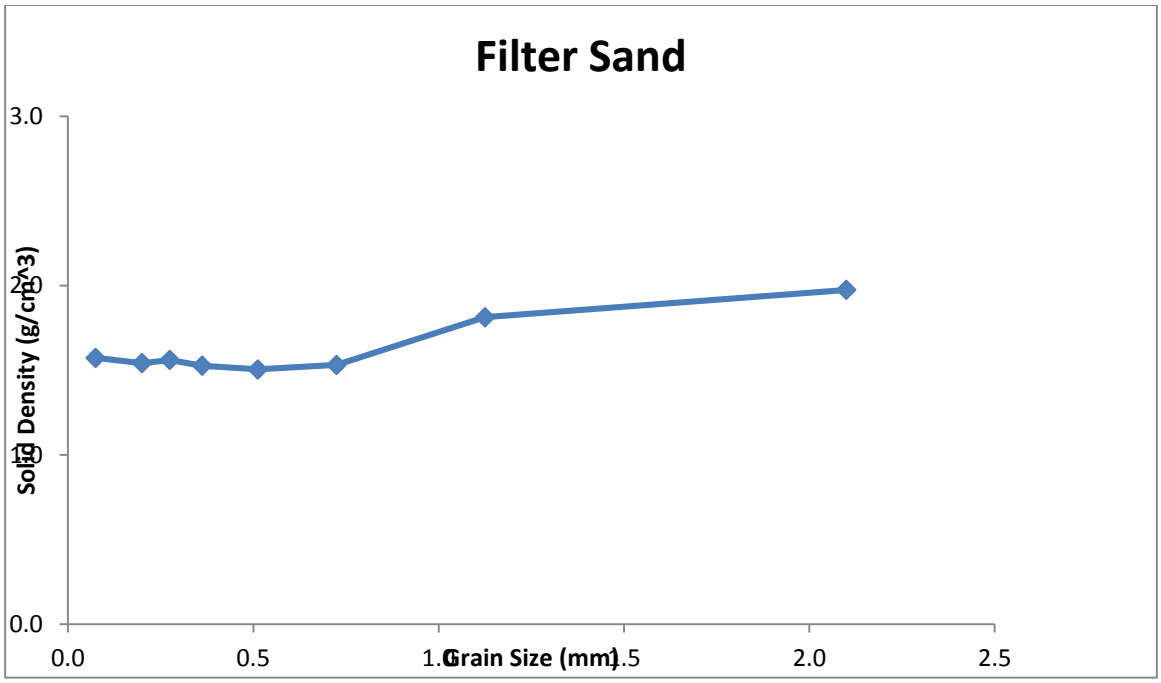
Filter Sand
3.0
2.0
1.0
0.0
Solid Density (g/cm^3)
0.0
0.5
1.0
1.5
2.0
2.5
Grain Size (mm)

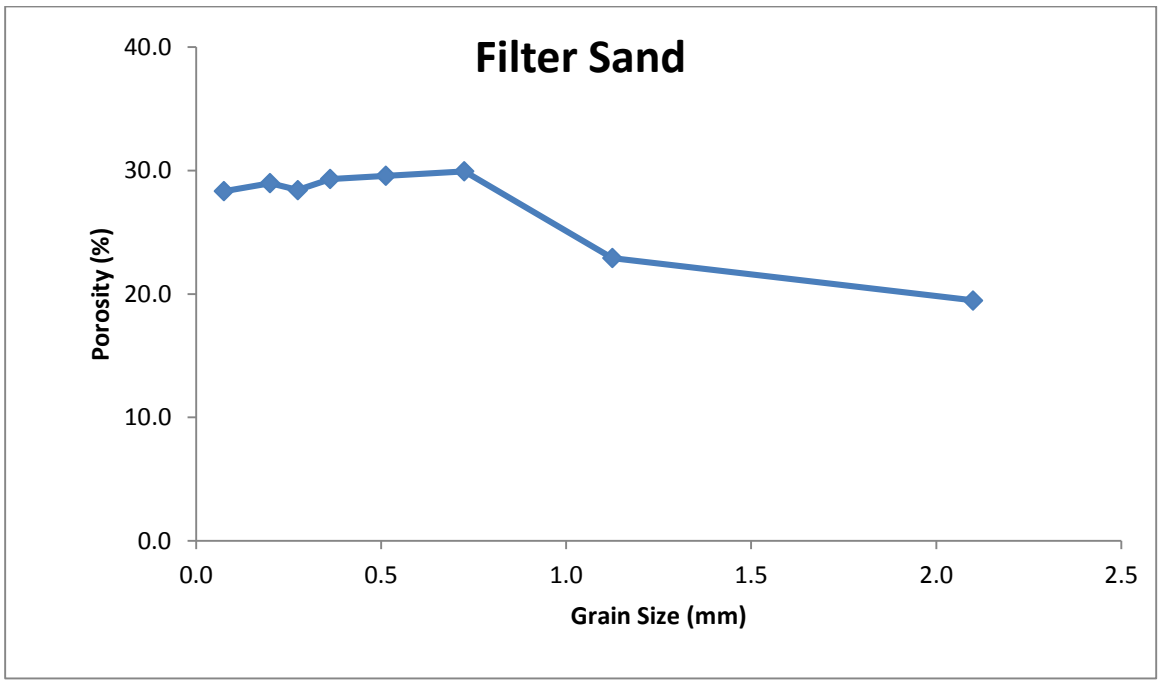
Filter Sand
40.0
30.0
20.0
10.0
0.0
Porosity (%)
0.0
0.5
1.0
1.5
2.0
2.5
Grain Size (mm)

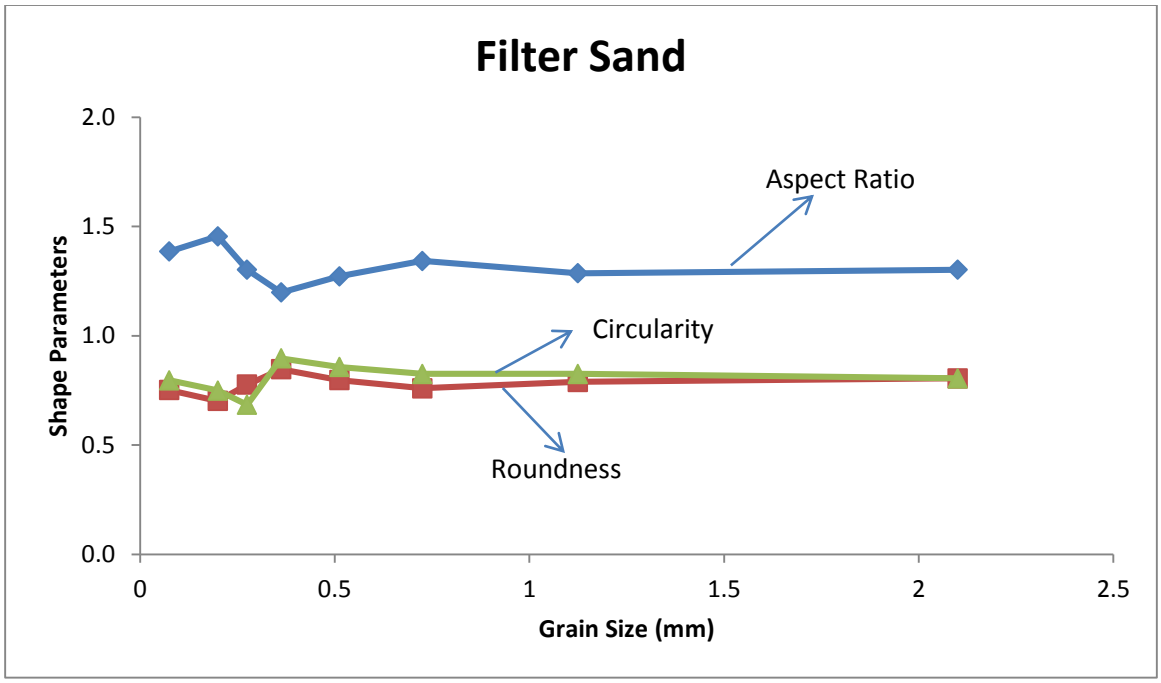
Filter Sand
Shape Parameters
2.0
1.5
1.0
0.5
0.0
0
0.5
1
1.5
2
2.5
Grain Size (mm)
Aspect Ratio
Circularity
Roundness

| Crushed Garnet | | | | |
|---|---|---|---|---|
| Sample ID | Roundness | Aspect Ratio | Circularity | Grain Size |
| | | | | |
| B1 | 0.66 | 1.58 | 0.71 | 0.045 |
| B2 | 0.58 | 1.76 | 0.68 | 0.12 |
| B3 | 0.77 | 1.31 | 0.70 | 0.225 |
| | | | | |
| | | | | |

| Sample ID | Grain Size (mm) | Solid Density (g/cm^3) | Specifc Gravity | Porosity (%) |
|---|---|---|---|---|
| B1 | 0.045 | 2.08 | 2.08 | 32.23 |
| B2 | 0.12 | 2.20 | 2.20 | 30.78 |
| B3 | 0.225 | 2.26 | 2.27 | 29.26 |

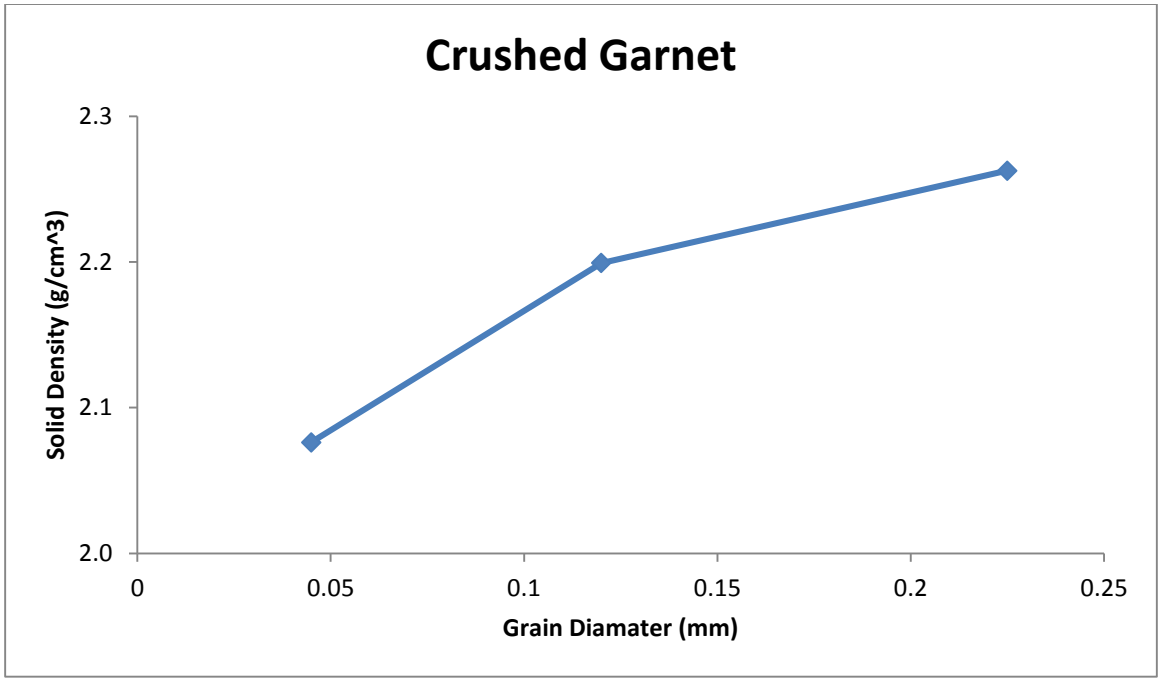

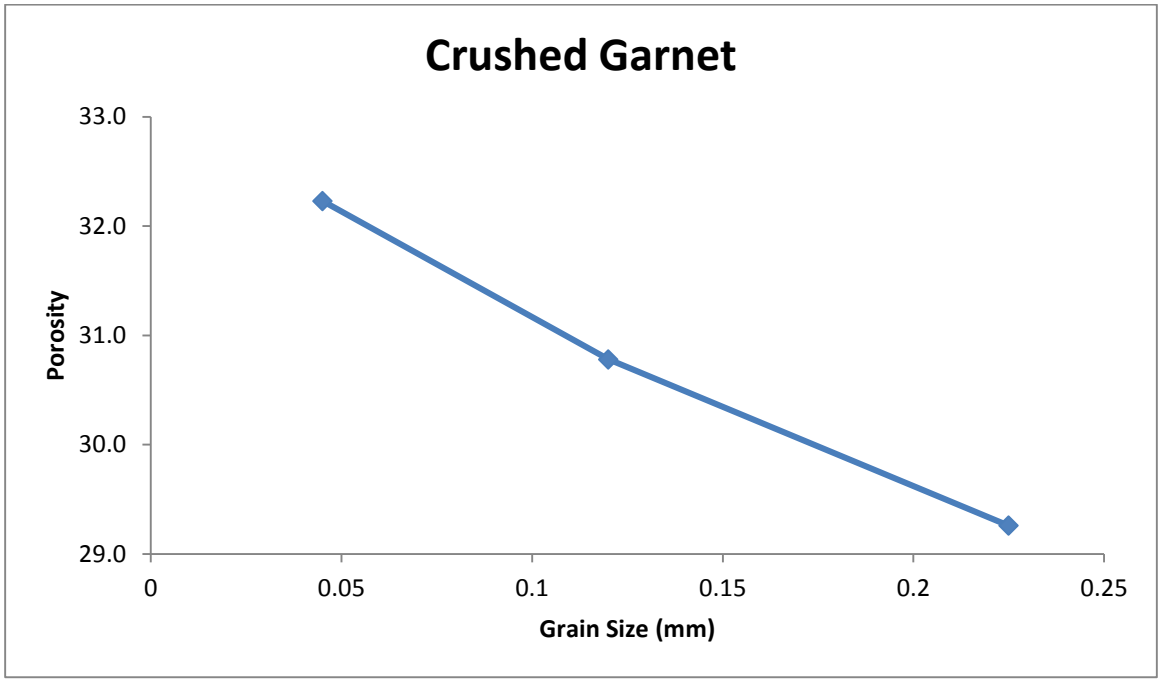
Crushed Garnet
33.0
32.0
31.0
30.0
29.0
Porosity
0
0.05
0.1
0.15
0.2
0.25
Grain Size (mm)

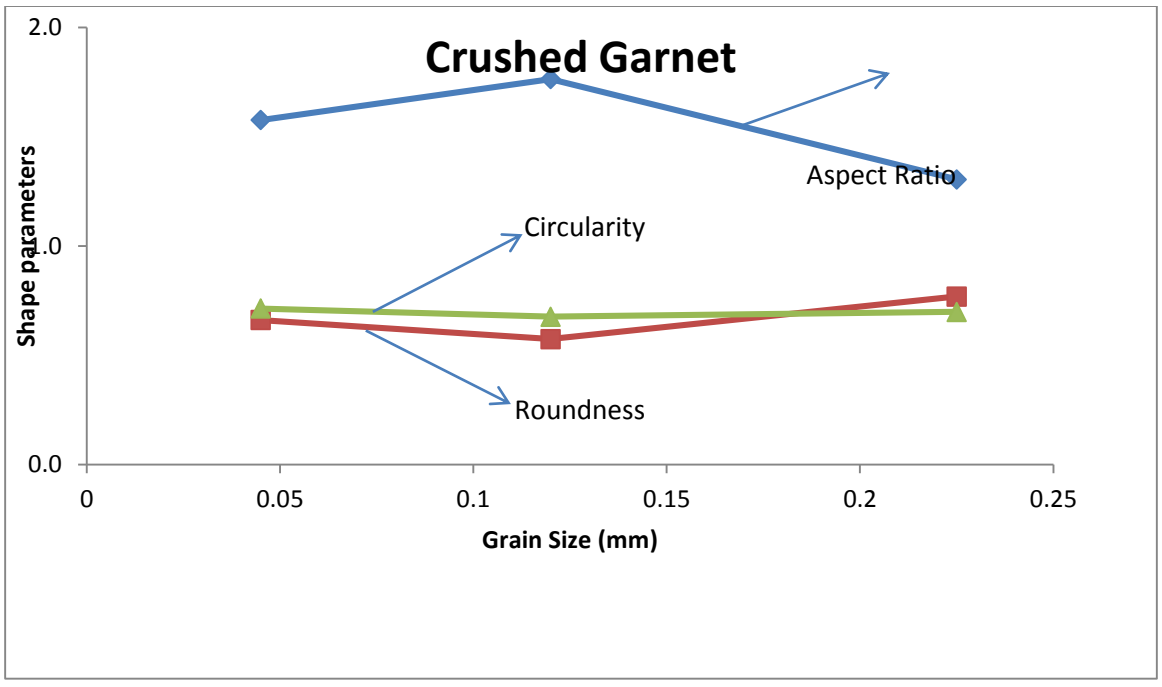
Crushed Garnet
2.0
1.0
0.0
Shape parameters
Aspect Ratio
Circularity
Roundness
0
0.05
0.1
0.15
0.2
0.25
Grain Size (mm)

| Shale Cutting | | | | |
|---|---|---|---|---|
| Sample ID | Grain Size (mm) | Solid Density (g/cm^3) | Specifc Gravity | Porosity (%) |
| E1 | 1.015 | 1.57 | 1.58 | 28.34 |
| E2 | 1.29 | 1.54 | 1.55 | 28.98 |
| E3 | 1.88 | 1.56 | 1.56 | 28.43 |
| E4 | 2.36 | 1.53 | 1.53 | 29.32 |

| Sample ID | Roundness | Aspect Ratio | Circularity | Grain Size |
|---|---|---|---|---|
| | | | | |
| E1 | 0.79 | 1.28 | 0.86 | 1.015 |
| E2 | 0.77 | 1.38 | 0.82 | 1.29 |
| E3 | 0.78 | 1.32 | 0.76 | 1.88 |
| E4 | 0.66 | 1.62 | 0.70 | 2.36 |

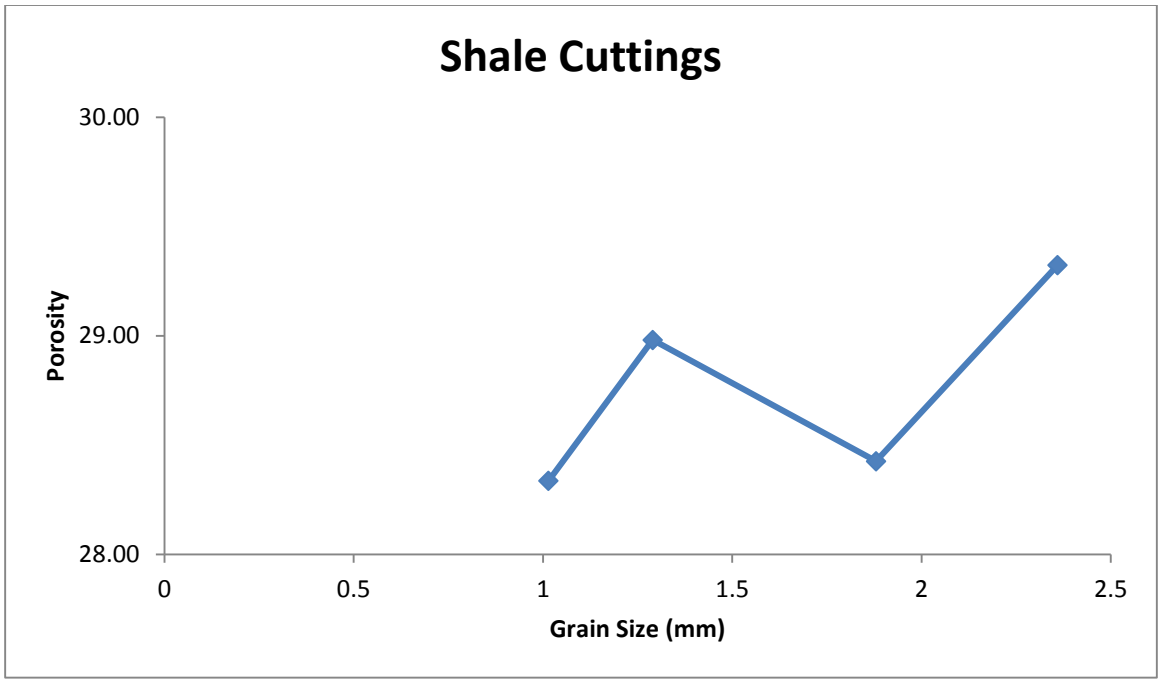
Shale Cuttings
30.00
29.00
28.00
Porosity
0
0.5
1
1.5
2
2.5
Grain Size (mm)

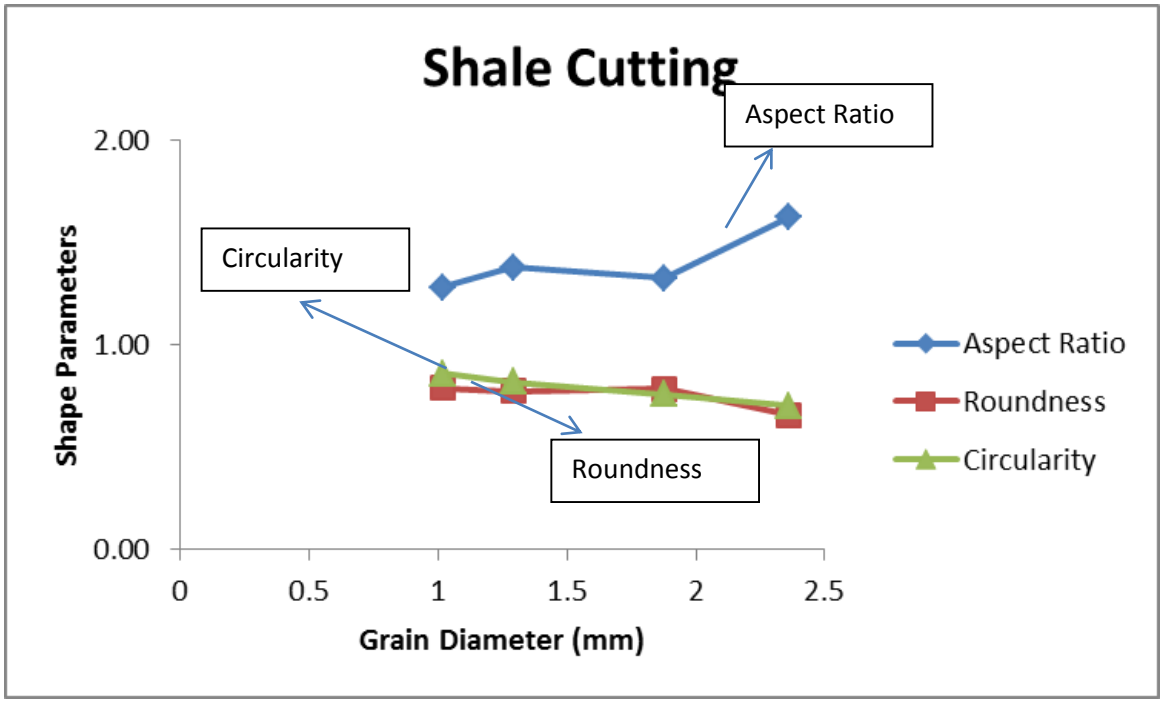
Shale Cutting
Aspect Ratio
Circularity
Roundness
2.00
1.00
0.00
Shape Parameters
0
0.5
1
1.5
2
2.5
Grain Diameter (mm)
Aspect Ratio
Roundness
Circularity

# APPENDIX B

# FORCE-PENETRATION CURVES FOR ALL TESTS

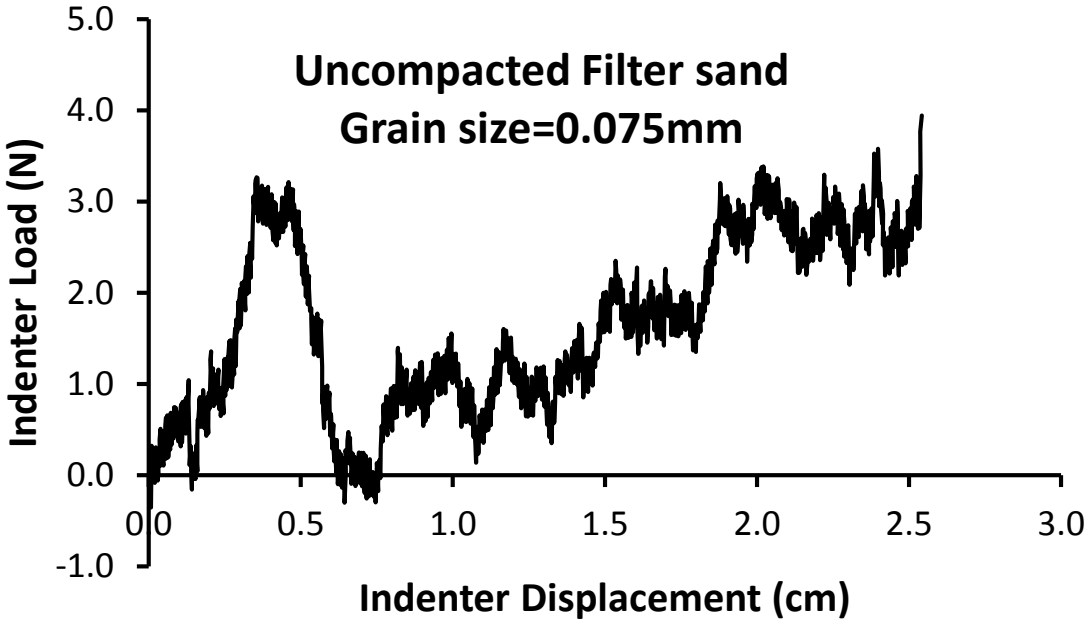
Uncompacted Filter sand
Grain size=0.075mm
Indenter Load (N)
5.0
4.0
3.0
2.0
1.0
0.0
-1.0
0.0
0.5
1.0
1.5
2.0
2.5
3.0
Indenter Displacement (cm)

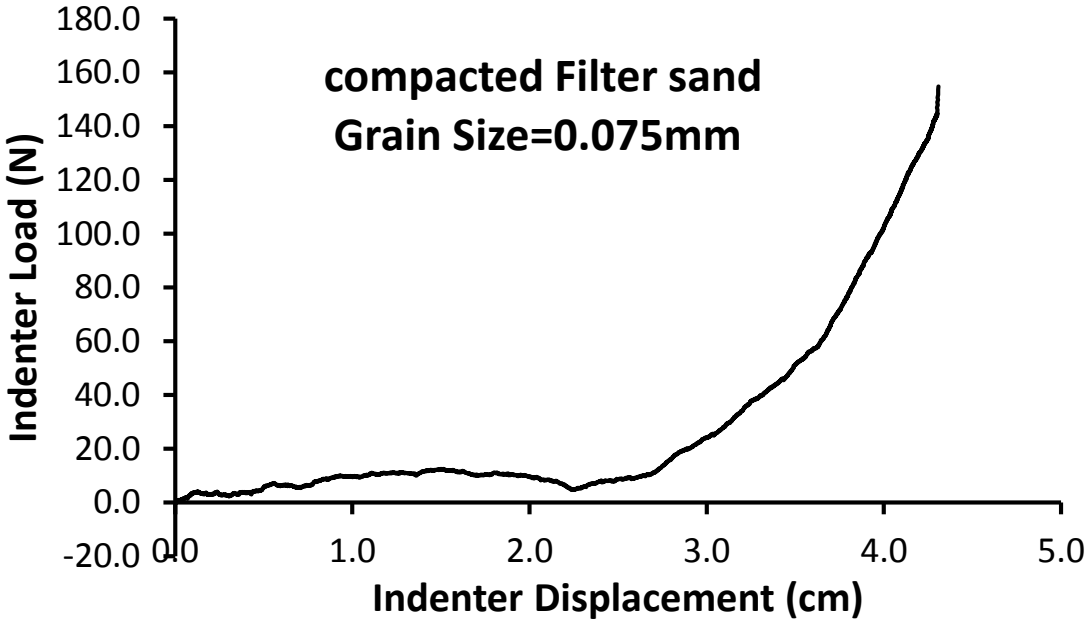
compacted Filter sand
Grain Size=0.075mm
Indenter Load (N)
180.0
160.0
140.0
120.0
100.0
80.0
60.0
40.0
20.0
0.0
-20.0
0.0
1.0
2.0
3.0
4.0
5.0
Indenter Displacement (cm)

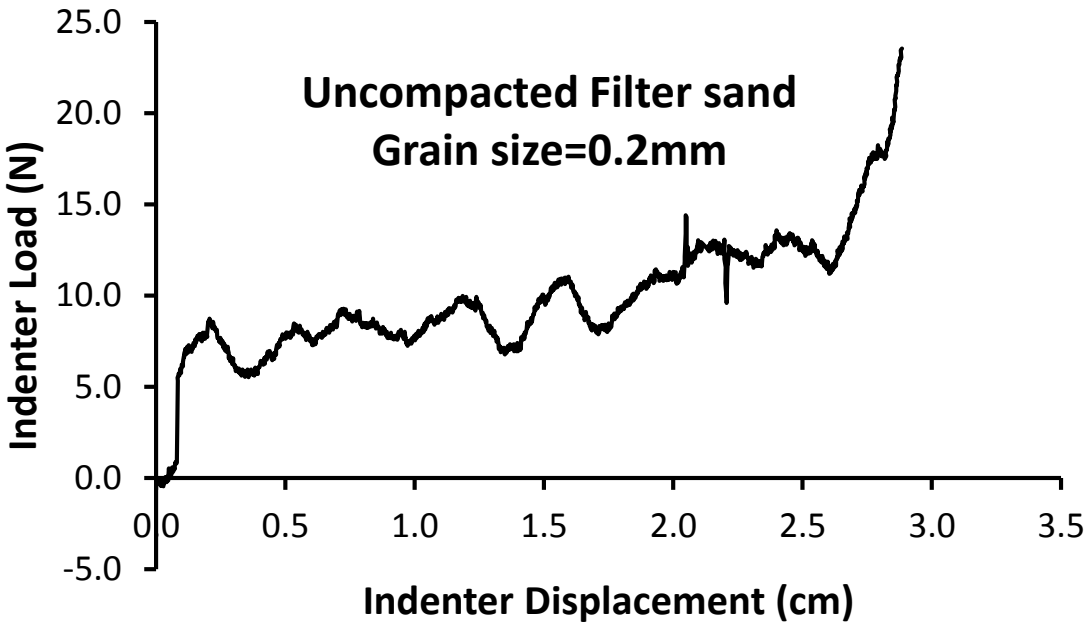
Uncompacted Filter sand
Grain size=0.2mm
Indenter Load (N)
25.0
20.0
15.0
10.0
5.0
0.0
-5.0
0.0
0.5
1.0
1.5
2.0
2.5
3.0
3.5
Indenter Displacement (cm)

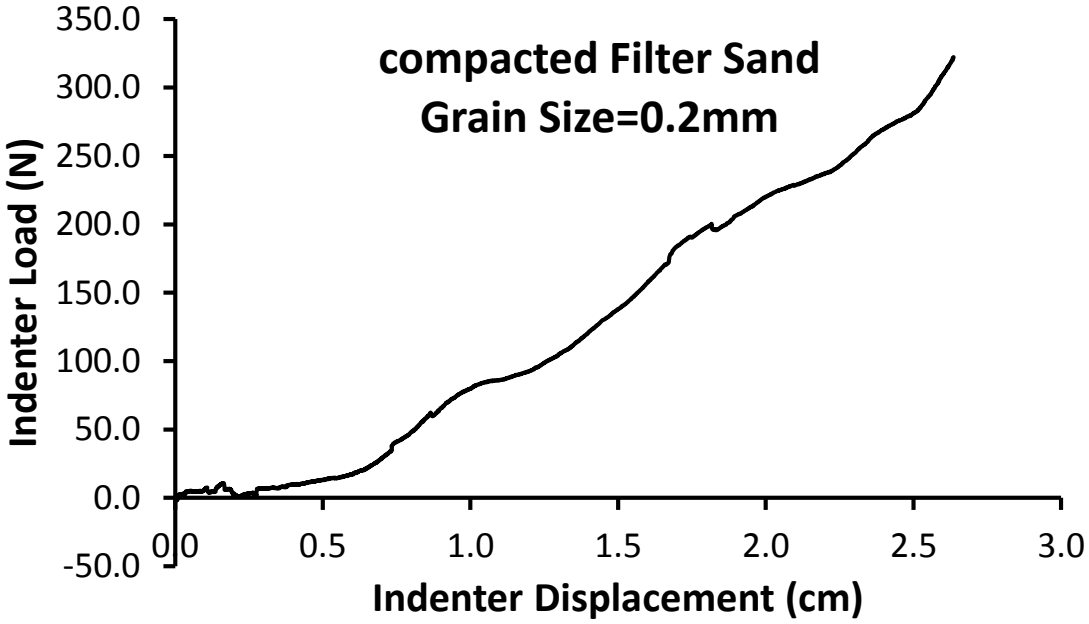
compacted Filter Sand
Grain Size=0.2mm
Indenter Load (N)
350.0
300.0
250.0
200.0
150.0
100.0
50.0
0.0
-50.0
0.0
0.5
1.0
1.5
2.0
2.5
3.0
Indenter Displacement (cm)

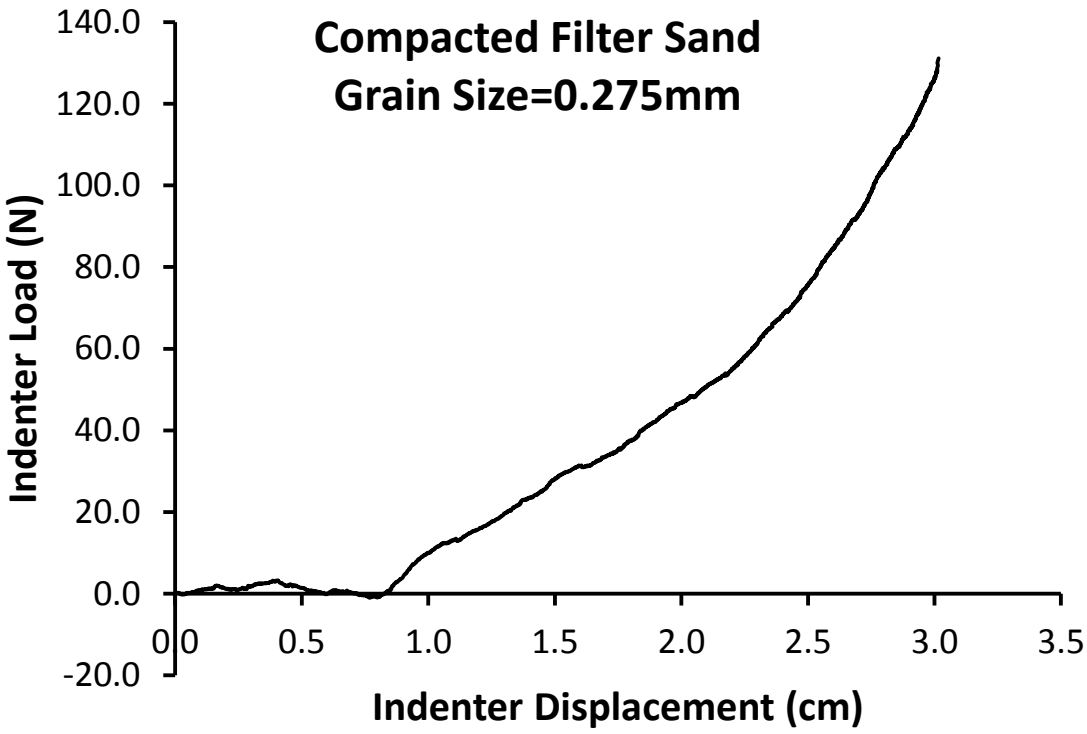
Compacted Filter Sand
Grain Size=0.275mm
Indenter Load (N)
140.0
120.0
100.0
80.0
60.0
40.0
20.0
0.0
-20.0
0
0.5
1.0
1.5
2.0
2.5
3.0
3.5
Indenter Displacement (cm)

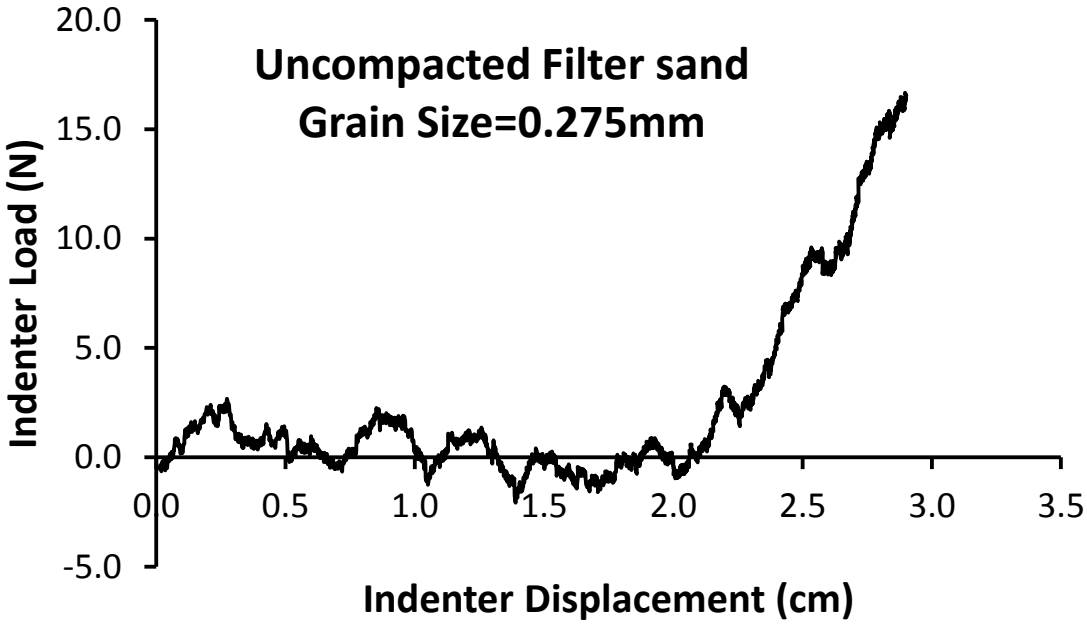
Uncompacted Filter sand
Grain Size=0.275mm
Indenter Load (N)
20.0
15.0
10.0
5.0
0.0
-5.0
0
0.5
1.0
1.5
2.0
2.5
3.0
3.5
Indenter Displacement (cm)

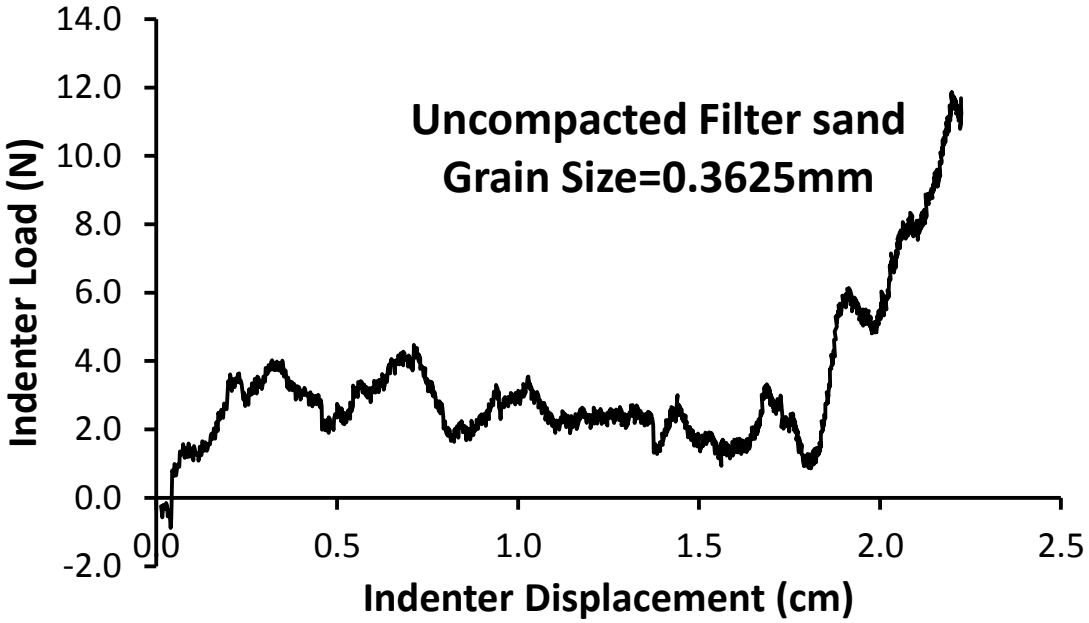
Uncompacted Filter sand
Grain Size=0.3625mm
Indenter Load (N)
Indenter Displacement (cm)
14.0
12.0
10.0
8.0
6.0
4.0
2.0
0.0
-2.0
0.0
0.5
1.0
1.5
2.0
2.5

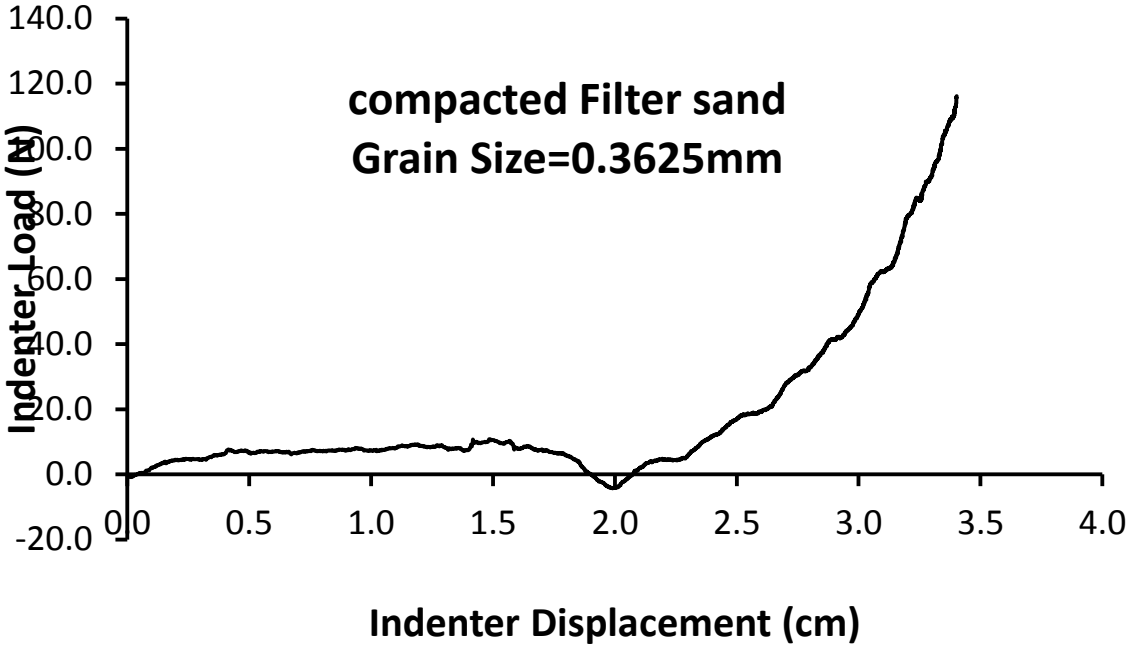
compacted Filter sand
Grain Size=0.3625mm
Indenter Load (N)
Indenter Displacement (cm)
140.0
120.0
100.0
80.0
60.0
40.0
20.0
0.0
-20.0
0.0
0.5
1.0
1.5
2.0
2.5
3.0
3.5
4.0

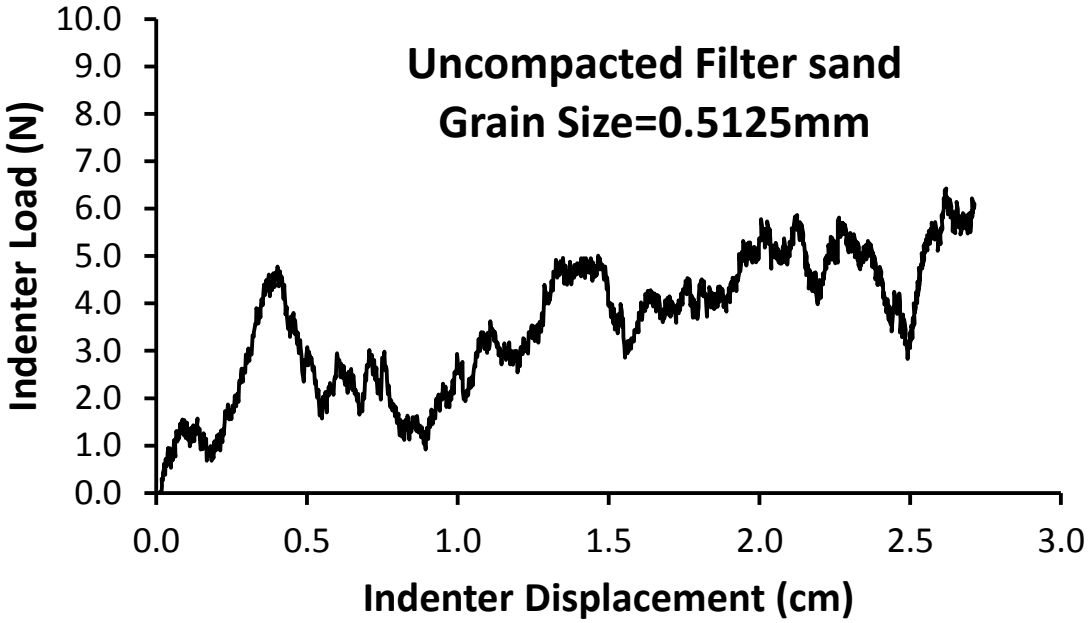
Uncompacted Filter sand
Grain Size=0.5125mm
Indenter Load (N)
10.0
9.0
8.0
7.0
6.0
5.0
4.0
3.0
2.0
1.0
0.0
0.0
0.5
1.0
1.5
2.0
2.5
3.0
Indenter Displacement (cm)

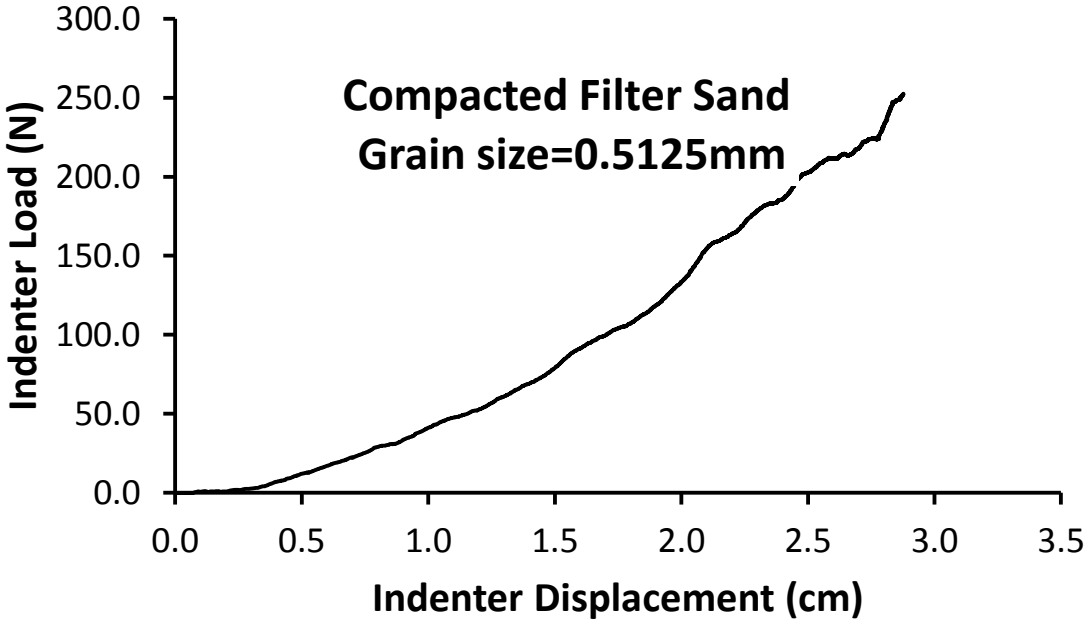
Compacted Filter Sand
Grain size=0.5125mm
Indenter Load (N)
300.0
250.0
200.0
150.0
100.0
50.0
0.0
0.0
0.5
1.0
1.5
2.0
2.5
3.0
3.5
Indenter Displacement (cm)

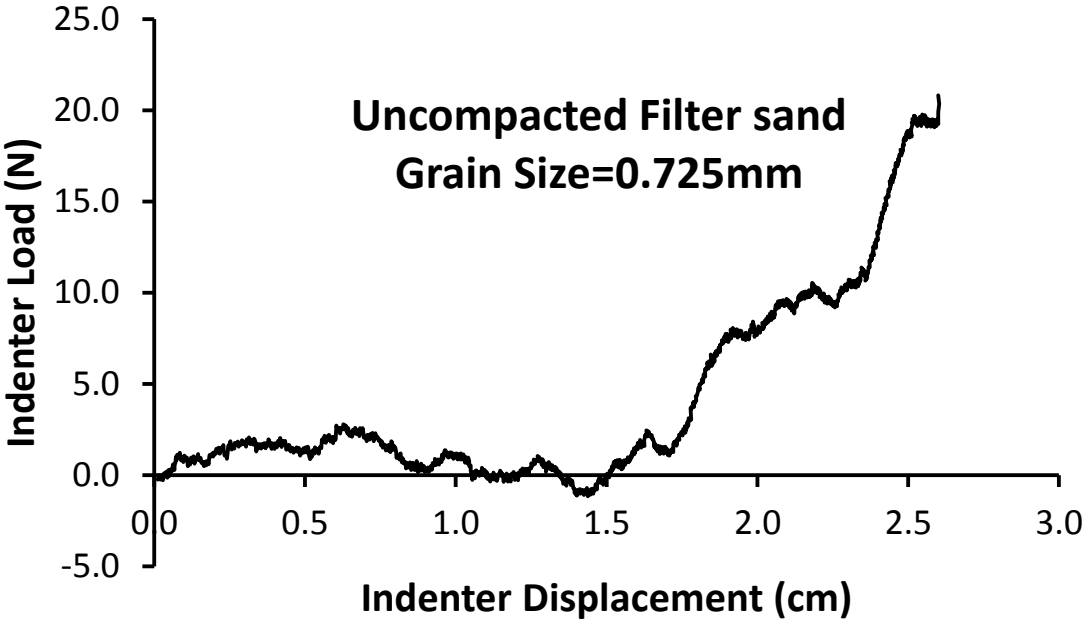
Uncompacted Filter sand
Grain Size=0.725mm
Indenter Load (N)
25.0
20.0
15.0
10.0
5.0
0.0
-5.0
0.0
0.5
1.0
1.5
2.0
2.5
3.0
Indenter Displacement (cm)

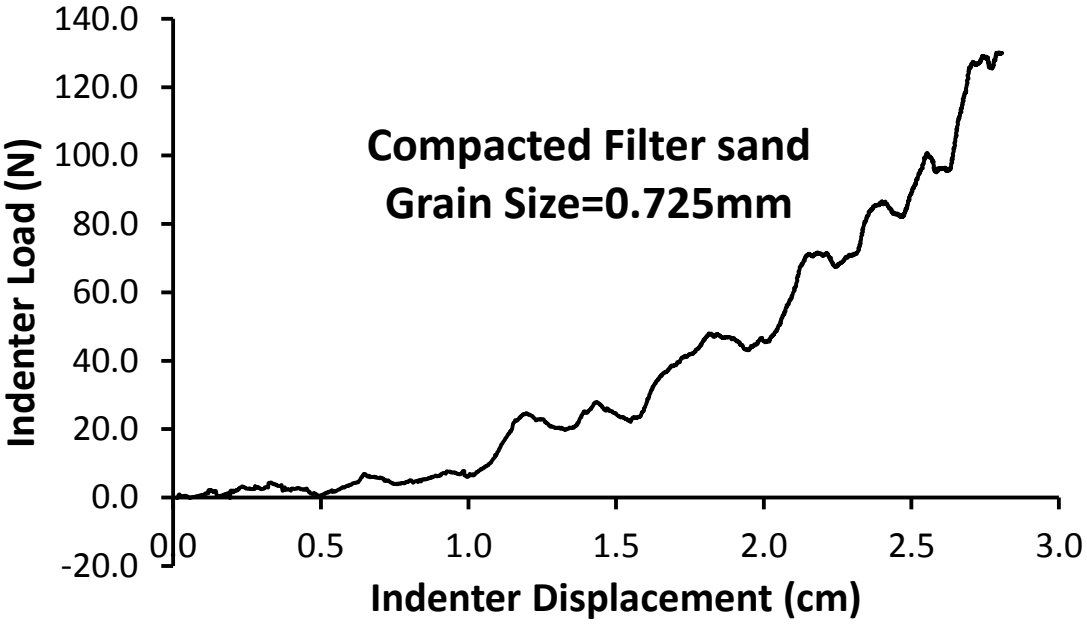
Compacted Filter sand
Grain Size=0.725mm
Indenter Load (N)
140.0
120.0
100.0
80.0
60.0
40.0
20.0
0.0
-20.0
0.0
0.5
1.0
1.5
2.0
2.5
3.0
Indenter Displacement (cm)

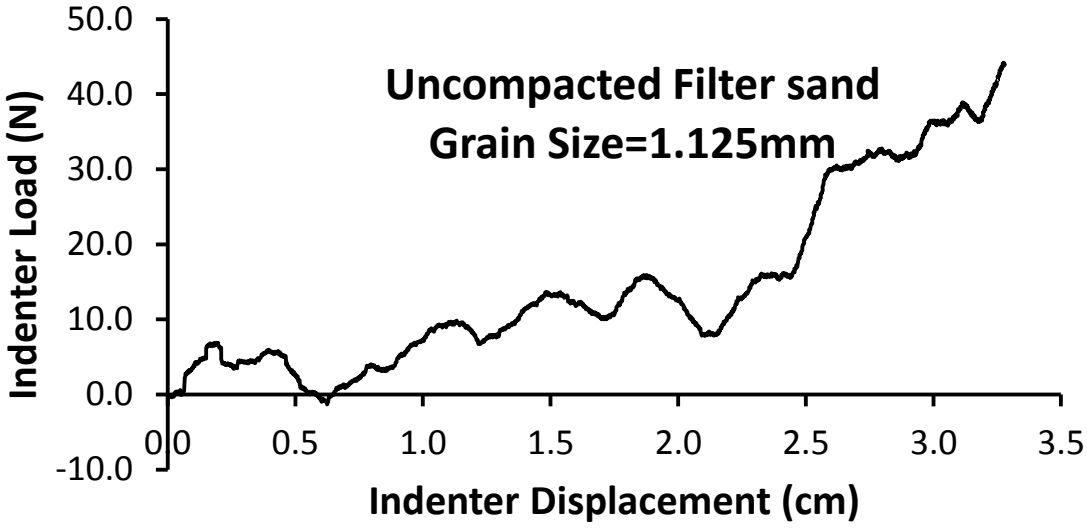
Uncompacted Filter sand
Grain Size=1.125mm
Indenter Load (N)
50.0
40.0
30.0
20.0
10.0
0.0
-10.0
0.0
0.5
1.0
1.5
2.0
2.5
3.0
3.5
Indenter Displacement (cm)

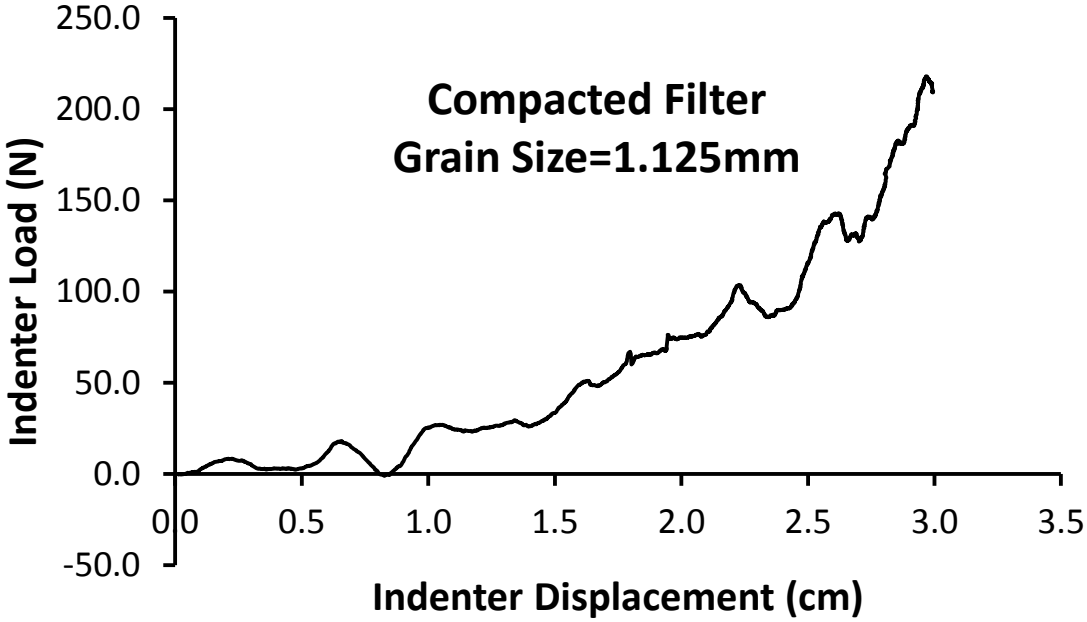
Compacted Filter
Grain Size=1.125mm
Indenter Load (N)
250.0
200.0
150.0
100.0
50.0
0.0
-50.0
0.0
0.5
1.0
1.5
2.0
2.5
3.0
3.5
Indenter Displacement (cm)

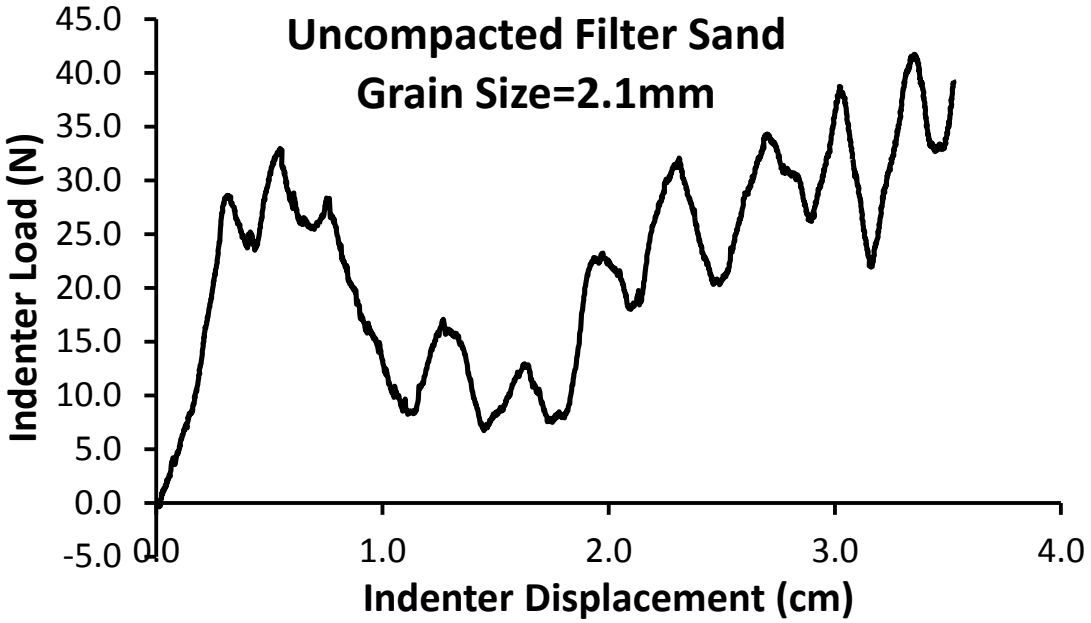
Uncompacted Filter Sand
Grain Size=2.1mm
Indenter Load (N)
45.0
40.0
35.0
30.0
25.0
20.0
15.0
10.0
5.0
0.0
-5.0
0.0
1.0
2.0
3.0
4.0
Indenter Displacement (cm)

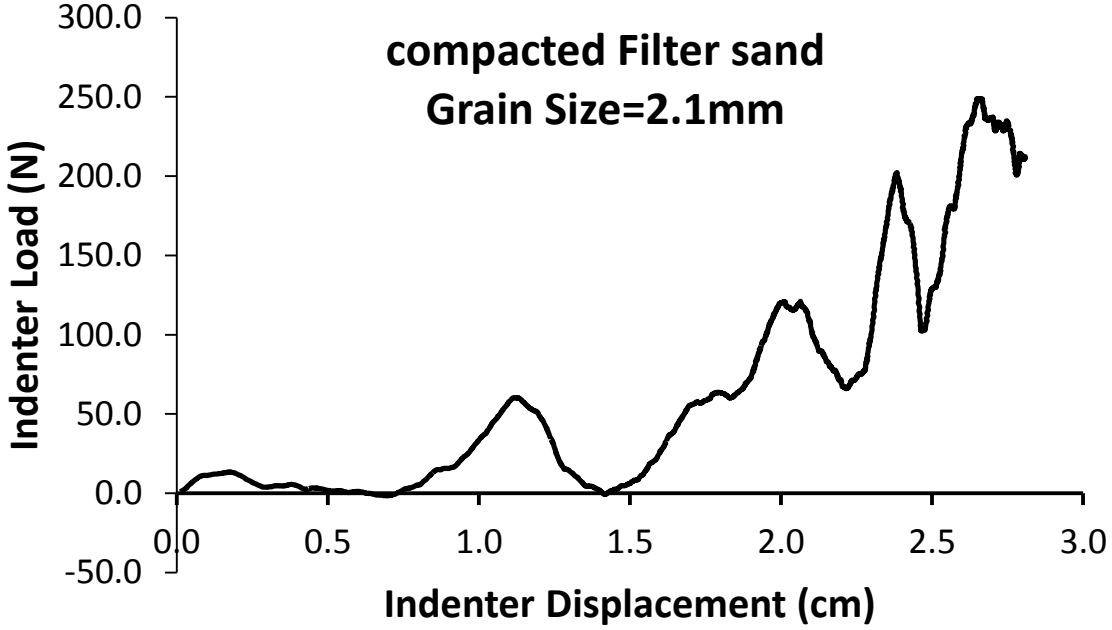
compacted Filter sand
Grain Size=2.1mm
Indenter Load (N)
300.0
250.0
200.0
150.0
100.0
50.0
0.0
-50.0
0.0
0.5
1.0
1.5
2.0
2.5
3.0
Indenter Displacement (cm)

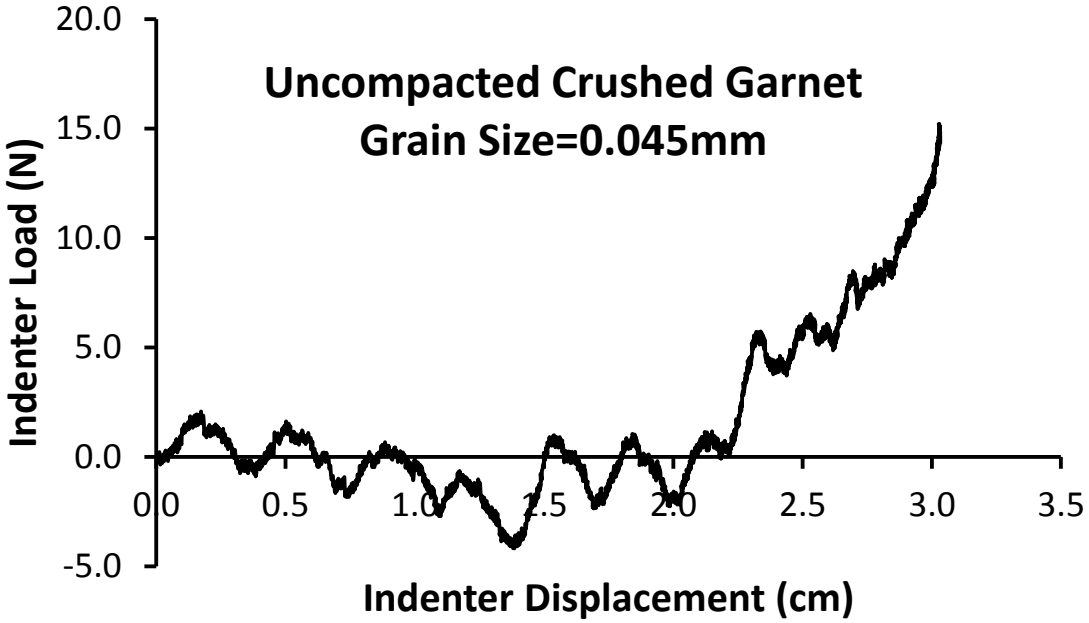
Uncompacted Crushed Garnet
Grain Size=0.045mm
Indenter Load (N)
20.0
15.0
10.0
5.0
0.0
-5.0
0.0
0.5
1.0
1.5
2.0
2.5
3.0
3.5
Indenter Displacement (cm)

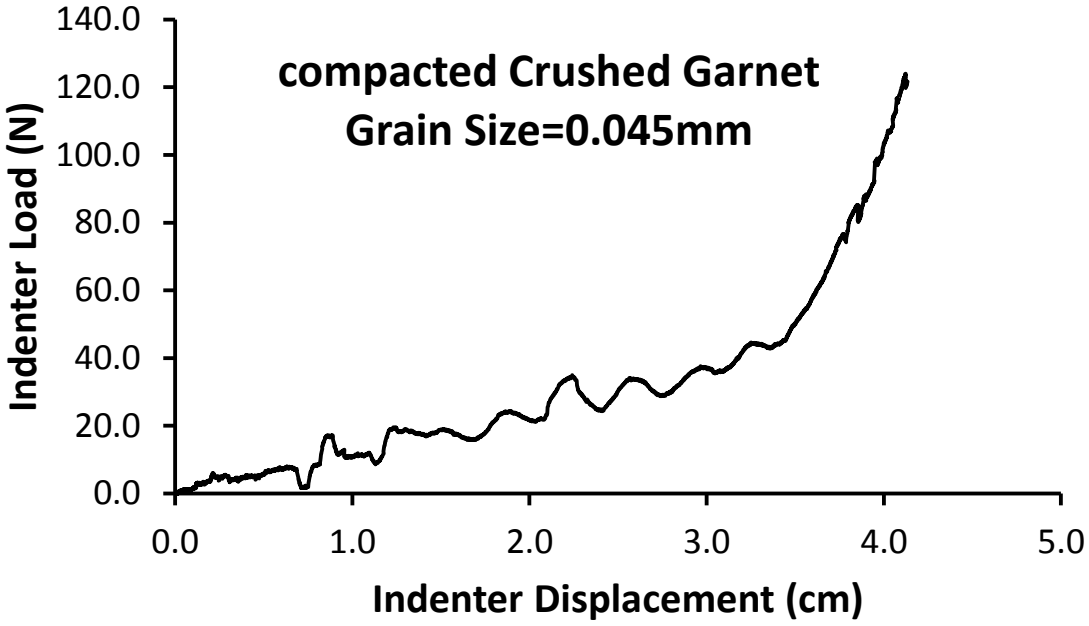
compacted Crushed Garnet
Grain Size=0.045mm
Indenter Load (N)
140.0
120.0
100.0
80.0
60.0
40.0
20.0
0.0
0.0
1.0
2.0
3.0
4.0
5.0
Indenter Displacement (cm)

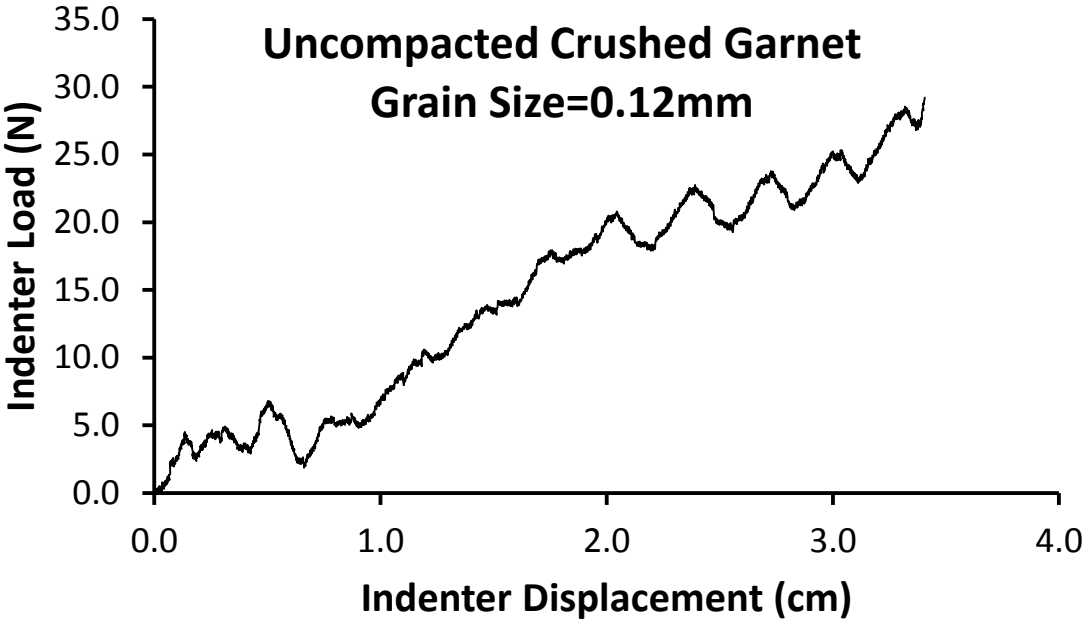
Uncompacted Crushed Garnet
Grain Size=0.12mm
Indenter Load (N)
35.0
30.0
25.0
20.0
15.0
10.0
5.0
0.0
0.0
1.0
2.0
3.0
4.0
Indenter Displacement (cm)

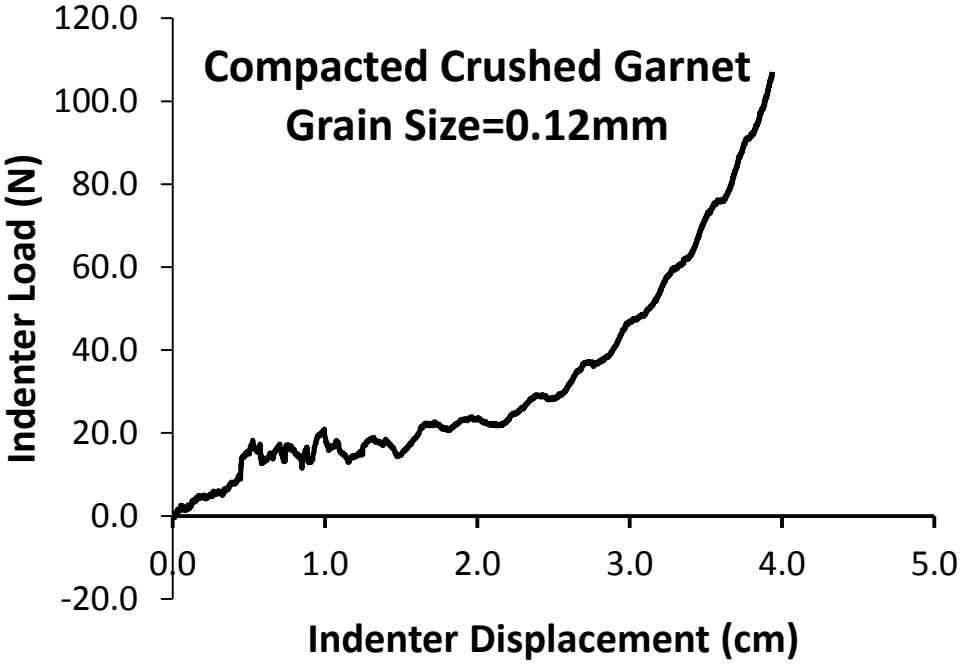
Compacted Crushed Garnet
Grain Size=0.12mm
Indenter Load (N)
120.0
100.0
80.0
60.0
40.0
20.0
0.0
-20.0
0.0
1.0
2.0
3.0
4.0
5.0
Indenter Displacement (cm)

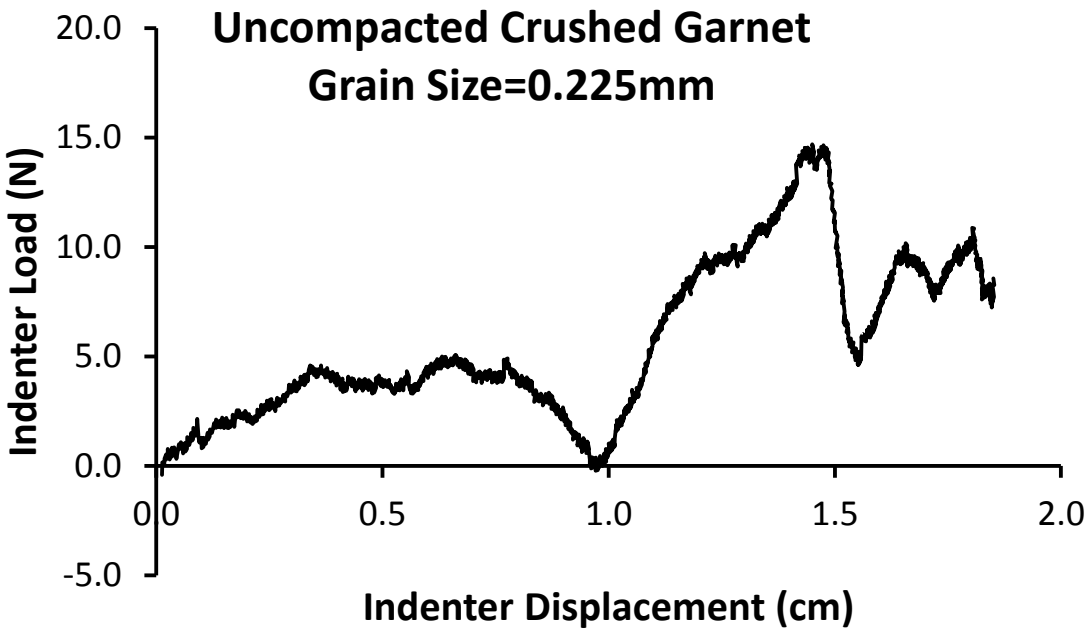
Uncompacted Crushed Garnet
Grain Size=0.225mm
Indenter Load (N)
20.0
15.0
10.0
5.0
0.0
-5.0
0.0
0.5
1.0
1.5
2.0
Indenter Displacement (cm)

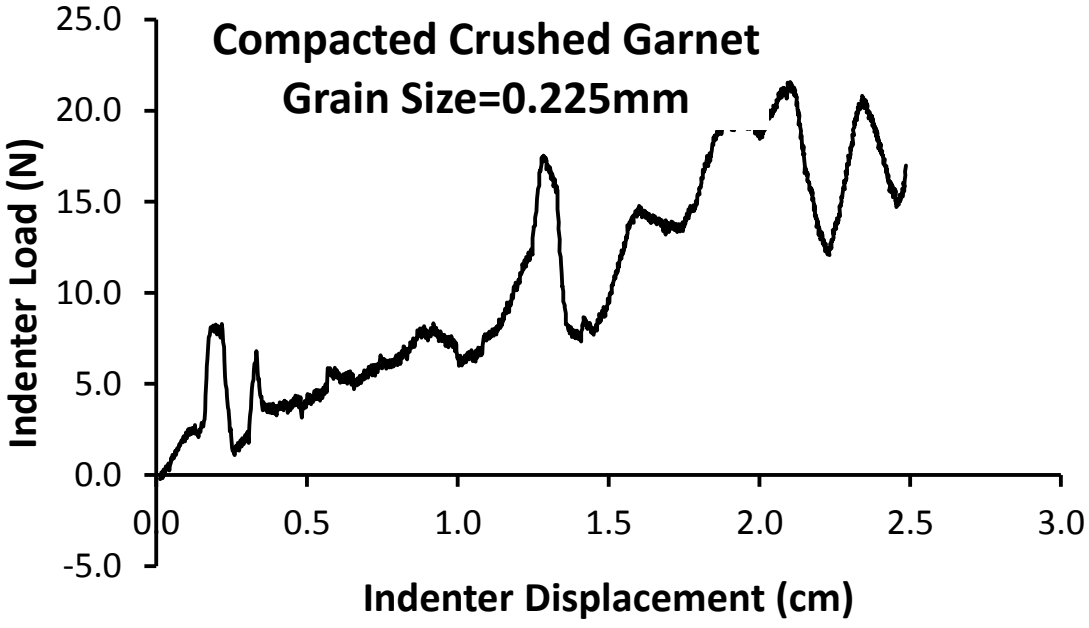
Compacted Crushed Garnet
Grain Size=0.225mm
Indenter Load (N)
25.0
20.0
15.0
10.0
5.0
0.0
-5.0
0.0
0.5
1.0
1.5
2.0
2.5
3.0
Indenter Displacement (cm)

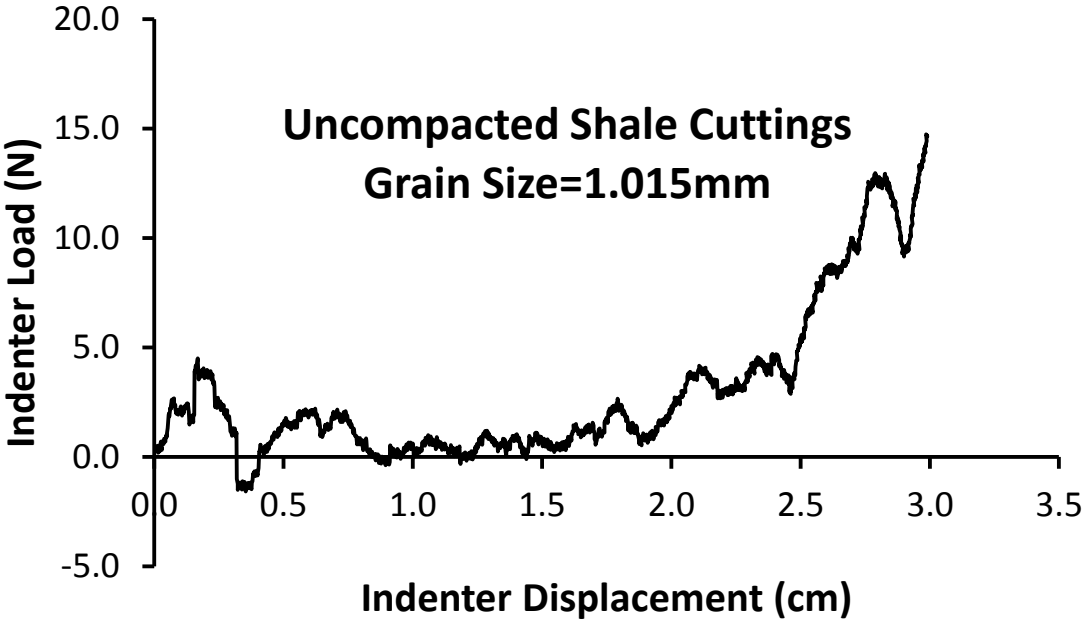
Uncompacted Shale Cuttings
Grain Size=1.015mm
Indenter Load (N)
20.0
15.0
10.0
5.0
0.0
-5.0
0.0
0.5
1.0
1.5
2.0
2.5
3.0
3.5
Indenter Displacement (cm)

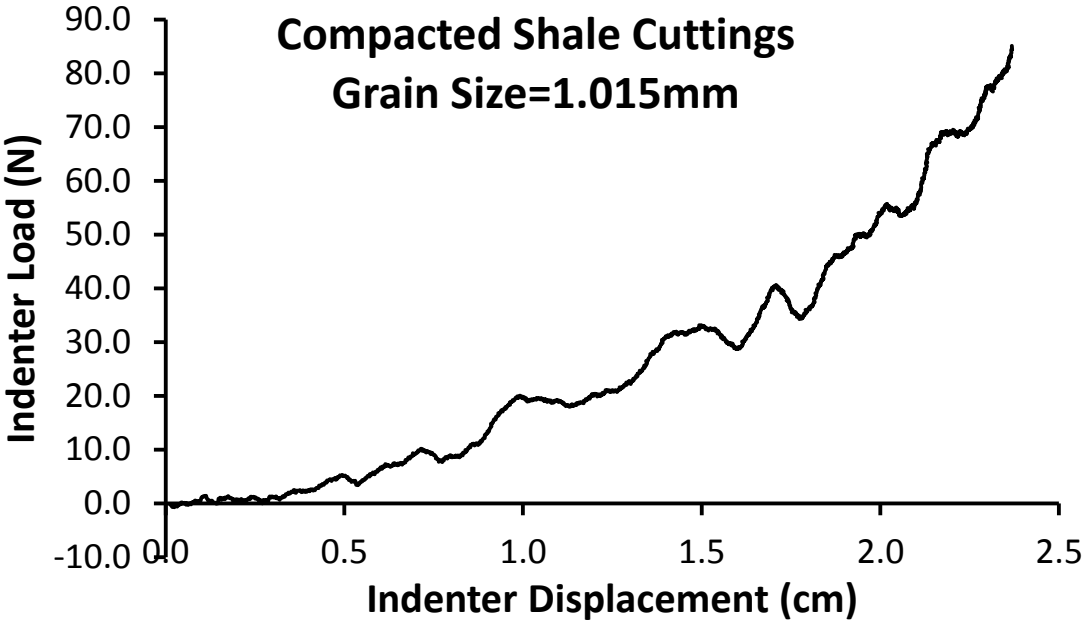
Compacted Shale Cuttings
Grain Size=1.015mm
Indenter Load (N)
90.0
80.0
70.0
60.0
50.0
40.0
30.0
20.0
10.0
0.0
-10.0
0.0
0.5
1.0
1.5
2.0
2.5
Indenter Displacement (cm)

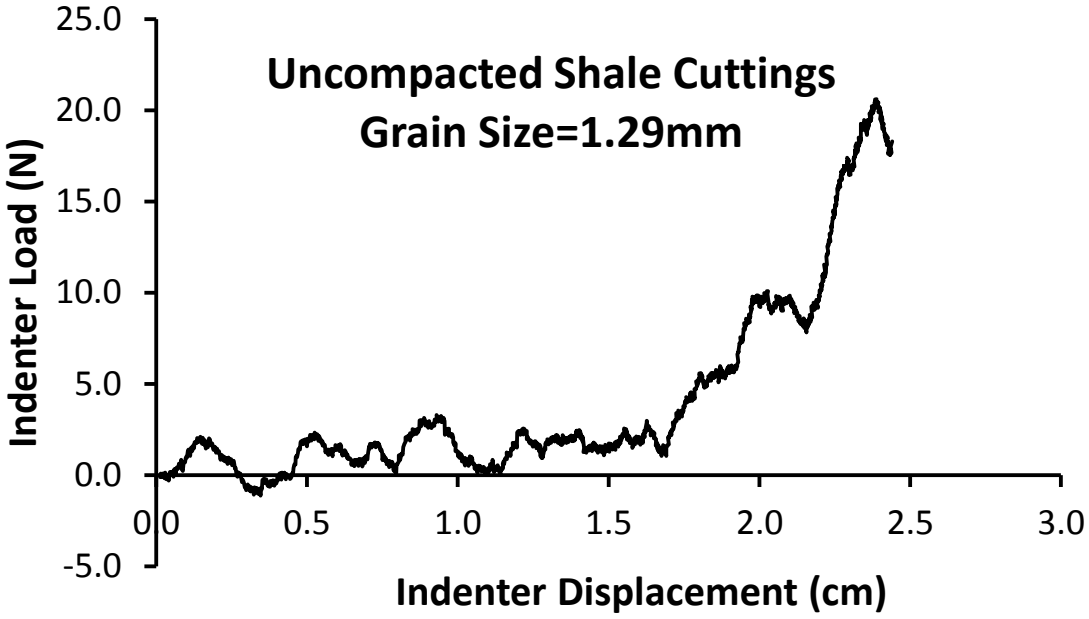
Uncompacted Shale Cuttings
Grain Size=1.29mm
Indenter Load (N)
25.0
20.0
15.0
10.0
5.0
0.0
-5.0
0.0
0.5
1.0
1.5
2.0
2.5
3.0
Indenter Displacement (cm)

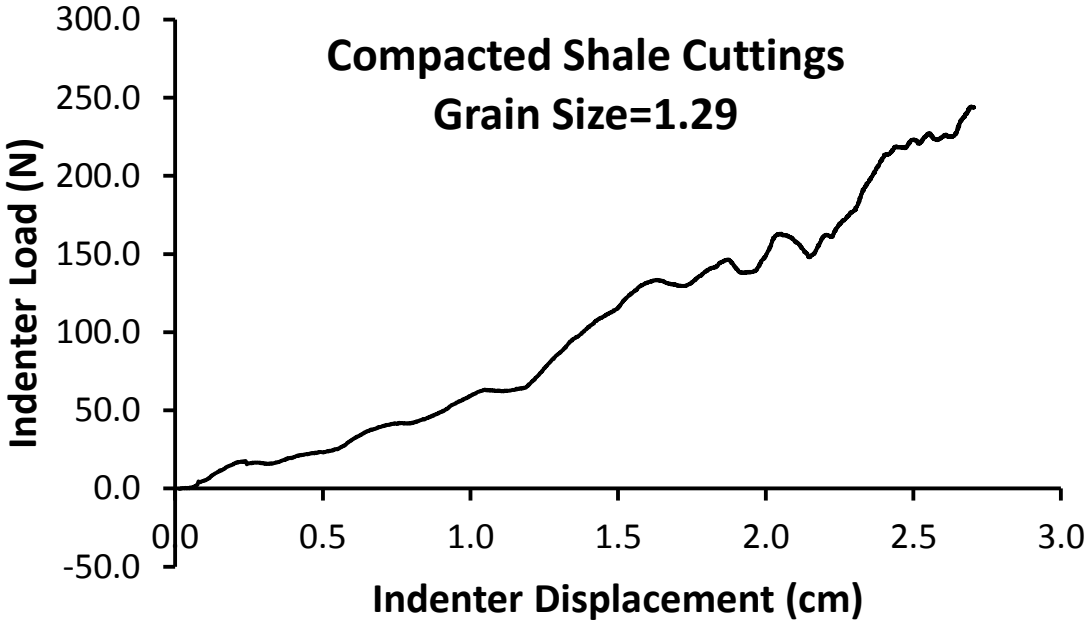
Compacted Shale Cuttings
Grain Size=1.29
Indenter Load (N)
300.0
250.0
200.0
150.0
100.0
50.0
0.0
-50.0
0.0
0.5
1.0
1.5
2.0
2.5
3.0
Indenter Displacement (cm)

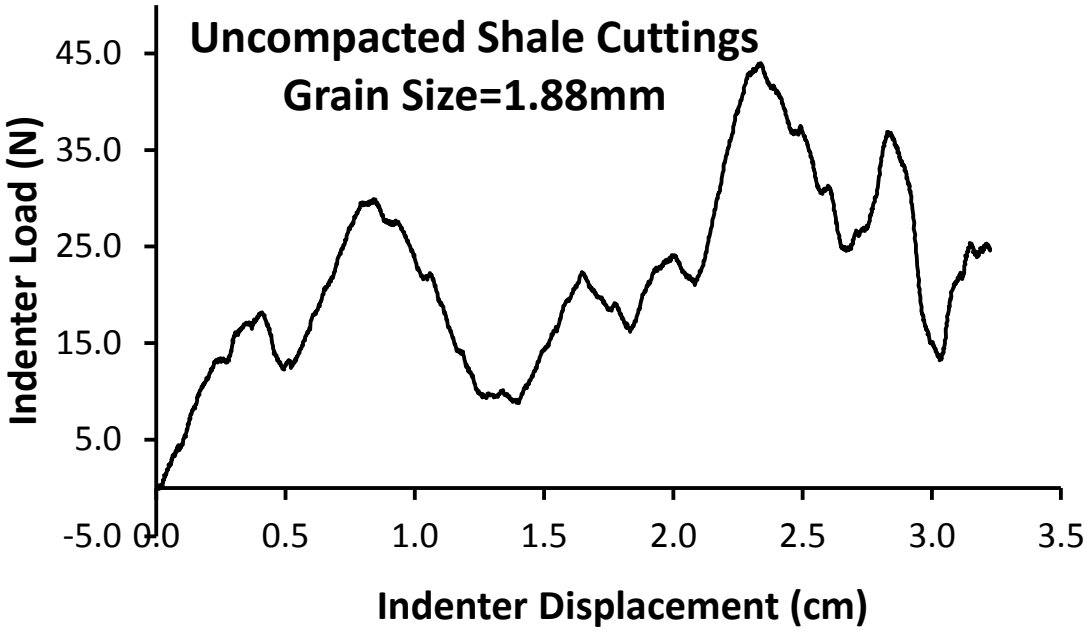
Uncompacted Shale Cuttings
Grain Size=1.88mm
Indenter Load (N)
45.0
35.0
25.0
15.0
5.0
-5.0
0.0
0.5
1.0
1.5
2.0
2.5
3.0
3.5
Indenter Displacement (cm)

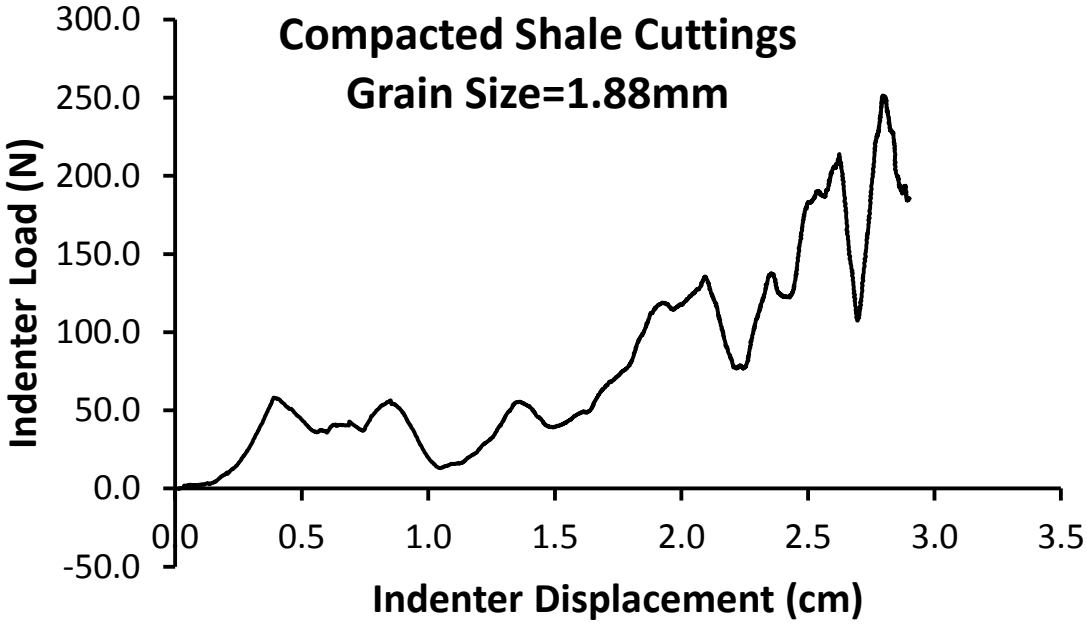
Compacted Shale Cuttings
Grain Size=1.88mm
Indenter Load (N)
300.0
250.0
200.0
150.0
100.0
50.0
0.0
-50.0
0.0
0.5
1.0
1.5
2.0
2.5
3.0
3.5
Indenter Displacement (cm)

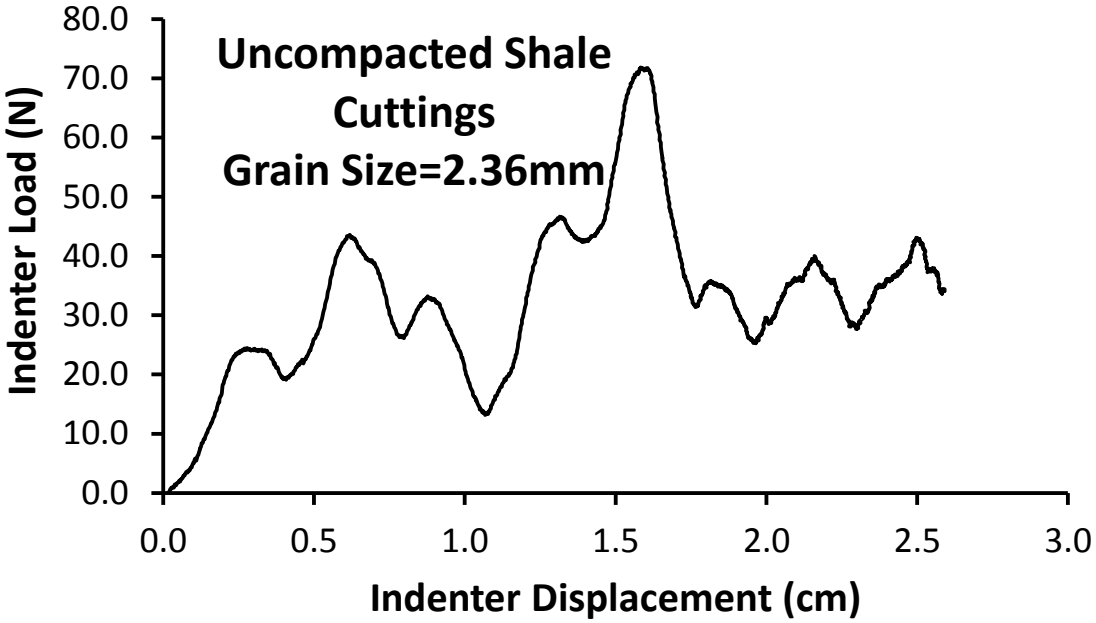
Uncompacted Shale
Cuttings
Grain Size=2.36mm
Indenter Load (N)
80.0
70.0
60.0
50.0
40.0
30.0
20.0
10.0
0.0
0.0
0.5
1.0
1.5
2.0
2.5
3.0
Indenter Displacement (cm)

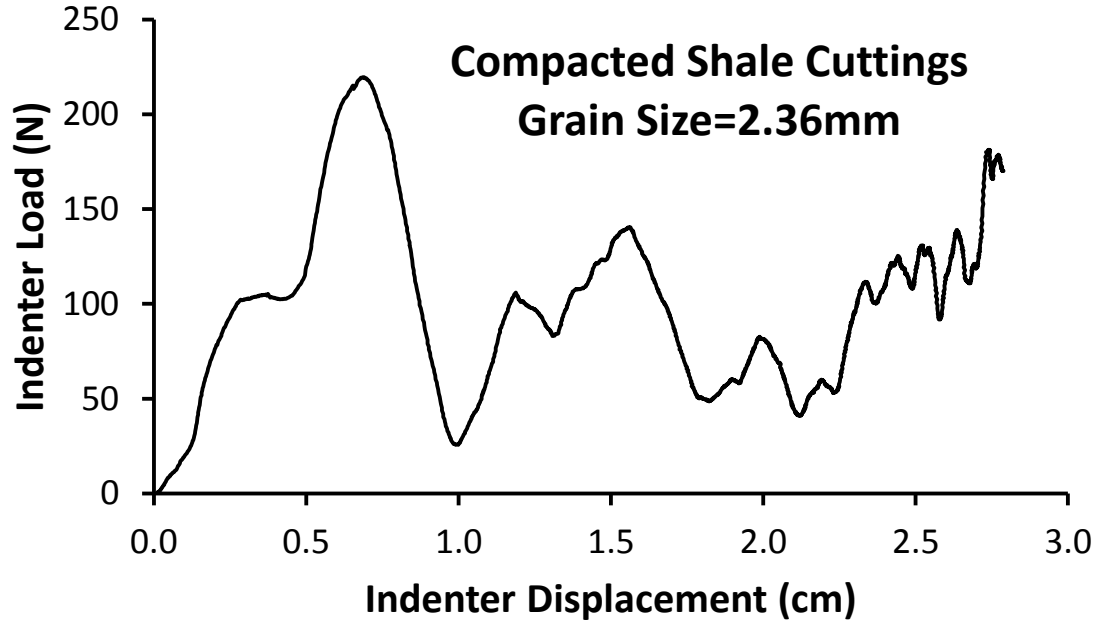
Compacted Shale Cuttings
Grain Size=2.36mm
Indenter Load (N)
250
200
150
100
50
0
0.0
0.5
1.0
1.5
2.0
2.5
3.0
Indenter Displacement (cm)

# APPENDIX C

# DATA TABLES

| | | | | Uncompacted Material | | | | |
|---|---|---|---|---|---|---|---|---|
| | Sample ID | Grain size | Aspect Ratio | Bulk Density | Circularity | Solid Density | Specific Energy | Specific Penetration |
| Filter Sand | A1 | 0.08 | 1.39 | 1.40 | 0.80 | 1.57 | 0.75 | 1.84 |
| | A2 | 0.20 | 1.46 | 1.42 | 0.75 | 1.54 | 3.04 | 7.79 |
| | A3 | 0.28 | 1.30 | 1.45 | 0.68 | 1.56 | 1.38 | 6.04 |
| | A4 | 0.36 | 1.20 | 1.40 | 0.90 | 1.53 | 1.33 | 4.87 |
| | A5 | 0.51 | 1.27 | 1.36 | 0.86 | 1.51 | 1.25 | 8.47 |
| | A6 | 0.73 | 1.34 | 1.33 | 0.83 | 1.53 | 1.54 | 5.82 |
| | A7 | 1.13 | 1.29 | 1.38 | 0.83 | 1.81 | 3.94 | 10.66 |
| | A8 | 2.10 | 1.30 | 1.37 | 0.81 | 1.97 | 7.39 | 23.40 |
| Crushed Garnet | B1 | 0.05 | 1.58 | 1.87 | 0.71 | 2.08 | 2.19 | 6.09 |
| | B2 | 0.26 | 1.76 | 2.01 | 0.68 | 2.20 | 9.66 | 18.76 |
| | B3 | 0.23 | 1.31 | 2.07 | 0.70 | 2.26 | 2.59 | 7.01 |
| Shale Cuttings | E1 | 0.78 | 1.28 | 1.37 | 0.86 | 1.56 | 0.92 | 3.98 |
| | E2 | 1.02 | 1.38 | 1.37 | 0.82 | 1.71 | 3.20 | 12.68 |
| | D1 | 1.44 | 1.32 | 1.27 | 0.76 | 2.09 | 5.76 | 12.61 |
| | D2 | 2.36 | 1.62 | 1.29 | 0.70 | 2.06 | 15.12 | 73.44 |

| Material Compacted | | | | | | | |
|---|---|---|---|---|---|---|---|
| Sample ID | Grain size | Aspect Ratio | Bulk Density | Circularity | Solid Density | Specific Energy | Specific Penetration |
| A1 | 0.08 | 1.39 | 1.58 | 0.80 | 1.57 | 22.68 | 68.65 |
| A2 | 0.20 | 1.46 | 1.47 | 0.75 | 1.54 | 28.20 | 63.42 |
| A3 | 0.28 | 1.30 | 1.55 | 0.68 | 1.56 | 21.55 | 42.81 |
| A4 | 0.36 | 1.20 | 1.47 | 0.90 | 1.53 | 19.52 | 34.26 |
| A5 | 0.51 | 1.27 | 1.49 | 0.86 | 1.51 | 37.21 | 72.25 |
| A6 | 0.73 | 1.34 | 1.45 | 0.83 | 1.53 | 24.13 | 58.83 |
| A7 | 1.13 | 1.29 | 1.50 | 0.83 | 1.81 | 47.23 | 91.24 |
| A8 | 2.10 | 1.30 | 1.46 | 0.81 | 1.97 | 27.38 | 81.85 |
| B1 | 0.05 | 1.58 | 2.11 | 0.71 | 2.08 | 13.29 | 22.45 |
| B2 | 0.26 | 1.76 | 2.27 | 0.68 | 2.20 | 28.47 | 28.47 |
| B2 | 0.23 | 1.31 | 2.25 | 0.70 | 2.26 | 8.47 | 23.76 |
| E1 | 0.78 | 1.28 | 1.49 | 0.86 | 1.56 | 40.12 | 94.84 |
| E2 | 1.015 | 1.38 | 1.84 | 0.82 | 1.71 | 13.72 | 90.77 |
| D1 | 1.44 | 1.32 | 1.43 | 0.76 | 2.09 | 63.89 | 118.03 |
| D2 | 2.36 | 1.62 | 1.32 | 0.70 | 2.06 | 28.22 | 121.46 |

## BIBLIOGRAPHY

Albert I, Tegzes P, Albert R, Sample J. G, Barabási A.L, Vicsek T, Kahng B, and Schiffer P. "Stick-slip fluctuations in granular drag," The American Physical Society. Phys. Rev. 2013 E 64, 031307.

Bragov A. M, Lomunov A.K, Sergeichev I.V, Tsembelis K, Proud W.G. "Determination of physicomechanical properties of soft soils from medium to high strain rates," *International Journal of Impact Engineering* vol. 35, 2008. Pp.967–976

Brzinskki III T.A, Mayor P, and Durian D.J. "Depth-Dependent Resistance of Granular Media to Vertical Penetration," *American Physical Society*. 2013. PRL 111. 168002.

Copur H, Bilgin N, Tuncdemir H, and Balci C. "A set of indices based on indentation tests for assessment of rock cutting performance and rock properties," *The South African Institute of Mining and Metallurgy*, 2003. SA ISSN 0038–223X/3.00 + 0.00.

Deketh H.J.R, Averez Grima M, Hergardern I.M, Giezen M, and Verhoef P.N.W. "Towards the prediction of rock excavation machine performance," Bulletin of Engineering Geology and the Environment 1998. Vol. 57, issue 1, pp 3-15.

Dollinger G. L, Handewith H. J, and Breeds C.D. "Use of the Punch Test for Estimating TBM Performance," *Tunneling and Underground Space Technology*, Vol. 13, No. 4, 1998. pp. 403-408.

Ehlers, W. and Avci, O, "Stress-dependent hardening and failure surfaces of dry sand," Int. J. Numer. Anal. Meth. Geomech, 2012. 37: 787–809. doi: 10.1002/nag.1121.

Hongbing Lu, Huiyang Luo, William L. Cooper, and Ranga Komanduri. "Effect of Particle Size on the Compressive Behavior of Dry Sand under Confinement at High Strain Rates," 2012 Conference Proceedings of the Society for Experimental Mechanics Series. *The Society for Experimental Mechanics*. Ch.67, 2013. Pp 523-530.

Huang J, Xua S, Hu S. "Effects of grain size and gradation on the dynamic responses of quartz sands," *International Journal of Impact Engineering* vol. 59, 2013. pp 1-10.

Kahraman S, Fener M, and Kozman E. "Predicting the compressive and tensile strength of rocks from indentation hardness index," *Southern African Institute of Mining and Metallurgy*, vol 112, 2012. SA ISSN 0038–223X/3.00 + 0.00.

Kahraman S, Gunaydin O. "Indentation hardness test to estimate the sawability of carbonate rocks," *Bull Eng. Geol. Environ* (2008) 67:507–511.

Marston J.O, Vakarelski I.U, and Thoroddsen S.T. "Sphere impact and penetration into wet sand," *American Physical Society*. Physical review 2012. 86, 020301(R).

Masafumi Iai. "Scaled experimental study on excavation of lunar regolith with rakes/rippers and flat blade," PhD. Dissertation Missouri University of Science and Technology. 2010

Nedderman, R. M. "Statics and kinematics of granular materials," 1992. *Cambridge University Press, Cambridge, ISBN 0* 521.40435: 5.

Robert P. Behringer, Heinrich M. Jaeger and Sidney R. Nagel. "Granular solids, liquids, and gasses," American Physical Society. 1996. Vol. 68, pp 1259-1273.

Saffet Yagiz. "Assessment of brittleness using rock strength and density with punch penetration test," *Tunneling and Underground Space Technology* vol. 24, 2009. pp 66–74.

Uehara J.S, Ambrose M.A, Ojha R.P, and Durian D.J. "Low-Speed Impact Craters in Loose Granular Media," American Physical Society. Vol 90, 2003. Num19.

Vanel Loic, Daniel Howell, Clark D, Behringer R .P, and Eric Clement. "Memories in sand: Experimental tests of construction history on stress distributions under sand piles," *The American Physical Society*, Vol. 60, No 4, 1999. Pp 5040-5043.

# VITA

Dennis Chieze Duru came from Ejemekwuru, Imo State, Nigeria. He received his Bachelor of Agricultural Technology in Crop Science and Technology from the Federal University of Technology, Owerri in Imo State, Nigeria. Successfully, he completed the National Youth Service Scheme (NYSC) in June, 2012.

Subsequently, Dennis gained admission to study Geological Engineering (M.S.) at Missouri University of Science and Technology in Rolla, Missouri. During this time, he worked at the Space Resources Laboratory at the Rock Mechanics and Explosives Research Center, where he carried out a number of space related projects. Analyzing rocks and soils was also part of the work he carried out at the research center. In addition, he served as a Graduate Research Assistant and Teaching Assistant at different times.

Dennis is an active member of different professional organizations including the Society of Exploration Geophysicists (SEG), Society of Petroleum Engineers (SPE), and the Association of Environmental and Engineering Geologists (AEG). He has presented and co-authored different conference papers. Dennis graduated with his Masters' in December, 2014.